Horizontal Tail and Aileron Sizing for Distributed Electric Propulsion Aircraft

T. Dundulis

Technische Universiteit Delft

TU Delft Delft University of Technology

Challenge the future

Horizontal Tail and Aileron Sizing for Distributed Electric Propulsion Aircraft

by

T. Dundulis

in partial fulfillment of the requirements for the degree of

Master of Science
in Aerospace Engineering

at the Delft University of Technology,
to be defended publicly on Tuesday April 23, 2024 at 1:00 PM.

Supervisors:	Dr. ir. R. de Vries,
	Dr. ir. R. Vos,
Thesis committee:	Dr. ir. M. F. M. Hoogreef,
	Dr. ir. E. van Kampen,

This thesis is confidential and cannot be made public until April 23, 2025.

TU Delft Delft University of Technology

PREFACE

This report is an extensive summary of the research I conducted to obtain my Master of Science degree in Aerospace Engineering at Delft University of Technology and to ultimately become an engineer. The entire Master's program presented significant challenges, yet it was undeniably the most rewarding experience of my life. Through the encountered struggles, I acquired valuable experience and, notably, enhanced my problem-solving skills, which are currently benefiting me and will continue to do so in my future career.

I would like to take this opportunity to express my gratitude, first and foremost, to my unofficial daily supervisor, Reynard de Vries, for the invaluable assistance and time devoted to ensuring the success of this project. Additionally, I extend my appreciation to Roelof Vos, who agreed to supervise this project and provided invaluable guidance on the most challenging aspects of my research. I also want to thank Alberto Ruiz Garcia for his contributions, particularly in addressing questions related to propeller effect modeling, which significantly facilitated the initiation of my research.

Finally, heartfelt thanks go to my family for their unwavering support throughout my academic journey. Without the assistance I received, reaching this milestone would not have been possible. Once again, a sincere thank you to everyone who contributed to my success in achieving my goal of becoming an engineer.

T. Dundulis
Delft, April 2024

ABSTRACT

A distributed propulsion aircraft can feature many benefits; however, the stability and control of such aircraft are different from those of conventional aircraft. The goal of this thesis is to evaluate the minimum horizontal tail and aileron size for DEP aircraft and compare it to a conventional aircraft. To do this, a tool is proposed capable of estimating the minimal horizontal tail and aileron size for different configurations and including or excluding propeller effects. The tool is capable of predicting the dynamic pressure increase at the wing and horizontal tail due to propeller slipstream, the change in angle of attack at the wing due to propeller upwash and downwash, and the increase in wing downwash. Using these quantities, the change in lift for the wing and horizontal tail can be estimated due to the propellers. Additionally, it can estimate the moment of inertia of the aircraft which is especially relevant for the roll of a DEP aircraft. The tool sizes the aircraft for stability, rotation at take-off, trim, and roll. The main limitation of the tool is that it does not account for sideslip (only two-dimensional movements), thus, for rolling the influence of sideslip is ignored. Furthermore, the tool is designed for use with conventional planform aircraft, and the wing can either have minimal sweep or no sweep at all. The tool was verified using examples from the references presenting the method. It was also validated using Saab 340 with T-tail wind tunnel data. There was a slight offset between the results due to the limitations of the tool modelling, however, the model was calibrated to the real-life data. In this report, three aircraft configurations are analyzed: twin turboprop aircraft excluding propeller effects, twin turboprop aircraft including propeller effects, and a DEP aircraft including propeller effects. The DEP aircraft features eight propellers, folding wing tips, a reserve fuel tank in the back of the fuselage, and a battery inside the aircraft wing.

First of all, the influence of propeller effects for the twin turboprop configuration is analyzed. The results show that propellers destabilize the aircraft due to propeller normal force and extra downwash generated; however, they help rotate faster at take-off due to increased lift and downwash. Moreover, propellers add additional damping during rolling.

Second of all, all three configurations are sized for the minimal tail size, and the results are compared. The twin turboprop aircraft (without propeller effects) features the smallest normalized tail size, closely followed by the DEP aircraft. The twin turboprop aircraft (with propeller effects) features the largest tail size. This is because the twin turboprop aircraft (with propeller effects) has the lowest stability due to the propeller destabilizing moment and extra downwash at the horizontal tail. However, the DEP aircraft featured a lower propeller destabilizing moment and a relatively shorter fuselage, increasing stability. Moreover, propeller effects increase the rotational performance, lowering the tail size for this maneuver. In general, the DEP aircraft features a 19% smaller normalized horizontal tail size.

Regarding roll, the twin turboprop aircraft had a higher requirement for roll due to lower aircraft mass. However, even with a lower requirement, the DEP aircraft needed the same normalized aileron size. This was due to the larger rolling moment of inertia (the normalized moment of inertia was approximately 30% higher than for the twin-turboprop aircraft due to the batteries being placed quite close to the fuselage - up to 34% of the half-span). Moreover, the distributed propellers added damping to the roll motion, even further reducing the roll performance of DEP aircraft.

Finally, a sensitivity analysis of the DEP aircraft was performed. This included the vertical position of the horizontal tail, battery placement in the wing, and reserve fuel placement. It was concluded that a T-tail is the optimal tail for a DEP aircraft, as the downwash at the tail is lower, thus making it more stable. Moreover, an analysis was done to see if the batteries could be placed throughout the whole wing; however, this resulted in a too big aileron. Using the whole space reserved for the aileron, the battery could be placed up to 55% of the span. Finally, moving the reserve fuel tank to the middle of the fuselage showed a better stability performance of an aircraft, reducing the tail size by about 10%.

Contents

List of Figures

List of Tables

NOMENCLATURE

ABBREVIATIONS

Abbreviation	Definition
a	Aileron
ac	Aerodynamic center
af	Airfoil
cg	Center of gravity
DEP	Distributed electric propulsion
DOF	Degree of freedom
e	Elevator
f	Flap
fus	Fuselage
h	Horizontal tail
mac	Mean aerodynamic chord
mg	Main gear
MOI	Moment of inertia
MTOW	Maximum take-off weight
OEI	One engine inoperative
p	Propeller
ph	Phugoid
prop	propeller
prop off	Without propeller effects
prop on	With propeller effects
r	Rudder
sp	Short period
T	thrust
w	Wing
wr	Wing root

SYMBOLS

Symbol	Definition	Unit
A	Aspect ratio	(-)
b	Wingspan	(m)
b_{p}	Blade width of the propeller	(m)
c	Chord	(m)
$C_D = \frac{D}{q_\infty S_{\mathrm{W}}}$	Aircraft drag coefficient	(-)
C_{D_f}	Aircraft skin friction drag	(-)
C_{D_0}	Aircraft zero-lift drag coefficient	(-)
$C_l = \frac{L_{\mathrm{A}}}{q_\infty S_{\mathrm{W}} b_{\mathrm{W}}}$	Rolling moment coefficient	(-)
$C_{l_\alpha} = \partial C_l \partial / \alpha$	Sectional lift coefficient with respect to angle of attack	(1/rad)
$C_{l_\beta} = \partial C_l / \partial \beta$	Rolling moment coefficient derivative with respect to sideslip	(1/rad)
$C_{l_{\delta_{\mathrm{a}}}} = \partial C_l / \partial \delta_{\mathrm{a}}$	Rolling moment coefficient derivative with respect to aileron deflection	(1/rad)

Symbol	Definition	Unit
$C_L = \frac{L}{q_\infty S_\mathrm{w}}$	Lift coefficient	(-)
$C_{L_\alpha} = \partial C_L / \partial \alpha$	Lift coefficient with respect to angle of attack	(1/rad)
$C_m = \frac{M_\mathrm{A}}{q_\infty S_\mathrm{w} b_\mathrm{w}}$	Pitching moment coefficient	(-)
C_{m_af}	Airfoil pitching moment coefficient	(-)
$C_{m_\alpha} = \partial C_m / \partial \alpha$	Pitching moment coefficient derivative with respect to angle of attack	(1/rad)
$C_{m_{\dot\alpha}} = \partial C_m / \partial (\dot\alpha \bar c / 2V_\infty)$	Pitching moment coefficient derivative with respect to pitch rate	(1/rad)
$C_{m_q} = \partial C_m / \partial (q_\infty \bar c / 2V_\infty)$	Wing and fuselage pitching moment coefficient	(-)
$C_{n_r} = \partial C_n / \partial (r b_\mathrm{w} / 2V_\infty)$	Yawing moment coefficient derivative with respect to yaw rate	(s/rad)
$C_{n_\beta} = \partial C_n / \partial \beta$	Yawing moment coefficient derivative with respect to sideslip	(1/rad)
$C_{N_{\alpha_\mathrm{p}}} = \partial C_N / \partial \alpha_\mathrm{p}$	Normal force derivative of the propeller	(1/rad)
e	Oswald efficiency factor	(-)
f	Propeller inflow factor	(-)
h	Height	(m)
i	Incidence angle	(rad)
I_{xx}	Roll mass moment of inertia	(kgm^2)
I_{yy}	Pitch mass moment of inertia	(kgm^2)
K_fus	Correlation parameter for fuselage moment	(-)
K_N	Normal force factor	(-)
K_1	Correlation parameter for additional wing lift due to power effects on the wing	(-)
l	Length	(m)
L	Lift	(N)
L_f	Fuselage length	(ft)
m	Mass	(kg)
M	Mach number (depending on context)	(-)
M	Moment (depending on context)	(Nm)
M_q	Pitch angular acceleration per unit pitch rate	(1/s)
M_α	Pitch angular acceleration per unit angle of attack	($1/\mathrm{s}^2$)
$M_{\dot\alpha}$	Pitch angular acceleration per unit rate of change of angle of attack	(1/s)
n	Number of propellers	(-)
N_p	Propeller normal force	(N)
p	Roll rate	(rad/s)
q	Dynamic pressure	(Pa)
q_∞	Freestream dynamic pressure	(Pa)
r	Radial distance	(m)
R	Radius	(m)
$\bar R_x$	Roll non-dimensional radii of gyration	(-)
$\bar R_y$	Pitch non-dimensional radii of gyration	(-)
S_w	Wing area	(m^2)
S_i	Area immersed in the propeller slipstream	(m^2)
SM	Static margin	(-)
t	Time	(s)
$T_c = \frac{T}{q_\infty S_\mathrm{w}}$	Thrust coefficient	(-)
U	Speed in x-axis	(m/s)
V_∞	Freestream air speed	(m/s)
$\bar V_H$	Horizontal tail volume coefficient	(-)
w	Width	(m)
W_f	Fuselage width	(ft)
x	Longitudinal position	(m)

Symbol	Definition	Unit
x_{ac}	Longitudinal position of aerodynamic center	(m)
x_{cg}	Longitudinal position of center of gravity	(m)
$X_u = \frac{-qS_w(C_{D_u}+2C_D)}{mU}$	Forward acceleration per unit change in speed	(m/s^2/rad)
y	Spanwise position	(m)
z	Vertical position	(m)
z_{h_T}	Distance from thrust axis to the quarter chord of the horizontal tail mean aerodynamic chord	(m)
z''_h	Vertical distance from the root chord plane of the wing to the quarter-chord point of horizontal tail mean aerodynamic chord	(m)
$Z_u = \frac{-qS_w(C_{L_\alpha}+C_D)}{m}$	Vertical acceleration per unit angle of attack	(m/s^2/rad)
$Z_\alpha = \frac{-qS_w(C_{L_u}+2C_L)}{mU}$	Vertical acceleration per unit change in speed	(1/s)
α	Angle of attack	(rad)
α_b	Angle of attack relative to body axis	(rad)
α_h	Angle of attack of propeller plane	(rad)
α_T	Angle of attack of thrust axis	(rad)
α_0	Zero lift angle of attack	(rad)
β'	Propeller blade angle	(rad)
δ	Control surface deflection	(rad)
$\frac{d\epsilon}{d\alpha}$	Downwash gradient	(-)
$-\frac{\delta\epsilon_u}{\delta\alpha}$	Upwash gradient at the propeller	(-)
ΔC_L	Extra lift	(-)
Δz_wake	Wing wake thickness	(m)
$\Delta\epsilon_\mathrm{h}$	Extra downwash	(rad)
γ	Pitch angle (depending on context)	(rad)
γ	Angle between the wing chord plane and the line connecting the trailing edge of the wing root chord and the quarter chord of the horizontal tail mean aerodynamic chord (depending on context)	(rad)
ϵ	Downwash angle	(rad)
η_h	Dynamic pressure ratio at horizontal tail	(-)
$\Lambda_{c/4}$	Quarter chord sweep	(rad)
$\Lambda_{c/2}$	Half chord sweep	(rad)
ζ	Damping ratio	(-)
ρ	Mass density	(kgm^3)
τ	Control surface effectiveness	(-)
ϕ	Bank angle	(rad)
ω	Angular velocity	(rad/s)
ω_n	Undamped natural frequency	(rad/s)

1

INTRODUCTION

The aviation industry has committed to achieving a 75% reduction in carbon dioxide and a 95% reduction in nitrogen oxide emissions by 2050, as outlined in Flightpath 2050 [13]. Consequently, extensive research is underway in the aviation sector to minimize the environmental impact of aircraft [14]. One promising avenue to meet the goals of Flightpath 2050 involves the use of renewable electricity to power aircraft. This has led to the emergence of innovative concepts for electrically driven aircraft, such as the distributed electric propulsion (DEP) aircraft, exemplified by the X-57 Maxwell demonstrator shown in Figure 1.1.

Figure 1.1: X-57 Maxwell demonstrator (NASA image) [1].

The feasibility of DEP aircraft relies on the advantages offered by electric engines, which exhibit a lower weight penalty when scaled down compared to combustion engines [15]. By utilizing electric propulsion and powering the aircraft with green electricity, zero emissions can be achieved during flight, aligning seamlessly with the goals of Flightpath 2050.

In addition to achieving zero-emission flight when powered fully by green electricity, a DEP aircraft provides several advantages over conventional counterparts. The propeller-induced velocity increases lift over

the wing, enabling a reduction in the wing surface area for a given perfromance requirement and maximum lift coefficient. Furthermore, the distributed propulsion spreads the engine weight across the entire wing, reducing maximum stresses during flight [16]. This configuration allows for an increased wing aspect ratio by decreasing the chord length, resulting in lower drag and improved overall aircraft performance [17]. Electric propulsors, compared to combustion engines, offer enhanced efficiency and reduced noise [18, 19]. Moreover, DEP aircraft feature a better take-off and landing performance, enabling lower-speed operations [20].

Another potential advantage of a DEP aircraft is the possible reduction of control surfaces. Active control mechanisms, such as differential thrust, can minimize the need for traditional control surfaces like the vertical tail or rudder [1, 21]. Propeller and aerodynamic surface interaction may further enhance the effectiveness of these control surfaces. Previous studies have shown that control surfaces in the propeller's slipstream are more effective [22]. This reduction in control surfaces could lead to a decrease in aircraft wetted surface area, subsequently reducing drag and overall weight, thereby improving performance and energy efficiency. Thus, the primary objective of this research is to **determine the minimum size of control and stabilizing surfaces for a distributed propulsion aircraft that complies with regulatory and recommended requirements**.

1.1. KNOWLEDGE GAP

Most of the DEP control and stability research has already been done on the vertical tail and rudder reduction, as presented in Section 2.2. Additionally, most of this research was focused on engine inoperative conditions [6, 16, 23] and rudder replacement by differential thrust [1, 21, 24, 25]. Furthermore, only one paper was found on DEP aircraft horizontal tail sizing; Fouda et al. [26] adapted the approach from the conventional tail design due to the smaller wing area of distributed propulsion aircraft. This resulted in a slightly lower tail volume; however, the authors did not take into account the propeller slipstream and horizontal tail aerodynamic interactions. Thus, the approach should be modified for better results.

No literature on aileron or elevator sizing was found for distributed propulsion aircraft. Moreover, the sizing of the control surfaces was not done for all critical flight conditions; the focus was mostly on crosswind landings and one engine inoperative condition. Only a few articles focus on the propeller and control and stability surface interaction. Finally, no research was found that focuses on the additional directional and lateral inertia created by the widely spread propellers, which should affect the stability and control of the aircraft.

Due to extensive research conducted on the vertical tail and rudder, it has been decided to exclude them from this study. The focus will solely be on longitudinal stability and control, as well as lateral control. Furthermore, doing a more in-depth study would require a 6-DOF analysis, which is left out of scope due to time constraints. Additionally, the horizontal tail position will be analyzed to see its optimal position and determine if a T-tail, crucifix, or conventional tail is a better choice for DEP aircraft, as no studies for DEP aircraft tail configurations have been done. Following the research gap identified in the literature, research questions have been made. These are presented in the section below.

1.2. RESEARCH QUESTIONS

Research questions, which should be answered by the end of this research and fill in the knowledge gap discussed in Section 1.1, are listed below:

How does the sizing of longitudinal stability, longitudinal control, and lateral control surfaces of a distributed-propulsion aircraft compare to a twin-propeller aircraft sized for the same mission, with and without accounting for propeller effects?

- What are the critical flight conditions for distributed propulsion aircraft's stability and control surfaces?
- How do the propellers affect the aircraft's control and stability performance?
  - What effect does the propeller slipstream have on the control and stability surfaces of the aircraft?
  - What effect does the different pitch and roll inertia due to distributed propulsors have on the control and stability of the aircraft?
- What is the sensitivity of the horizontal tail and aileron size to key design choices of a DEP aircraft?
  - What is the impact of the vertical position of the horizontal tail?
  - What is the impact of battery placement?

  - What is the impact of reserve fuel placement?

- By how much can the control and stability surfaces be reduced (or increased) compared to the reference twin-propeller aircraft?

  - By how much can the horizontal tail be reduced (or increased)?
  - By how much can the aileron be reduced (or increased)?

1.3. REPORT OUTLINE

To guide the reader, a report structure is presented in this section. First of all, in Chapter 2, background information is presented. This includes the explanation of basic propeller aerodynamics and the effect of propellers on aircraft stability based on literature. Additionally, the state-of-the-art literature on DEP aircraft is also discussed there with the requirements that have to be met for an aircraft. In Chapter 3, the methodology of the work is presented. This includes the presentation of three configurations to be analyzed in this report. Moreover, an overview of the model is given, with an explanation of how different aerodynamic forces and moments are modeled or various aerodynamic effects. In Chapter 4, the verification and validation of the model made is discussed. This includes the verification of the downwash, wing wake, and propeller effects; validation of propeller effects and moment of inertia of the aircraft. Moreover, a sensitivity analysis is performed on calibration coefficients, derived from validation, and ground effect. The results are shown and discussed in Chapter 5. This includes the discussion of propeller effects on stability and control, the final design, and a sensitivity analysis horizontal tail, battery, and fuel placement. Finally, conclusions and recommendations of the work performed are given in Chapter 6.

2

BACKGROUND

This chapter discusses all the relevant background information. Firstly, propeller effects are analyzed to acquaint the reader with the basics of propeller aerodynamics. Following this, a state-of-the-art literature study is presented, used to identify the knowledge gap and formulate the research questions in Chapter 1. Finally, a set of requirements is highlighted for the aircraft design.

2.1. PROPELLER AERODYNAMICS

In this section, the basics of propeller aerodynamics are presented. The main function of a propeller is to create thrust, and in doing so, it often induces significant changes in a vehicle's aerodynamic properties. The effects of a propeller on the forces and moments acting on a vehicle can be classified into two categories: those caused by the direct action of the propeller forces and those caused by the propeller slipstream.

2.1.1. PROPELLER FORCES

The propeller produces forces and moments in all directions, as illustrated in Figure 2.1. The primary goal of the propeller is to generate thrust force, propelling the aircraft forward. As a side effect, torque is generated due to the drag experienced by the blades, resulting in a moment around the center of the propeller.

Normal and side forces result from the varying loading on the propeller blades at an angle of attack (or sideslip for side force). The loading on the propeller changes as the rotating blade shifts position. When the angle of attack increases, the loading on the upward-moving propeller blade decreases, while on the downward-moving blade, it increases due to different local angles of attack. This asymmetric propeller disc loading is responsible for producing the propeller's normal force. However, at a 0° angle of attack, both sides experience the same angle of attack, resulting in uniform loading, and no normal force is generated.

For this study, the normal force caused by the propeller could be interesting to research, as it affects the stability and control of the aircraft. In other research, it has been discovered that normal force can impact the stability of an aircraft [27]. The normal force is generated when there is an angle of attack or sideslip (side force) at the propeller. Moreover, normal forces are also generated in a roll (a change in the angle of attack occurs due to a rolling motion). Thus, the propeller produces normal and side force for the three heading changes (pitch, yaw, and roll), and these forces should be considered for the aircraft's stability and controllability.

2.1.2. PROPELLER SLIPSTREAM

This section discusses important parameters describing the flow caused by a propeller: axial velocity (responsible for the increase in dynamic pressure in the slipstream), swirl velocity, and contraction. These parameters describe the flow contained in the slipstream tube of the propeller, as illustrated in Figure 2.2.

Starting with axial velocity, originating from Newton's Third Law, where thrust is the reaction force of the accelerated airflow. Increasing the axial velocity generated by the propeller disk enhances the thrust force. Although the propeller's thrust axis may not always be parallel to the streamwise direction due to different angles of attack, the axial velocity has only one component in the thrust axis direction, always parallel to thrust. This velocity typically reaches its maximum at about 75% of the propeller radius due to the highest loading occurring at that spot.

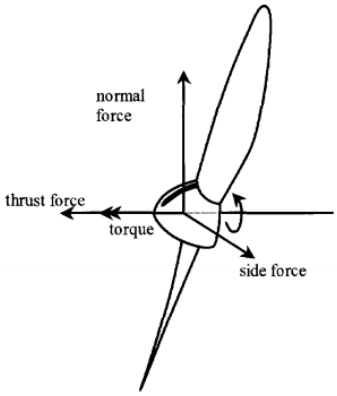

Figure 2.1: The most important forces and moments acting on the propeller [2].

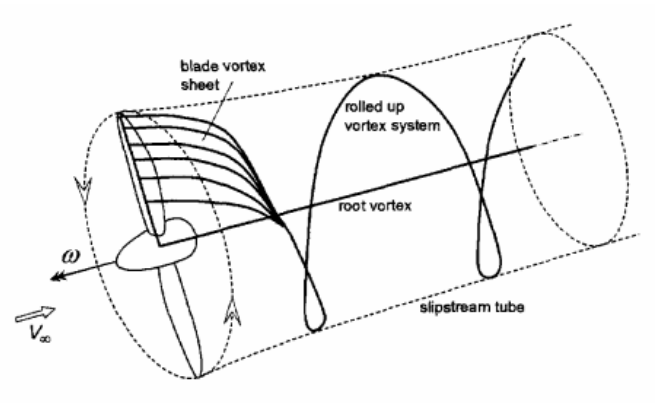

Figure 2.2: Helical vortex system and slipstream tube generated by a propeller [2].

Another velocity induced by propeller interaction is the swirl or tangential velocity. This velocity, resulting from the propeller-produced torque, does not exist before entering the propeller slipstream (unless the flow itself has some vorticity). After passing through the propeller disc, swirl velocity attains a certain value and remains fairly constant (changing slightly due to slipstream contraction as momentum must remain the same) throughout the slipstream in the axial direction. However, in the presence of the wing, this velocity component decreases throughout the wing, a phenomenon known as swirl recovery.

The propeller-induced slipstream reduces in size over the axial distance traveled due to the mass flow conservation of the propeller's increased velocity. Moreover, the nacelle affects the slipstream of the propeller, as seen in Figure 2.3. The slipstream at the nacelle does not contract as fast as the theoretical slipstream; however, after leaving the nacelle, the slipstream experiences a much larger reduction in size.

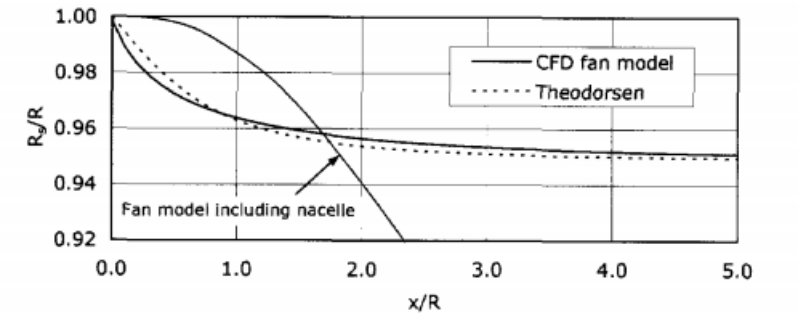

Figure 2.3: Comparison of slipstream contraction ratio calculated with a propeller model [2] and the model of Theodorsen [3].

2.1.3. PROPELLER-WING INTERACTION

When the slipstream of a propeller passes over an aerodynamic surface, it influences its performance. First, the propeller-induced axial velocity increases the flow speed over the wing, resulting in an increase in lift in the propeller slipstream, as shown in Figure 2.4. Second, the tangential velocity changes the local angle of attack at the wing. Since the swirl velocity acts in different directions on the wing depending on the side of the propeller, the local lift is increased on the side of the propeller going upwards and decreased on the side going downwards, as seen in Figure 2.5. Additionally, the increase in dynamic pressure can vary depending on the side of the slipstream due to different blade loadings at different angles of attack.

In general, induced velocity (or an increase in dynamic pressure) can enhance the lifting performance of any surface covered in the slipstream [22]. Therefore, an aileron positioned inside a propeller slipstream will have higher effectiveness [28]. This could allow for a reduction in aileron size or improved roll performance.

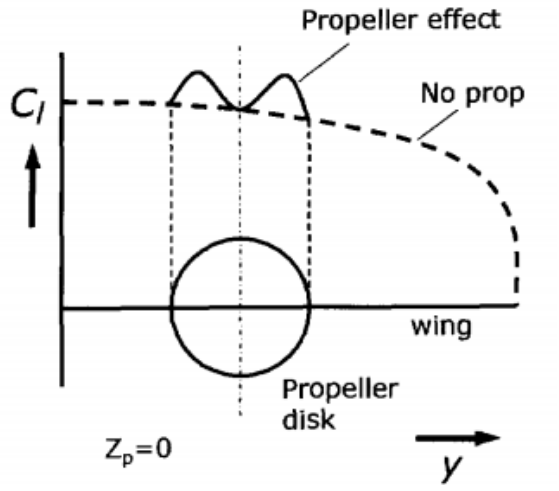

Figure 2.4: Change in local wing lift coefficient due to the axial velocity increase in the slipstream [2].

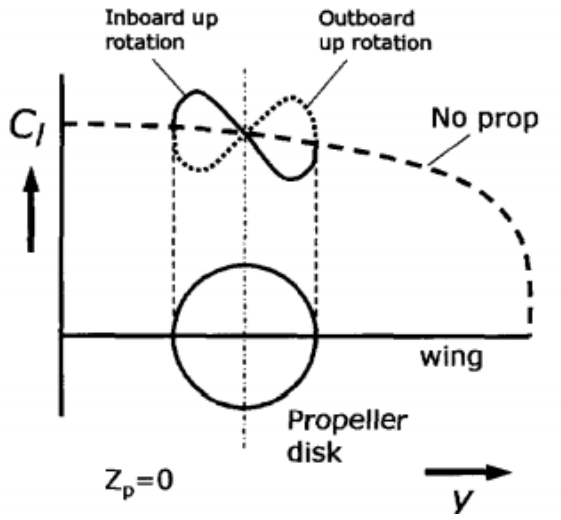

Figure 2.5: Change in local wing lift coefficient due to the swirl velocity increase in the slipstream [2].

2.1.4. PROPELLER EFFECT ON LONGITUDINAL STABILITY

The primary stability surface responsible for the conventional aircraft's longitudinal stability is the horizontal tail. Additionally, the horizontal tail allows for aircraft trimming. Key considerations in the design of the horizontal tail include the downwash caused by the wing and the change in dynamic pressure due to the wake of the wing or the propeller slipstream [4]. It should be noted that the slipstream follows the downwash created [29]. Propeller aircraft could potentially compensate for wing wake by having increased dynamic pressure at the wake due to the slipstream.

In addition to the slipstream following the downwash, propellers can increase the downwash angle. A study by Bouquet and Vos [9] showed that an increase in downwash due to the propellers provides better take-off performance, as more negative lift is produced by the tail. However, the study stated that for other flight conditions, tail effectiveness decreases due to higher downwash, especially for low-tail configurations. The effectiveness of such configurations drops further, even besides the higher dynamic pressure due to the propeller slipstream. A study by Shuai et al. [30] obtained similar results, noting that the propeller slipstream-induced reduction in the horizontal tail's efficacy is the primary cause of longitudinal stability degradation. However, the downwash angle at the horizontal tail dropped as the angle of attack grew for counter-rotating and inboard-up propellers, contradicting previous findings. In general, Shuai et al. [30] state that the dynamic pressure increase in the slipstream does improve the performance of the horizontal tail. However, the location of the slipstream depends on the angle of attack, flap deflection, and power setting [31]. Both authors agree that accounting for propeller effects is crucial for stability, even in preliminary design phases.

Finally, the increase in dynamic pressure on the wing affects the stability of the aircraft. One study by Bouquet [32] investigates the effects of the propeller slipstream on the stability and control of aircraft. The author notes that the tail-off pitching moment becomes more negative due to the propeller slipstream going over the wing. However, this effect changes with power settings, adding complexity to the aircraft's trimming.

2.1.5. PROPELLER EFFECT ON DIRECTIONAL STABILITY

The primary stability surface responsible for the conventional aircraft's directional stability is the vertical tail. One key condition in vertical tail design is the one-engine-inoperative (OEI) condition. A study focused on the vertical tail by Schroijen et al. [33] showed that during the one-engine-inoperative condition, the propeller slipstream has a significant impact on the vertical tail's performance. A distinct increase in the yawing moment due to propeller slipstream interaction was observed during this study. The increased side force on the fin, caused by the asymmetrical lift distribution over the wing or flap due to the propeller slipstream, was the most likely reason for this rise in the yawing moment. By creating a side wash at the location of the fin, the asymmetric wing trailing vortex sheet increases the fin's input to the yawing moment. Thus, during the one-engine-inoperative condition, the behavior of the vertical tail of a propeller aircraft changes drastically. Similar results were obtained by Keller and Rudnik [34]. Under the OEI condition, the author obtained results that showed a significant increase in directional stability. The generated yawing moment increased by 130%

due to the asymmetric flow-induced sidewash at the vertical tail. Besides the asymmetric flow, the vertical tail can benefit from the increase in dynamic pressure when being inside the propeller slipstream, as stated by Soikkeli [35].

Another study focused on the vertical tail by van Wonderen [29] showed that the configuration of the aircraft has a significant impact on how the propeller slipstream affects the aircraft, with the wing position and propeller position having the greatest impact. The author also states that due to the crossflow caused by the propeller slipstream, the vertical tail effectiveness increases. Additionally, a side force is generated in the case of asymmetric thrust conditions. Furthermore, it was observed that for a high-wing configuration under a positive sideslip, the effectiveness of the vertical tail decreases due to the circulation created by the asymmetric lift distribution, as seen in Figure 2.6. However, an increase in tail effectiveness was observed for the low-wing configuration. Finally, the author states that the side force produced by the vertical tail at a sideslip angle under the influence of the propeller slipstream rises by 5% to 7% when considering the entire aircraft configuration. Also, the rotation direction of the propellers has a significant impact on the yawing moment coefficient. Moreover, the yawing moment will be considerably higher if the critical engine fails, primarily due to the increased crossflow over the fuselage and vertical tail, agreeing with other studies.

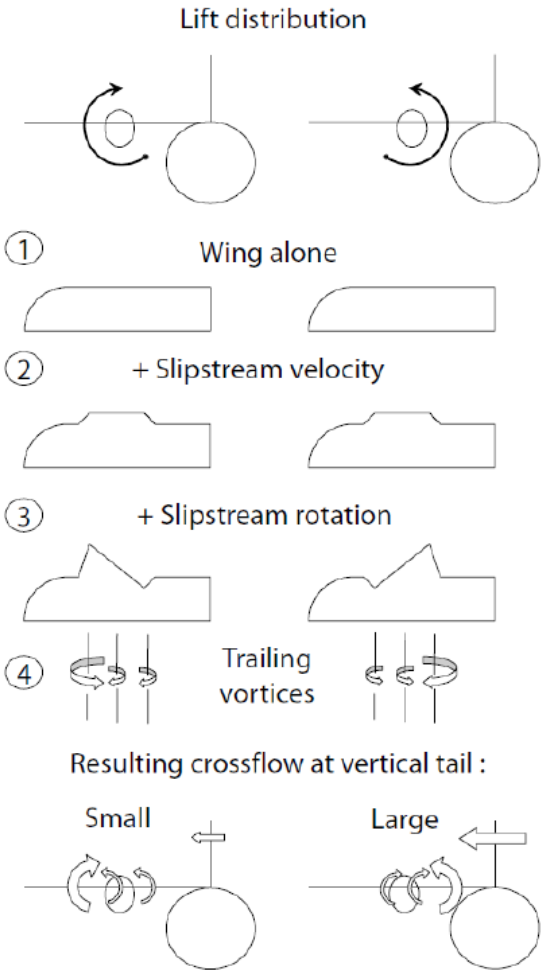

Figure 2.6: Illustration of the asymmetric lift spanwise lift distribution for an outboard up and inboard up rotating propeller and the effect on the vertical tail [4].

2.2. DISTRIBUTED PROPULSION AIRCRAFT STABILITY AND CONTROL

Much research is being conducted on the distributed electric propulsion concept [1, 19]. This research mainly focuses on flight performance; however, there is also research on stability and control [21, 28]. Some of the research has obtained non-beneficial results for DEP aircraft. For instance, Kim et al. [36] obtained results

that showed distributed propellers deteriorate the longitudinal and directional stability of an aircraft due to the normal and side force produced, which is also the case for conventional propeller aircraft [9]. However, it should be noted that the aircraft analyzed was still stable. Thus, these effects allow the design of a stable and controllable DEP aircraft; nonetheless, they should be accounted for.

Another part of the research has been primarily focused on the reduction of the vertical tail [5, 16] and rudder through differential thrust [24, 25]. Moreover, the majority of this research has been focused on specific flight conditions, like one engine inoperative (OEI), while neglecting other possible critical conditions during a flight.

2.2.1. RUDDER REDUCTION THROUGH DIFFERENTIAL THRUST

Distributed electric propulsion aircraft can derive significant benefits from employing differential thrust. The larger moment arms of the propellers and shorter response times (electrical engines) enable these propulsors to be effectively utilized for controlling and stabilizing the aircraft [1, 21]. By adjusting the thrust on each side differentially, a yawing moment is generated, a concept known as differential thrust. While conventional aircraft (turbo-fan) have employed differential thrust during emergencies [21], electric engines allow its use during regular flight conditions.

The use of differential thrust enables directional control, potentially allowing for the removal or reduction of the rudder. State-of-the-art studies have demonstrated the possibility of entirely replacing the rudder for aircraft control. Freeman and Klunk [24] developed a linear time-invariant state-space model, showing that equivalent controllability can be achieved with differential thrust compared to maneuvers performed by the rudder. Similar results were obtained by Kou et al. [25], who developed a differential thrust yaw controller demonstrating comparable controllability to a rudder-based yaw controller. The possibility of eliminating the rudder through the use of differential thrust was also explored by Hoogreef and Soikkeli [5, 35] in a simulated one-engine-inoperative condition. However, the authors emphasized that such conditions lead to a drastic reduction in lift due to failed propulsors, as depicted in Figure 2.7. This induces a rolling moment and a decrease in altitude. Moreover, the reduction in available thrust due to differential thrust may limit climb or acceleration.

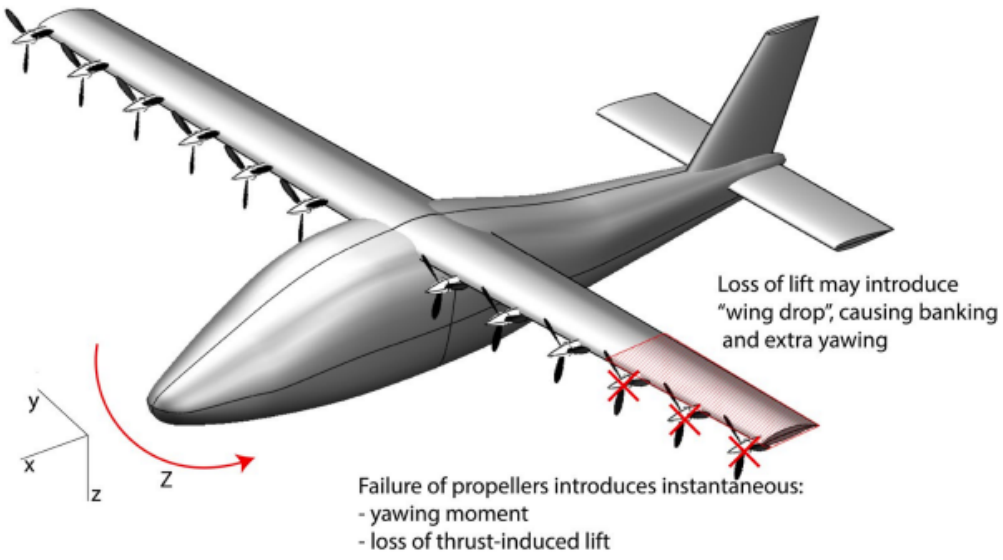

Figure 2.7: Illustration of effects induced by engine inoperative conditions [5].

A critical consideration in differential thrust operation is the rolling moment generated due to asymmetric lift, which influences Dutch roll performance. Pfeifle et al. [37] determined that strong Dutch roll damping can be achieved, providing yaw and roll control through differential thrust. However, these studies [5, 35, 37] highlight the need for a 6-degrees-of-freedom (6-DOF) analysis or experimental analysis, as yaw control through differential thrust is highly coupled to roll motion.

2.2.2. VERTICAL TAIL REDUCTION

Several studies have focused on reducing the size of the vertical tail. This is possible because considering a one-engine-inoperative condition in a DEP aircraft results in a smaller thrust asymmetry. In the event of engine failure, the remaining engine(s) must provide sufficient thrust for a certain climb performance, leading to oversized engines and consequently, a larger vertical tail and rudder surface to balance the increased moment.

Ameyugo et al. [16] estimated a potential 90% reduction in fin size when considering a one-engine-inoperative condition. However, the authors noted that even with such a significant reduction, differential thrust should be used to maintain the aircraft's stability and controllability. They emphasized that current regulations do not permit such reductions, as the aircraft must remain stable and controllable even without fuel or energy. Additionally, Biser et al. [6] demonstrated a vertical tail reduction of 32% and 45% for 6-engine and 12-engine aircraft, respectively. However, this reduction led to poorer Dutch roll performance, reaching level 2 handling qualities, which is insufficient for commercial aircraft, as shown in Figure 2.8. The authors argued that handling qualities could be improved by utilizing a controller-augmented flight control system. Furthermore, they suggested that even in emergencies, level 2 handling qualities would be acceptable.

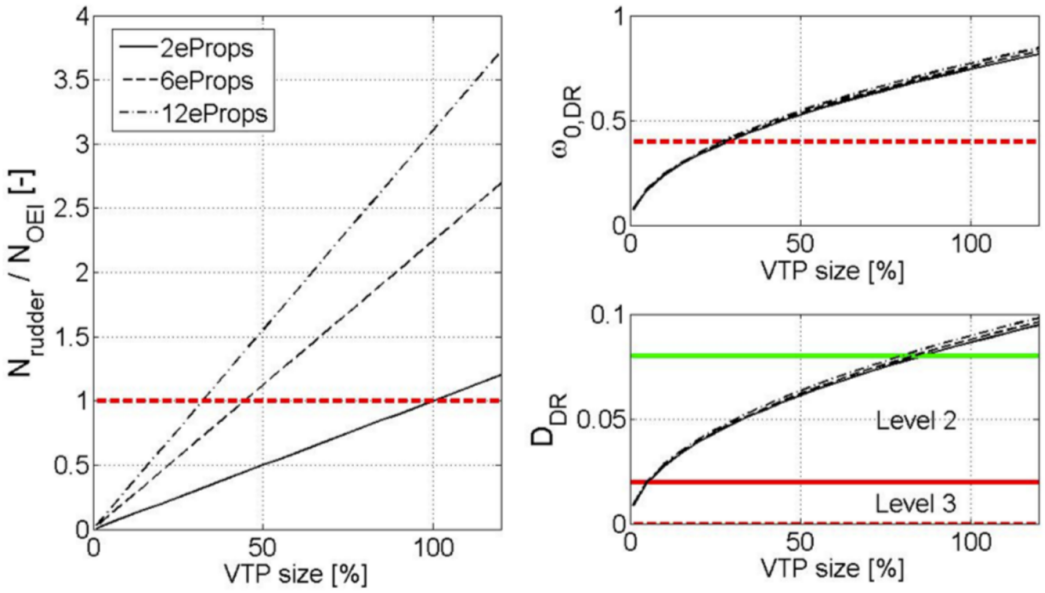

Figure 2.8: OEI and Dutch roll characteristics for variation of the vertical tail size [6].

Nguyen Van et al. [28] conducted a comprehensive study on the stability and control of DEP aircraft, considering various critical conditions. They concluded that differential thrust is most compromised at high velocities, being inversely proportional to velocity, while vertical tail effectiveness increases quadratically with velocity [28]. The critical flight phases identified were take-off, best climb, and final landing due to low or high power. The authors affirmed that the rudder can be replaced by differential thrust and that DEP aircraft are most advantageous for neutral directional static stability, potentially achieving a 45% reduction in vertical tail size. In another study, Nguyen Van et al. [23] used the ATR72 as a base aircraft to assess potential stability and control surface reduction. However, they explained that the vertical tail could not be reduced due to the important level arm of engines located at the wing tip. Nonetheless, at low speeds, differential thrust could control the aircraft, with control diminishing at higher speeds where control and stability surface effectiveness increase while differential thrust effectiveness decreases, as observed in previous research [23]. The authors suggested that the vertical tail should be reduced to allow for better differential thrust control. Lastly, Nguyen Van et al. [38] developed an aircraft model to analyze vertical tail and rudder reduction. The authors estimated a 60% reduction in vertical tail size for this model, emphasizing the need for future research to analyze the full flight envelope and estimate the fin size reduction.

As the DEP aircraft concept is emerging, there is ambiguity in its certification. Conventional requirements may lead to an under- or over-constrained DEP aircraft design. Klunk et al. [21] analyzed FAR Part 25 requirements and, taking these requirements into account, sized the vertical tail considering the Boeing 737-800 as a reference. Additionally, the authors argued that for a distributed propulsion system, different conditions than

one engine inoperative should be considered. Thus, one side inoperable (OSI) and two propulsors inoperable (TPI) were introduced for the vertical tail sizing of the DEP aircraft. Nevertheless, for both conditions, significant vertical tail area reductions were achieved when compared to a conventional Boeing 737-800. While a vertical tail reduction was still achieved, it is crucial to apply relevant requirements for a DEP aircraft, as Klunk et al. did.

2.3. REQUIREMENTS

This chapter presents the relevant stability and control requirements. Firstly, the pertinent requirements from CS-25 are discussed. Subsequently, recommended requirements are presented, which, although not mandatory, are considered beneficial. Additionally, other potential requirements for a distributed electric propulsion aircraft are examined. Given that DEP aircraft represent a novel concept, this examination primarily involves an analysis of state-of-the-art literature to incorporate suggestions from various authors regarding DEP aircraft requirements. Finally, a list of requirements to be addressed in this study is outlined.

2.3.1. CS-25 REQUIREMENTS

The analysis of CS-25 was conducted to identify the applicable requirements for stability and control surface sizing. These requirements were selected from the sections on controllability and maneuverability, trim, stability, ground handling characteristics, miscellaneous flight requirements, and control systems in CS-25. The relevant requirements can be found in Appendix A. It's important to mention that stick forces and stick force gradients are beyond the scope of the preliminary design in this study. Additionally, it should be noted that CS-25 provides an acceptable method for demonstrating compliance with roll capability, covering a bank angle range from -30° to 30° within 11 seconds. However, in this thesis, the ailerons will be designed for requirements set for good aircraft handling presented in the next section.

2.3.2. REQUIREMENTS FROM LITERATURE

Control and stability reference requirements were gathered from Sadraey [10]. The list of these requirements is presented in Table 2.1. The aircraft under consideration were assumed to be Class II and Class III (a more detailed overview of the aircraft is presented in Chapter 3) with a Category B flight phase. Level 1 handling qualities were assumed, requiring the least effort from the pilot. It should be noted that some of the listed requirements will not be verified, as they are outside the scope of this study. The final requirements addressed by this study are presented in Section 2.3.3.

Table 2.1: Requirements from Sadraey [10].

Requirement	Value
Rotation time during take-off	3-5 s
Take-off pitch angular acceleration	4-6°/s^2
The damping ratio of the phugoid mode	≥0.04
Short period damping ratio	0.3-2.0
Time to achieve a 45° bank angle[1]	1.9 s
Time to achieve a 30° bank angle[2]	2 s
Crosswind speed	30 knots
Time to double amplitude in spiral mode	≤20 s
Dutch roll damping ratio	≥0.08
Dutch roll frequency	≥0.4 rad/s
Dutch roll damping ratio times frequency	≥0.15 rad/s

CS-25 requirements state that the aircraft must be stable and controllable during all flight phases. However, during take-off, there is a brief period where total power loss would result in catastrophic consequences, as the aircraft cannot return to the runway or maneuver to a safe landing [39]. On the other hand, the duration of this window is very short, so it can be neglected [39]. Additionally, the risk can be mitigated by including system redundancy, but this is outside the scope of this study (total loss of power is unacceptable in the aerospace industry, especially for CS-25 aircraft; via good systems engineering and safety assessment practices, this can be overcome).

Another potential failure is flight control. All-electric aircraft require an electronic system for flight control [39], which has a possibility of failure. The design of such control systems is beyond the scope of this

study; however, the aircraft should be stable even without these control systems [39]. This is because the certification of such systems is costly [39] (when considering an unstable aircraft), as the failure of such systems would result in an unstable aircraft.

2.3.3. FINAL REQUIREMENTS

The final requirements for three configurations (as presented in Chapter 3) are listed in Table 2.2. These requirements were compiled from CS-25 [40], Sadraey [10], and Garrett T. Klunk et al. [21]. The resulting list is presented in Table 2.2. Requirements highlighted in green are mandatory (coming from regulations), those in yellow are recommended, and requirements in red are considered out of scope due to limitations preventing their verification in this study. It is essential to note that the verification of red-highlighted requirements would necessitate a 6-DOF model (or a real-life model), which was not developed in this study due to time constraints. Moreover, the recomendatory roll requirement will be used instead of the one from CS-25. The recommendatory one is more critical than the one in CS-25 (achieving the recommended one will also comply with CS-25) and this will also allow the pilots to have better handling qualities of the aircraft. The short period and phugoid requirements are in yellow, as the values are recommended for achieving Level 1 handling qualities. Conversely, the first requirement states that the aircraft must be stable, making the short period and phugoid requirements mandatory for minimum stability (positive damping). The recommended values aim to enhance aircraft handling. Each applicable requirement will be tested for every critical flight condition.

Table 2.2: Final requirements for control and stability surface sizing (green: hard requirement, yellow: recommended requirement, red: out of scope).

Requirement	Value	Source
Static longitudinal stability (C_{m_α})	<0	-
Dynamic longitudinal stability (C_{m_q})	<0	[10]
Time to achieve a 60° bank angle	11 s	[40]
Rotation time during take-off	3-5 s	[10]
Take-off pitch angular acceleration	4-6°/s^2	[10]
Time to achieve a 45° bank angle [1]	1.9 s	[10]
Time to achieve a 30° bank angle [2]	2 s	[10]
Short period damping ratio	0.3-2.0	[10]
Damping ratio of phugoid mode	≥0.04	[10]
Static directional stability (C_{n_β})	>0	-
Dynamic directional stability (C_{n_r})	<0	[10]
Static lateral stability (C_{l_β})	<0	-
Banked turn against inoperable engine(s)	≥20°	[40]
Heading change against inoperable engine(s)	≥15°	[40]
Bank angle at minimum control speed with inoperable engine(s)	<5°	[40]
Crosswind speed	25 knots	[40]
Crosswind speed	30 knots	[10]
Time to double amplitude in spiral mode	≤20 s	[10]
Dutch roll damping ratio	≥0.08	[10]
Dutch roll frequency	≥0.4 rad/s	[10]
Dutch roll damping ratio times frequency	≥0.15 rad/s	[10]

[1] For aircraft up to 30 tons.
[2] For aircraft above 30 tons.

3

METHODOLOGY

This chapter presents the methodology employed in the study. It includes the presentation of three aircraft configurations to be analyzed, an explanation of the model, and techniques for estimating propeller effects, moments of inertia, and aerodynamic parameters. This serves to elucidate the working principles of the model, their strengths, and their limitations. Finally, each of the aircraft maneuvers is addressed and its implementation in the model is explained.

3.1. CONFIGURATIONS

In this section, three different aircraft configurations are discussed. These configurations will be used in the study to size the aircraft's stability and control surfaces and observe the effects of different configurations. It should be noted that the configurations are designed for the same mission, thus, the specifications and geometries differ for the twin turboprop and DEP aircraft, besides the number and size of engines. Sizing the configurations for the same mission is done, as to provide the best comparison for a real-life application of a DEP aircraft. Moreover, the selection of these configurations aims to achieve two objectives: understanding the stability and control of a distributed electric propulsion aircraft and assessing the general contribution of propeller effects to the stability and control of an aircraft.

An overview of the main parameters of the aircraft is provided in Table 3.1. As the DEP aircraft is designed for the same mission (same payload and range), the aircraft's weight is much higher due to the heavy batteries. Because of this the wing area is larger for the DEP aircraft. On the other hand, the fuselage is relatively shorter due to the consistent payload.

Table 3.1: Main aircraft parameters for configurations.

Full name	Configuration 1	Configuration 2	Configuration 3
Short version	Config 1	Config 2	Config 3
Number of propellers (-)	2		8
Battery placement	-		Wing
Fuel placement	Wing		Fuselage
MTOW (kg)	28100		75989
Wing area (m^2)	64.43		148.1
Wing span (m)	27.7		42
Fuselage length (m)	30.37		33.73
Fuselage diameter (m)	3.38		2.84

The primary goal of this study is to determine the optimal design of the horizontal tail size and aileron size. This is achieved by finding the minimal size for different wing positions and sizing the ailerons for the optimal wing position and horizontal tail size. The minimal size is found by analyzing all the different flight conditions to determine the limiting case. These flight conditions are presented in Table 3.2.

Table 3.2: Different flight conditions for the configurations and their specifications (thrust coefficient per propeller).

Flight condition	Configuration 1 and 2		Configuration 3		Flap deflection (deg)
	V_∞ (m/s)	T_c/n (-)	V_∞ (m/s)	T_c/n (-)	
Stall	54	0	57.4	0	30
Rotation	59.2	0.184	65.7	0.044	15
Approach	74.6	0	74.6	0	20
Cruise	181.9	0.015	185.8	0.003	0
Dive	227.4	0.010	232.3	0.002	0
Climb	86.8	0.091	89.6	0.019	0
Top climb	172.6	0.019	173.9	0.005	0
Landing	74.6	0.035	74.6	0.008	20
Stall (with thrust)	54	0.127	57.4	0.032	30

3.1.1. CONFIGURATION 1: TWIN TURBOPROP WITHOUT PROPELLER INTERACTION EFFECTS

Figure 3.1 and Figure 3.2 presents the first aircraft configuration. It shares the same specifications and geometries as Configuration 2; however, it does not feature any propeller effects (besides the thrust force). The mass of engines will be accounted for, but there will be no propeller effects—only thrust vectors. The control and stability surface design will be done using conventional design methods, as these are suitable for such configurations. Configuration 1 is chosen as it provides a base case for which no modification in design methods is needed.

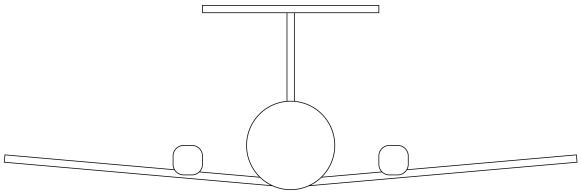

Figure 3.1: Front view of Configuration 1.

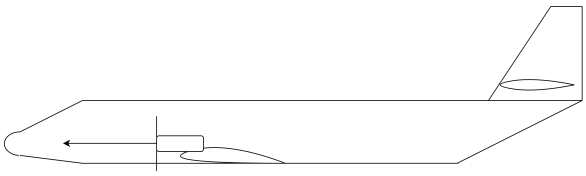

Figure 3.2: Side view of Configuration 1.

3.1.2. CONFIGURATION 2: TWIN TURBOPROP WITH PROPELLER INTERACTION EFFECTS

Configuration 2, visualized in Figure 3.3 and Figure 3.4, maintains the same specifications and geometries as Configuration 1 but includes propeller interaction effects. These propellers will affect the wing's and horizontal tail's performance and produce normal force. All of these effects will be considered in the design process. Configurations 1 and 2 will be compared to observe the propeller effect on the design of stability and control surface size. Thus, Configuration 2 achieves two goals: it enables the validation of the implemented design updates by comparing them to real-life aircraft or wind tunnel test data, and it provides a more realistic base case—an aircraft with twin engines.

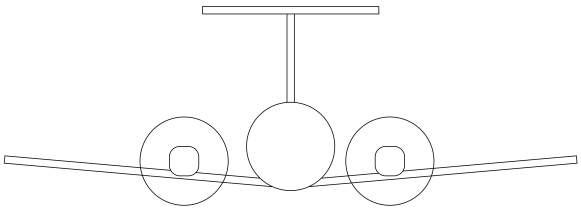

Figure 3.3: Front view of Configuration 2.

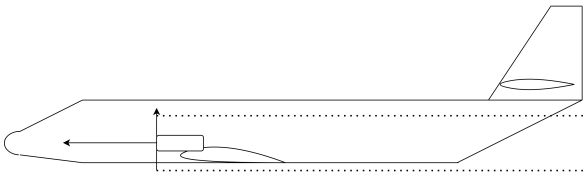

Figure 3.4: Side view of Configuration 2.

3.1.3. CONFIGURATION 3: DISTRIBUTED ENGINES WITH PROPELLER INTERACTION EFFECTS

Finally, Figure 3.5 and Figure 3.6 present the last configuration. Configuration 3 features distributed electric propellers (four on each side) and a different aircraft geometry due to heavy batteries placed in the wing. To account for this, all results will be normalized. The same methodology used for sizing the twin-engine aircraft will be applied. Due to smaller propellers and a larger number of them, different results should be obtained.

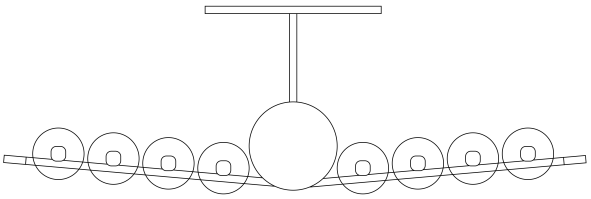

Figure 3.5: Front view of Configuration 3.

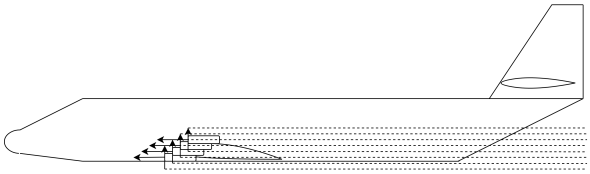

Figure 3.6: Side view of Configuration 3.

Moreover, besides the different slipstream properties, the aircraft will feature a different mass moment of inertia distribution (the heavy batteries are placed in the wing and propellers are distributed), which will be accounted for in this study. Additionally, the aircraft also features folding wing tips, which will limit the outer aileron position. The aircraft also has a small fuel tank in the back of the fuselage, which will affect the center of gravity range. A sensitivity analysis of the battery distribution in the wing and reserve fuel tank location is presented in Section 5.3. Finally, a top view of the aircraft is presented in Figure 3.7, to visualize the different components featured in the aircraft. A more detailed overview of the geometry of the aircraft can be found in de Vries' work [41].

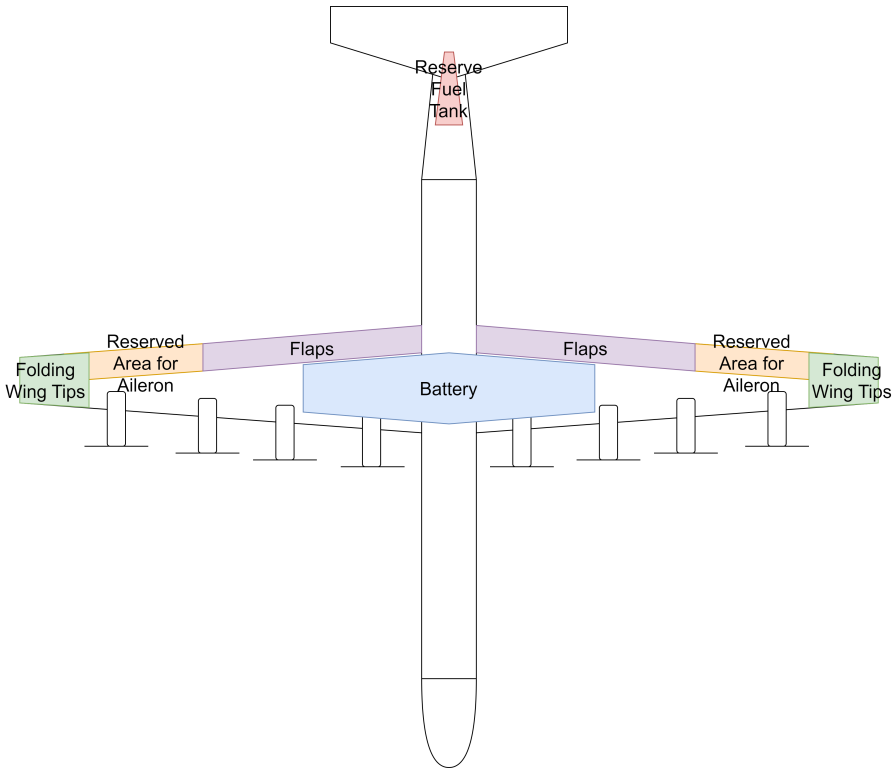

Figure 3.7: Top view of Configuration 3.

3.2. MODEL

Based on the requirements set in Chapter 2, the aircraft has to be designed for sufficient stability, rotation performance, and roll performance. Additionally, the aircraft should be capable of trimming during all flight phases. To estimate the aircraft's performance for each of the flight criteria, a code was constructed in Python 3.10.9. The developed program is considered to be in the low/mid-fidelity range; thus, some assumptions were made and presented later in this section. This was done so that it would be possible to find the optimal aircraft's stability and control surface size in a reasonable amount of time and effort. Moreover, in the current design phase of Configuration 3, high accuracy of results is not needed. Finally, the program structure and the sizing process are also presented later.

3.2.1. ASSUMPTIONS

Designing the control and stability surfaces of an aircraft is a complex process. Thus, to achieve some preliminary results at the early stage of the design, assumptions have to be made. These help simplify the problem while still maintaining a sufficient level of accuracy. Below are all the assumptions, along with their reasoning for the code and general methodology:

- Swirl velocity contribution to the lifting surfaces will be neglected. Zhao [30] in his study mentioned that downwash and propeller slipstream are key in estimating the horizontal tail performance. The downwash is accounted for in this study, while only the increase in dynamic pressure is included from the propeller slipstream. On the other hand, this is the most influencing effect [2].
- For rolling motion, the effect of propellers on the horizontal and vertical tail is neglected. The methodology used does not allow for the estimation of propeller effects at the tail in a rolling motion. However, the contribution of the tail to the damping is minimal (Figure 3.8); thus, these effects can be neglected.
- No stall flow separation at the wing is modelled.
- The battery and the fuel tank are assumed to have a uniform density.
- The propeller parameters were not provided; thus, the most fitting ones were selected.
- The elevator size is tied to the horizontal tail; thus, while the elevator is not explicitly sized, changing the horizontal tail size also changes the elevator size. This is done to lower the design variables for the sizing process. The elevator covers the full-span of the horizontal tail and is 30% chord length of the horizontal tail.
- For multiple propellers placed on the wing, the propeller induced dowwnash at the horizontal tail is assumed to be equal to the average of each propeller's separate contribution.
- Propellers and fuselage fuel tanks (in the aft of the fuselage) are modeled as point masses for mass moment of inertia calculation.
- The payload is assumed to be uniformly loaded on the aircraft. The uniform loading of the payload (the "potatoes" in the loading diagram) is relevant for landing gear positioning, which is not done in this report.
- The horizontal tail center of gravity and mass are assumed to be constant; thus, they remain constant with a changing horizontal tail size.
- Rolling moment due to sideslip is not included.
- Aircraft roll control is provided only through ailerons (no spoilers or other control surfaces).

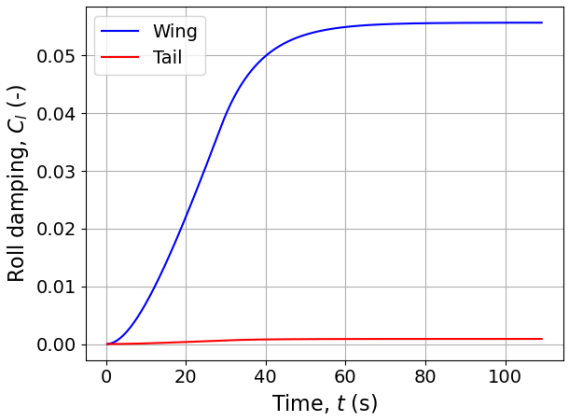

Figure 3.8: Wing and tail damping during roll maneuver.

3.2.2. PROGRAM STRUCTURE

The program structure for estimating aerodynamic surface forces is shown in Figure 3.9. This module is placed inside the aircraft class as a function, which calls other smaller functions (modules). This module is represented as "Aero" and "Output". The explanation of each module is presented below:

- **Aero** - responsible for distributing the inputs to other functions and estimating simple inputs like lift curve slopes.
- **Output** - takes all the outputs from different modules and turns them into lift coefficients; this is mainly used for the horizontal tail, where different angles are summed to get the local angle of attack and dynamic pressures are summed to get the local dynamic pressure.
- **Induced area** – gets the slipstream geometry: the induced wingspan, the slipstream path after the wing, etc.
- **Flap lift** – gets extra lift due to flap.
- **Wing lift** – gets the final lift of the wing and propeller. This includes the effect of the flap and propeller. Also, it outputs the wing moment coefficient, taking into account the flap and the slipstream.
- **Downwash** – gets the downwash of the wing.
- **Dynamic pressure** – gets the dynamic pressure ratio at the horizontal tail due to wing wake.
- **Propeller downwash** – gets extra downwash due to propellers.
- **Propeller dynamic pressure** – gets the extra dynamic pressure due to the propeller slipstream at the horizontal tail.

Geometry, α, T_c, M, δ_f, δ_e									
Aero	Geometry, α, T_c	Geometry, $C_{L\alpha}$, δ_f	Geometry, $C_{L\alpha}$, α, T_c, $C_{L,prop\ off}$	Geometry, α	Geometry, α	Geometry, T_c	Geometry, α, T_c	Geometry, α, C_{Lah}	
	Induced Area		Slipstream geometry				Slipstream geometry		
		Flap Lift	ΔC_L						
			Wing Lift	C_{Lw}	C_{Lw}			C_{Lw}, C_{Lp}, C_{mw}	
				Down-wash		ε_h	ε_h	ε_h	
					Dynamic Pressure			Dynamic pressure ratio	
						Propeller Down-wash	$\Delta\varepsilon_h$	$\Delta\varepsilon_h$	
							Propeller Dynamic Pressure	Dynamic pressure ratio	
								Output	C_{Lw}, C_{Lp}, C_{Lh}, C_{mw}

Figure 3.9: N2 chart for calculating lift components of the aircraft.

3.2.3. TAIL SIZING

To ensure a fair comparison of all three configurations, it is crucial to design them for optimal performance. The key parameter to consider is the horizontal tail size and wing location. While reducing the aileron or elevator size may not result in significant mass savings compared to the horizontal tail (as the removed aileron or elevator surface would be compensated by the wing), the horizontal tail is notably influenced by the wing position. Therefore, to determine the optimal horizontal tail size, variations in the wing position will be explored.

The elevator spanwise and chordwise positions will be kept constant, and the aileron will be sized in the final step, as it does not impact the wing position. In the trim and stability modules, various flight conditions and wing positions will be inputted. For rotation, only different wing positions will be considered, with only one flight condition for this maneuver. Different horizontal tail sizes corresponding to different wing positions will be obtained, with the largest size serving as the limiting factor.

Among all the different wing positions, the smallest limiting horizontal tail size will be selected to achieve the optimal wing and horizontal tail positioning and sizing, respectively. Following this, the sizing for ailerons will be carried out, as illustrated in Figure 3.10, summarizing the tail sizing process.

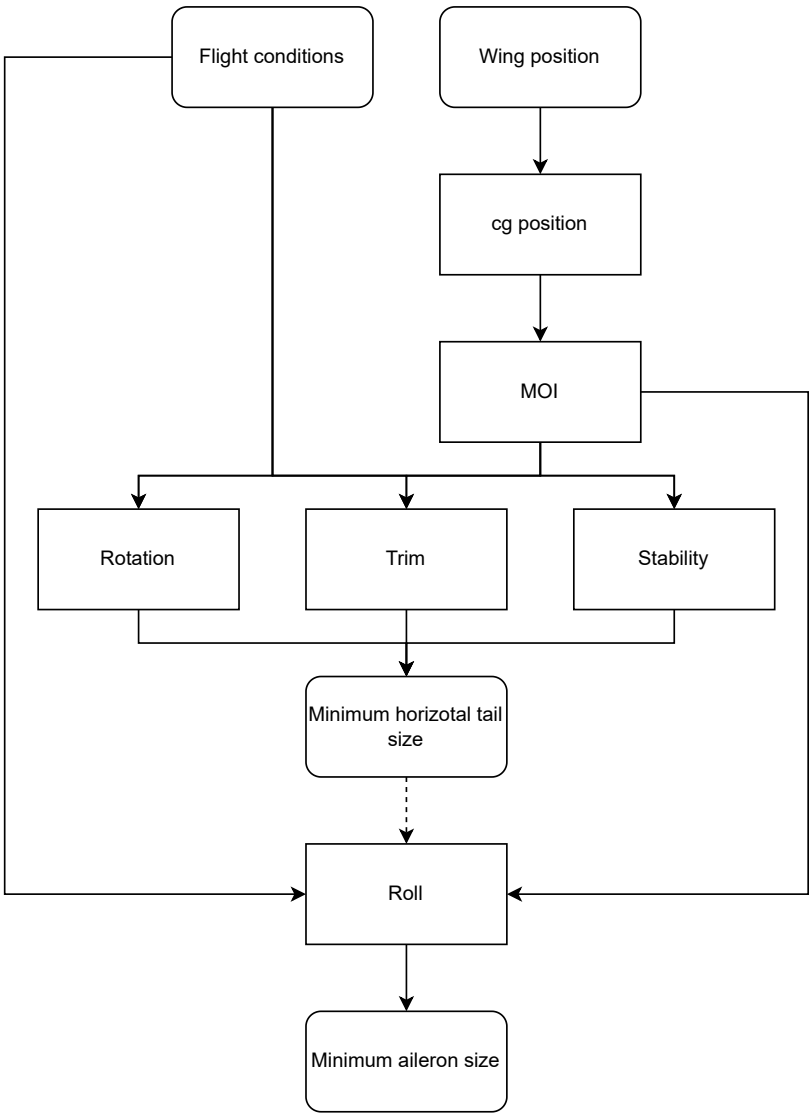

Figure 3.10: Horizontal tail and aileron sizing for a given wing position.

3.3. MOMENT OF INERTIA

In this research, pitching and rolling motions will be analyzed in time and space. Thus, to find the acceleration of the motion, the moment of inertia of the aircraft should be known. This can be predicted with the equations from Raymer [11]. For the roll axis, Equation 3.1, and for the pitch axis, Equation 3.2 can be used. In Table 3.3, common radii of gyration values are given.

$$I_{xx} = \frac{b^2 m \bar{R}_x^2}{4} \tag{3.1}$$

$$I_{yy} = \frac{l_{fus}^2 m \bar{R}_y^2}{4} \tag{3.2}$$

Table 3.3: Nondimensional radii of gyration [11].

Aircraft	$\bar{R}_x$	$\bar{R}_y$
Single-engine prop	0.25	0.38
Twin-engine prop	0.34	0.29
Twin turboprop transport	0.22	0.34
Jet transport: fuselage-mounted engines	0.24	0.36
2 wing-mounted engines	0.25	0.38
4 wing-mounted engines	0.31	0.33

The reference aircraft is a twin turboprop transport aircraft; thus, radii of gyration for this type will be used. Of course, a DEP aircraft will feature different systems, which will have different mass distributions. The key difference is the absence of fuel in the wings, the battery, which could be in the fuselage or the wing, and the distributed propellers. The methods to account for these differences and get an approximate moment of inertia are presented in the following sub-sections. The reference moment of inertia will be estimated with Equations 3.1 and 3.2. From these reference values, the fuel and twin propeller contributions will be subtracted, and the distributed propulsion and battery system contributions will be added to get the new moment of inertia.

3.3.1. FUEL

A wing fuel tank has a complex shape for which to estimate the moment of inertia. A general equation should be used - Equation 3.3. However, the approach can be simplified by discretization. The fuel tank is split into many spanwise sections, as seen in Figure 3.11. The shapes are still similar to the fuel tank; however, with a much denser discretization, the shapes can be assumed to be equal to rectangles. Then the formula for a rectangle can be used (Equation 3.4 and Equation 3.5), which accounts for the shape and distance from the reference point (center of gravity of the aircraft)

$$I = \int \rho r^2 dV \tag{3.3}$$

$$I_{xx} = \rho wch \cdot (w^2 + h^2) + \rho wch \cdot (\Delta y)^2 \tag{3.4}$$

$$I_{yy} = \rho wch \cdot (c^2 + h^2) + \rho wch \cdot (\Delta x)^2 \tag{3.5}$$

The fuel tanks are assumed to be placed from 10% to 70% of the half span. These values are taken from the ATR 72 fuel tank layout [42]. This aircraft is similar to the aircraft in question. Moreover, it is assumed that the tank is placed between the spars, which are located at 15% and 60% of the chord. Finally, the average height of the fuel tank is estimated by interpolating the surface area of the tank (xz plane), where root and tip surface areas are inputs. These surface areas are easily obtained by finding the integrated area of the top and bottom surfaces bounded by spars. The area varies linearly throughout the wingspan.

For Configuration 3, there is also a fuel tank in the back of the aircraft. However, it is a reserve fuel, and its weight is low. As the distance to the center of gravity is high, it will be assumed to be a point mass.

3.3.2. BATTERY

For a battery placed inside the wing (Configuration 3), the same approach as for the fuel tank in the wing is used. While the battery cannot be as effectively stored as fuel in the wing, the estimation tool will provide an estimate of the battery's moment of inertia inside the wing.

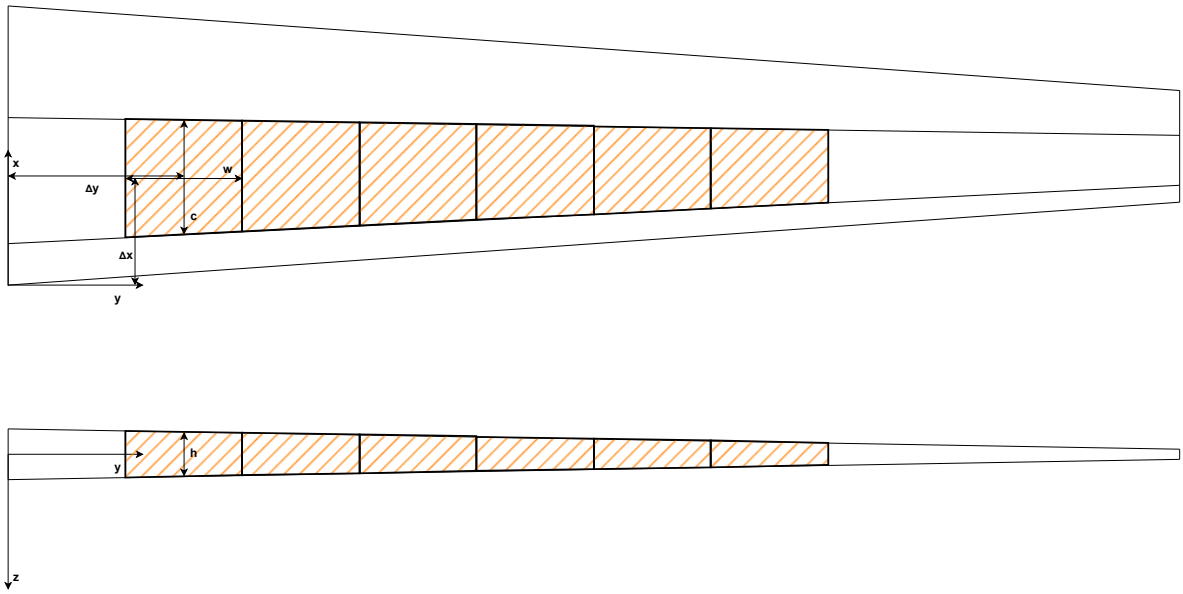

Figure 3.11: Discretization of the fuel tank

The batteries in Configuration 3 are placed inside the wing. To ensure the lowest rolling moment of inertia, they are placed as close to the fuselage as possible. Considering a battery density of 2000 kg/m^3 [43], the batteries can be placed up to at least 34% of the wing span, as seen in Figure 3.7. Of course, for structural wing performance, it would be better if the batteries were more spread out (optimally placing them throughout the whole wing). This would reduce the rolling performance of the aircraft. Thus, a sensitivity analysis of the battery placement will be performed to see if the aircraft can still meet the requirements for rolling with outer-placed batteries.

3.3.3. PROPELLERS AND MOTORS

In this study, propellers and engines will be considered as point masses. This is a valid assumption because the influence of shape is reduced if the object is further away from the reference axis. To prove the validity of the assumption, a simple calculation was performed, and the results are presented in Table 3.4.

Table 3.4: Comparison for the reference case for point mass approach and simplified actual.

Reference axis	Total (kg·m^2)	Point mass (kg·m^2)	Difference
x	32754	32560	0.6%
y	4964	3697	25.5%

As seen in Table 3.4, the assumption for finding the mass moment of inertia around the x-axis is valid. For the y-axis, the assumption might not seem valid. However, one should keep in mind that the engine's center of gravity is much closer to the y-axis than to the x-axis; thus, the shape plays a bigger role. Due to this, there is a big difference between both approaches. However, this difference is minor when compared to the total mass moment of inertia, where the fuselage will have the biggest influence. Moreover, this will have even less influence on distributed propulsion, as the shape factors scale quadratically with the dimensions; thus, the difference will be even lower. For twin turboprop aircraft, the engine contribution is accounted for in Equation 3.2.

3.4. AERODYNAMIC MODELS

The aircraft under analysis possesses a specific geometry, yet only a restricted set of aerodynamic coefficients is available. Consequently, it becomes imperative to estimate several aerodynamic coefficients to derive the pertinent forces and moments required for simulations. This section outlines the methods employed to determine these coefficients.

3.4.1. FUSELAGE

In general, for low angles of attack, the fuselage only contributes to the drag of the aircraft. Thus, for stability and control, this is not relevant. On the other hand, at higher angles of attack, the fuselage starts creating a destabilizing moment. Due to this, for instance, during take-off rotation, it is important to account for this moment created by the fuselage.

For this study, the assumption is made that at a zero pitch angle, the fuselage generates no moment. Although, in reality, the fuselage introduces a slight moment owing to its asymmetric curvature, this effect is minimal when contrasted with moments at non-zero pitch angles. Consequently, there is a need to estimate the moment derivative concerning the angle of attack. This is accomplished using Equation 3.6 as detailed in [11]. The pitching moment factor is extracted from a figure provided in the book [11].

$$C_{m_{\alpha_{fus}}} = \frac{K_{fus} W_f^2 L_f}{c S_w} \tag{3.6}$$

3.4.2. WING

The wing lift coefficient without propeller effects can be estimated using Equation 3.7 and the lift slope of the wing (horizontal tail and vertical tail also) can be estimated using Equation 3.8 (Equation 3.9 and Equation 3.10 shows the estimation of some of the variables) presented by Roskam [44].

$$C_L = C_{L_\alpha}(\alpha - \alpha_0 + i_w) \tag{3.7}$$

$$C_{L_\alpha} = \frac{2\pi A}{2 + \sqrt{\frac{A^2\beta^2}{k^2}\left(1 + \frac{\tan^2 \Lambda_{c/2}}{\beta^2}\right) + 4}} \tag{3.8}$$

$$\beta^2 = 1 - M^2 \tag{3.9}$$

$$k = \frac{C_{l_\alpha}}{2\pi/\beta} \tag{3.10}$$

Wing zero lift pitching moment is found with the Datcom method [45] presented in Eqwuation 3.11. This is only used for the main wing, as the pitching moment of the horizontal tail is zero (symmetric airfoil).

$$C_{m_0} = C_{m_{\text{af}}} \frac{A \cos^2 \Lambda_{c/4}}{A + 2\cos \Lambda_{c/4}} \tag{3.11}$$

The aircraft will also have some damping with the pitch rate. When an aircraft rotates, a dynamic angle of attack is created, which depends on the rotation speed. This damping is relevant for the take-off rotation and can be estimated with Equation 3.12 [46]. This damping is mostly affected by the horizontal tail, and the wing contribution is minimal [44]. Due to this, the model will always predict a negative pitch rate moment derivative, and the requirement for the negative pitch rate moment derivative will always be met.

$$C_{m_q} = -2 C_{L_{\alpha_h}} \eta_h \bar{V}_h (\bar{x}_{ac_h} - \bar{x}_{cg}) \tag{3.12}$$

Finally, the aircraft drag should be estimated. This will only be used for take-off rotation, where it has a noticeable effect. For aircraft roll, stability, and trim, drag is not required [10]. The drag is estimated using the drag polar (Equation 3.13). The Oswald efficiency factor can be predicted with Equation 3.14.

$$C_D = C_{D_0} + \frac{C_L^2}{\pi A e} \tag{3.13}$$

$$e = 1.78(1 - 0.045 A^{0.68}) - 0.64 \tag{3.14}$$

3.4.3. DOWNWASH

The downwash at the horizontal tail affects the performance of the tail and elevator. Thus, it is essential to be able to predict it to estimate the performance of these control and stability surfaces. Downwash is caused by the wing lift and is also altered by the propeller setting. Wing downwash occurs since lift is generated by producing downward flow velocity. This causes a change in the angle of attack at the horizontal tail. A method taken from Datcom [45] is presented below for finding the wing downwash. The effective aspect ratio and effective wing span can be found using Figure 3.12.

Using the effective aspect ratio obtained, the low-speed downwash gradient is achieved with the help of Figure 3.13. The downwash gradient at infinity can be calculated with Equation 3.15.

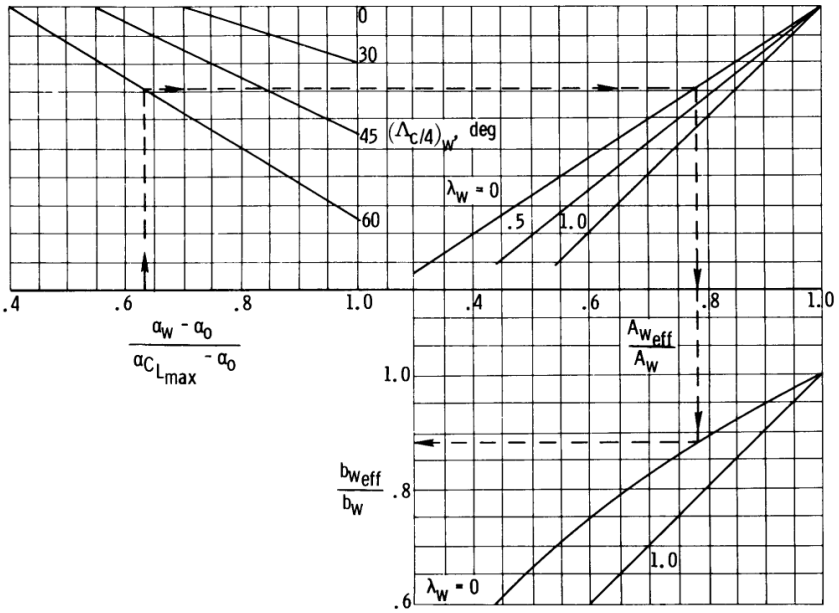

Figure 3.12: Effective wing aspect ratio and span for low speeds [7].

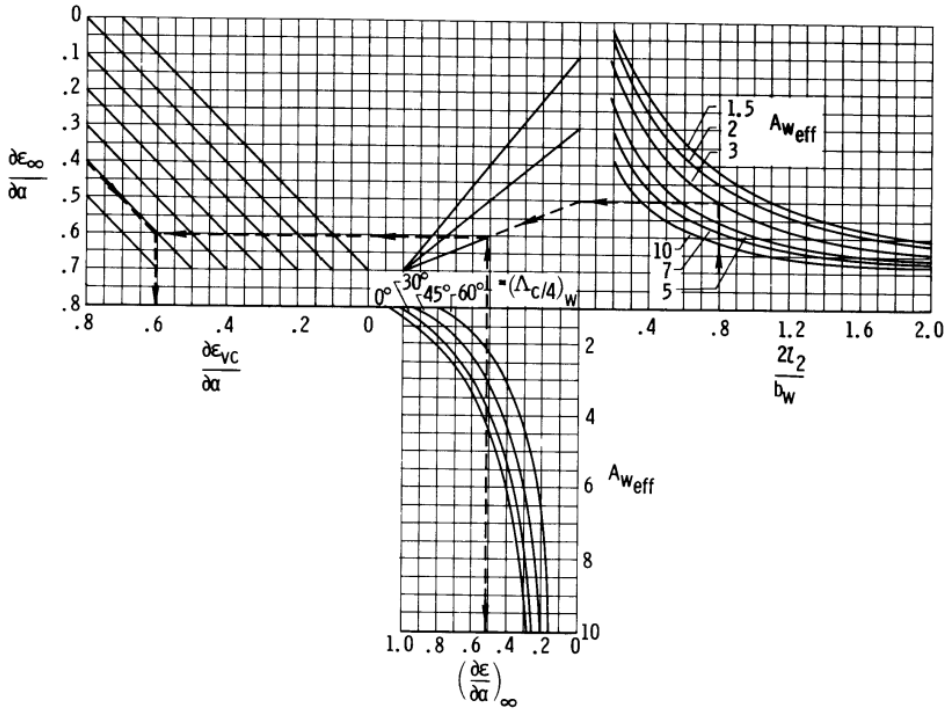

Figure 3.13: Downwash at the plane of symmetry and height of vortex core for low speeds [7].

$$\frac{\delta \epsilon_\infty}{\delta \alpha} = \frac{2}{\pi A_w} (C_{L_\alpha})_w \tag{3.15}$$

Depending on the flow separation of the main wing (which can be determined with Figure 3.14), the vertical distance of the horizontal tail quarter chord point relative to the vortex core can be found. For trailing edge separation, Equation 3.16 is used, and for the leading edge - Equation 3.17.

The span of the wing vortices at the tail is estimated with Equation 3.18. The span of completely rolled-up vortices is found with Equation 3.19 and the distance of rolled-up vortices is found with Equation 3.20. Finally, the downwash at the tail is found with Equation 3.21 and Figure 3.15.

$$a = z_{\mathrm{h}} - l_{\mathrm{eff}}\left(\alpha_{\mathrm{w}} - \frac{0.41 C_{L_{\mathrm{w}}}}{\pi A_{\mathrm{w_{eff}}}}\right) - \frac{b_{\mathrm{w_{eff}}}}{2}\tan\Gamma \tag{3.16}$$

$$a = z'_{\mathrm{h}} - (l_2 + l_3)\left(\alpha_{\mathrm{w}} - \frac{0.41 C_{L_{\mathrm{w}}}}{\pi A_{\mathrm{w_{eff}}}}\right) \tag{3.17}$$

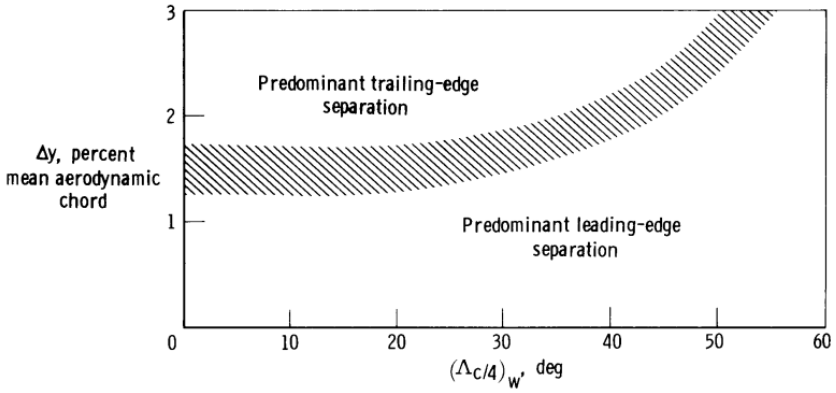

Figure 3.14: Type of flow separation as a function of airfoil and wing sweep for subsonic speeds [7].

$$b_{vor} = b_{\mathrm{w_{eff}}} - (b_{\mathrm{w_{eff}}} - b_{ru})\left(\frac{2 l_{\mathrm{eff}}}{b_{\mathrm{w}} l_{ru}}\right)^{1/2} \tag{3.18}$$

$$b_{ru} = \left(0.78 + 0.1(\lambda_{\mathrm{w}} - 0.4) + 0.003(\lambda_{c/4})_{\mathrm{w}}\right) b_{\mathrm{w_{eff}}} \tag{3.19}$$

$$l_{ru} = \frac{0.56 A_{\mathrm{w}}}{C_{L_{\mathrm{w}}}} \tag{3.20}$$

$$\left(\frac{\delta \bar{\epsilon}_{\mathrm{h}}}{\delta \alpha}\right)_{lowspeed} = \left[\frac{\frac{\delta \bar{\epsilon}_h}{\delta \alpha}}{\frac{\delta \epsilon_{vc}}{\delta \alpha}}\right]_{lowspeed} \left(\frac{\delta \epsilon_{vc}}{\delta \alpha}\right)_{lowspeed} \tag{3.21}$$

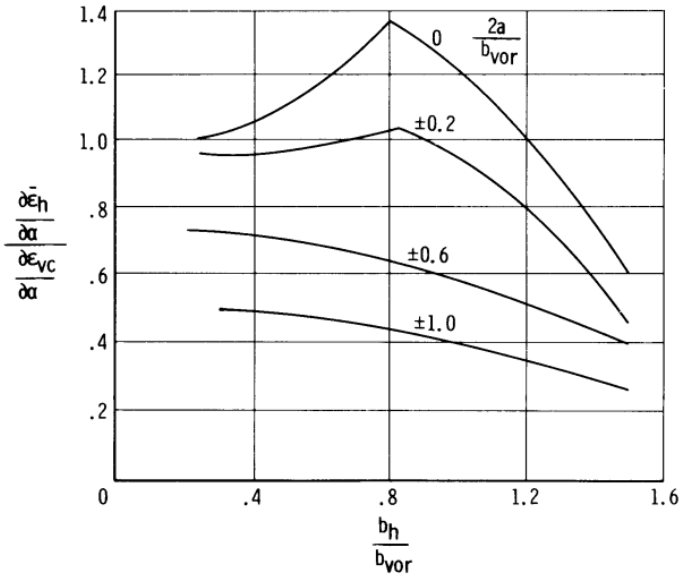

Figure 3.15: Average downwash acting on aft lifting surface for low speeds [7].

3.4.4. WING WAKE

Due to the friction over the wing, a slower region of flow is generated behind it called the wing wake. In this region, the dynamic pressure is smaller; thus, any surface located in this region will suffer lower effectiveness. This is common for a horizontal tail, which is located behind the wing. Due to this, the vertical placement of the horizontal tail is critical and is also within the scope of this study.

To estimate dynamic pressure due to the wing wake, the method presented by Wolowics and Yancey [7] can be used. The method predicts the location and size of the wake, and from this, the change in dynamic pressure is estimated. First of all, the wake size is found using Equation 3.22, where x is the distance from the wing root trailing edge. The maximum loss in dynamic pressure is obtained from Equation 3.23.

$$\frac{\Delta z_{\text{wake}}}{\bar{c}_w} = 0.68\sqrt{C_{D_{f_{\text{W}}}}\left(\frac{x}{\bar{c}_w}+0.15\right)} \tag{3.22}$$

$$\left(\frac{\Delta\bar{q}}{\bar{q}_\infty}\right)_0 = \frac{2.42C_{D_f}^{1/2}}{\frac{x}{\bar{c}_w}+0.3} \tag{3.23}$$

Knowing the maximum loss, it can be used to obtain the values depending on the vertical location (Equation 3.24). The vertical distance (body axis system) from the centerline of the wake to the quarter chord of the mean aerodynamic chord of the horizontal tail is found using Equation 3.25. Finally, the downwash angle at the plane of symmetry is estimated from Equation 3.26.

$$\left(\frac{\Delta\bar{q}}{\bar{q}_\infty}\right)_h = \left(\frac{\Delta\bar{q}}{\bar{q}_\infty}\right)_0 \cos^2\left(\frac{\pi}{2}\frac{z_h''}{\Delta z_{\text{wake}}}\right) \tag{3.24}$$

$$z_h'' = x\tan(\gamma+\epsilon_h-\alpha_w) \tag{3.25}$$

$$\epsilon_h = \frac{1.62C_{L_W}}{\pi A} \tag{3.26}$$

3.4.5. GROUND EFFECT

The ground effect mainly influences two parameters of the wing: lift curve slope and induced drag [47–50]. However, the effect of the ground effect on these parameters depends on the shape of the wing. For high-aspect wings, the induced drag is more affected, whereas the lift curve slope stays relatively the same [48, 51]. Similarly, for low aspect ratio wings, the ground effect significantly changes the lift curve slope, but the induced drag stays the same. This also meets CFD data [52] (aspect ratio of 20), where the drag changes close to the ground but the lift stays the same. As the configurations in the report feature high aspect ratio wings, only the change in induced drag is modeled. The induced drag reduction can be estimated using Equation 3.27 [48]. The induced drag coefficient is then multiplied by the outcome of Equation 3.27.

$$\phi = 1-\frac{1-1.32\frac{h}{b}}{1.05+7.4\frac{h}{b}} \tag{3.27}$$

3.4.6. ROLL DAMPING

In this study, the aircraft's rolling motion will be analyzed. However, the problem with this motion is that the lifting surfaces will encounter different local angles of attack along the wingspan. Due to this, the lifting surfaces will be discretized into many spanwise sections. Each of these sections will generate a force, which will produce a moment around the aircraft. To find the force, the lift curve slope of each section needs to be estimated.

The spanwise lift curve slope distribution is estimated with Schenk's approximation [53]. This approximation is used for lift distribution but can also be used for lift curve slope in the case of a less swept wing because the local angle of attack is similar at all sections.

The result from AVL and the one obtained by Schrenk's approximation is shown in Figure 3.16 to verify the usage of Scherenk's approximation. It can be seen that Schrenk underestimates the lift slope until the tip and overestimates it at the tip. However, the difference is small. Moreover, when computing the moment created, the difference is only 2.3% between the two approaches. However, with the Schrenk approximation, no coupling to external programs is needed, and it can be used for different planforms (low-sweep wings), thus, it is used in this study to estimate roll damping.

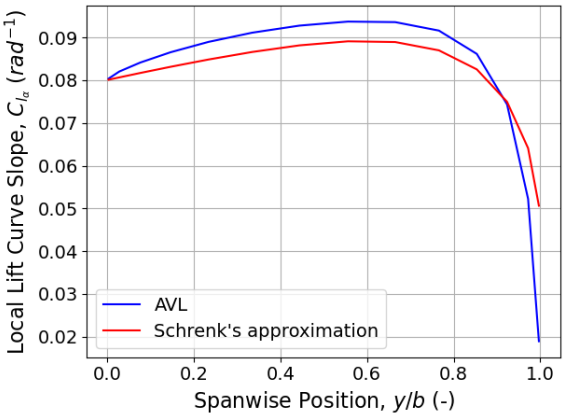

Figure 3.16: AVL and estimated by Schrenk's approximation lift curve slope spanwise distribution.

3.4.7. CONTROL SURFACE DEFLECTIONS

By deflecting control surfaces, forces controlling the aircraft are generated. There are mainly three control surfaces: the elevator, aileron, and rudder. These are responsible for longitudinal, lateral, and directional control, respectively. This study will only focus on the elevator and aileron designs.

Elevators mainly provide longitudinal control for the aircraft. In a conventional aircraft, this control is applied through an elevator deflection or throttle setting [10]. The derivative of the horizontal tail lift coefficient concerning elevator deflection is shown in Equation 3.28. This depends on the horizontal tail lift curve slope and control surface effectiveness, which can be obtained from a figure presented by Sadraey [10].

$$C_{L_{h_{\delta_e}}} = -C_{L_{\alpha_h}} \tau_e \tag{3.28}$$

Ailerons are control surfaces mainly used to provide roll control to the aircraft. They are situated at the ends of the wing, as the rolling moment is highest there. Ailerons typically extend from about 50% to about 90% of the span; however, a lower aileron span is desired to allow for more space for the flaps [11].

For the moment derivative due to aileron deflection, the calculation is a bit more complex. Again, the lift curve slope and control surface effectiveness are used. However, because the aileron does not cover the whole span of the wing and the position affects the moment, a normalization has to be applied. This coefficient depends on the aileron placement and area and is normalized to the surface area of the wing and wingspan, as shown in Equation 3.29 [10].

$$C_{l_{\delta_a}} = \frac{2C_{L_{\alpha_w}} \tau}{Sb} \int_{y_i}^{y_0} cy\,dy \tag{3.29}$$

3.5. PROPELLER EFFECTS

As discussed before, the propeller can directly and indirectly impact the aircraft. Direct impact comes from the thrust force and normal force, while indirect effects come from the slipstream-affected aerodynamic forces. The arrangement of the vehicle's parts has a significant impact on those caused by slipstream effects. But it is possible to generalize in the ways that follow:

- When delivering positive thrust, the dynamic pressure behind the propeller is higher than the dynamic pressure in the free stream. The forces and moments acting on slipstream-involved aircraft parts are inversely correlated with the slipstream dynamic pressure.
- A downwash field is created behind the propeller aircraft as a result of the normal force acting on a propeller at the angle of attack. The angle of attack of the aircraft parts working in the propeller slipstream is altered by this downwash field.

To account for propeller effects, a method presented in Datcom [45] has been used and expanded by Wolowics and Yancey [7] (the original method was presented in a technical report [54] and also described by

Abzug [55]; however, these papers are inaccessible). This technique examines the lift coefficient increments caused by the effects of propeller power in the following order:

- Due to the downwash flow field behind the propeller, the piece of the wing in the propeller slipstream changes its angle of attack
- Dynamic pressure shift over the wing part in the propeller slipstream
- Downwash-induced lift change and dynamic pressure changes acting on the horizontal tail

The basic approach to accounting for propeller effects will be the adjustment of aerodynamic coefficients. All aerodynamic coefficients will be normalized to the wing surface area and freestream dynamic pressure. Thus, every effect will be accounted for in the coefficient itself. For the wing, the lift coefficient is expressed in Equation 3.30. The wing lift consists of the lift generated without propeller effects (Equation 3.7) and the change in lift due to the increase in dynamic pressure in the slipstream and the change in the local angle of attack.

$$C_L = C_{L_\alpha}(\alpha_b - \alpha_0 + i_w) + (\Delta C_L)_{\Delta\bar{q}_w} + (\Delta C_L)_{\epsilon_p} \tag{3.30}$$

The horizontal tail lift coefficient is expressed in Equation 3.31. It depends on the local angle of attack (which depends on the body axis angle, wing incidence angle, downwash, propeller-induced downwash, and elevator deflection) and the dynamic pressure ratio (which depends on wing wake and propeller slipstream). Again, everything is normalized concerning the main wing area and freestream dynamic pressure.

$$C_{L_h} = C_{L_{\alpha_h}}(\alpha_b + i_h - \epsilon_h - \Delta\epsilon_h + \tau\delta_e)\left(\frac{\bar{q}_h}{\bar{q}_\infty} + \frac{\Delta\bar{q}_h}{\bar{q}_\infty}\right)\frac{S_h}{S_w} \tag{3.31}$$

Finally, the propellers will also generate a force when exposed to an angle of attack. The formula for it is presented in Equation 3.32. f is the propeller inflow factor, which can be obtained from a figure provided by Wolowics and Yancey [7].

$$\left(\Delta C_L\right)_{N_p} = f\left(C_{N_\alpha}\right)_p \alpha_p \frac{S_p}{S_w}\cos\alpha_T \tag{3.32}$$

To get the aerodynamic coefficients for the wing, horizontal tail, and propeller, the dynamic pressure increase at the wing needs to be known, as does the change in angle of attack in the slipstream, propeller-induced downwash, dynamic pressure at the horizontal tail, and the propeller normal force coefficient. The methods of obtaining these parameters are discussed below.

3.5.1. DYNAMIC PRESSURE INCREASE AT THE WING

The increase in dynamic pressure over the immersed part of the wing is found using Equation 3.33. This is only for the slipstream immersed part; thus, the area covered by the slipstream should be known. In Figure 3.17, the slipstream coverage of the wing is shown.

$$\frac{\Delta\bar{q}_w}{\bar{q}} = \frac{S_w(T_c'/n)}{\pi R_p^2} \tag{3.33}$$

To estimate the slipstream dimensions over wing, method [45] below is presented. First of all, the span that emerges in the propeller slipstream is evaluated with Equation 3.34. To estimate the parameters for this equation, Equation 3.35, Equation 3.36, and Equation 3.37 are used [7].

$$b_i = 2\sqrt{{R_\mathrm{p}}^2 - (z_s - z_\mathrm{w})^2} \tag{3.34}$$

$$z_s = -{x_\mathrm{p}}'(\alpha_b - \epsilon_u - \epsilon_\mathrm{p}) + z_T \tag{3.35}$$

$$-\epsilon_u = -\frac{\delta\epsilon_u}{\delta\alpha}(\alpha_\mathrm{w} - \alpha_0) \tag{3.36}$$

$$\epsilon_\mathrm{p} = \frac{\delta\epsilon_\mathrm{p}}{\delta\alpha_\mathrm{p}}\alpha_\mathrm{p} \tag{3.37}$$

The upwash gradient can be predicted using Figure 3.18. The downwash gradient is found by Equation 3.38. The constants are obtained from Figure 3.19, and the normal force derivative is estimated with Equation 3.43. Finally, the increase in lift coefficient is found using Equation 3.39.

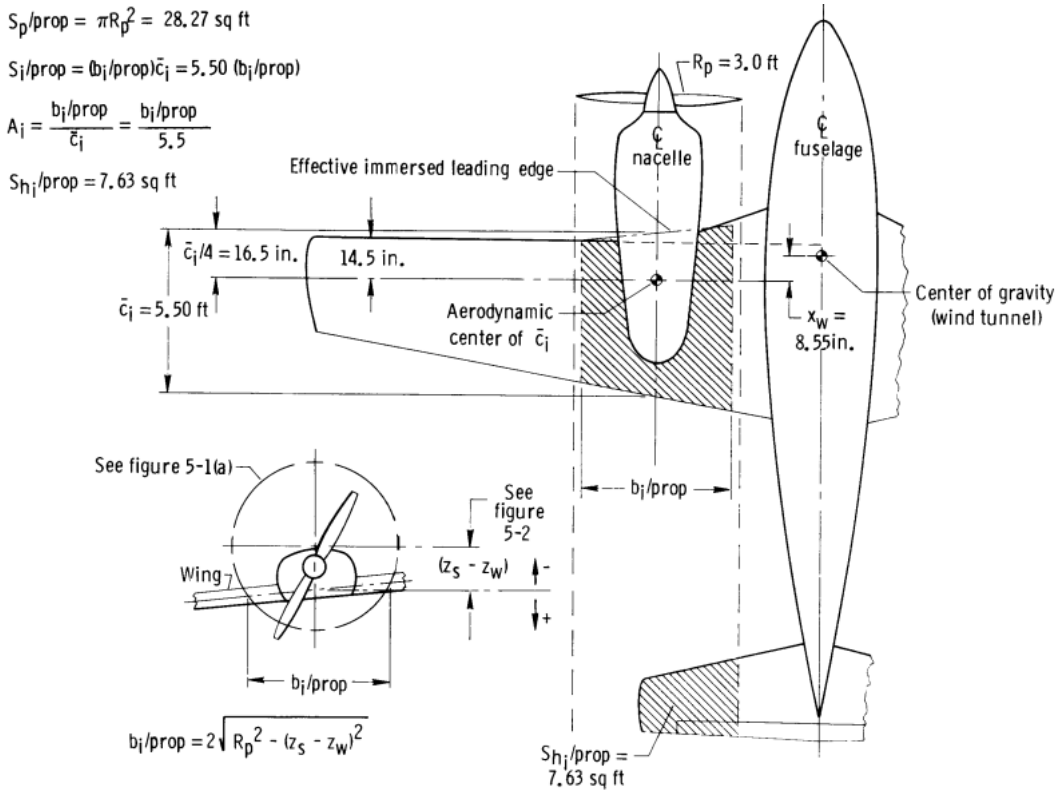

Figure 3.17: Definition sketches for calculation of immersed wing areas [7].

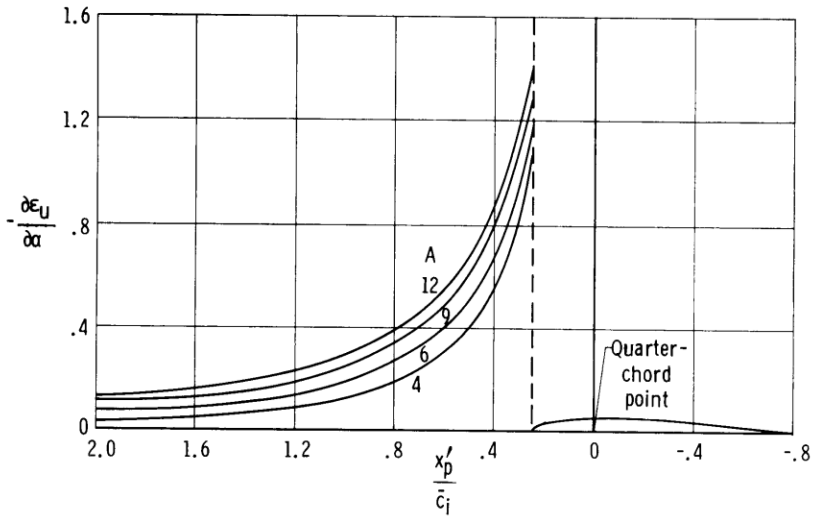

Figure 3.18: Upwash gradient at the plane of symmetry for unswept wings [7].

$$\frac{\delta \epsilon_p}{\delta \alpha_p} = C1 + C2\left(C_{N_\alpha}\right)_p \tag{3.38}$$

$$(\Delta C_L)_{\Delta \bar{q}_w} = nK_1 \frac{\Delta \bar{q}_w}{\bar{q}_\infty} (C_{L_W})_{\text{prop off}} \frac{(S_i)}{S_w} \tag{3.39}$$

K_1 is an empirical correlation parameter for additional wing lift due to the power effects on the wing obtained from a figure in Wolowics and Yancey [7] work.

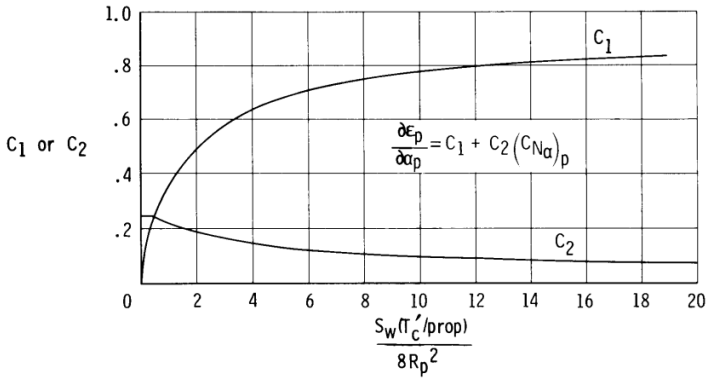

Figure 3.19: Factors for determining propeller downwash [7].

3.5.2. ANGLE CHANGE IN PROPELLER SLIPSTREAM

For the additional lift generated by the change in angle of attack due to the propeller downwash Equation 3.40 [7] is used. The change in the angle of attack is estimated with Equation 3.41.

$$(\Delta C_L)_{\epsilon_p} = n(1 + \frac{\Delta \bar{q}_w}{\bar{q}_\infty})\left(C_{L_\alpha}\right)_{w_{\text{prop off}}}(\Delta\alpha)_{S_i}\frac{(S_i/\text{prop})}{S_w} \tag{3.40}$$

$$(\Delta\alpha)_{S_i} = -\frac{\epsilon_p}{1 - \frac{\partial\epsilon_u}{\partial\alpha}} \tag{3.41}$$

3.5.3. PROPELLER INDUCED DOWNWASH

The slipstream affects the downwash at the horizontal tail [56]. The effect of propellers on the downwash can be estimated using Figure 3.20. The calculation of the downwash without propellers was discussed in a previous subsection.

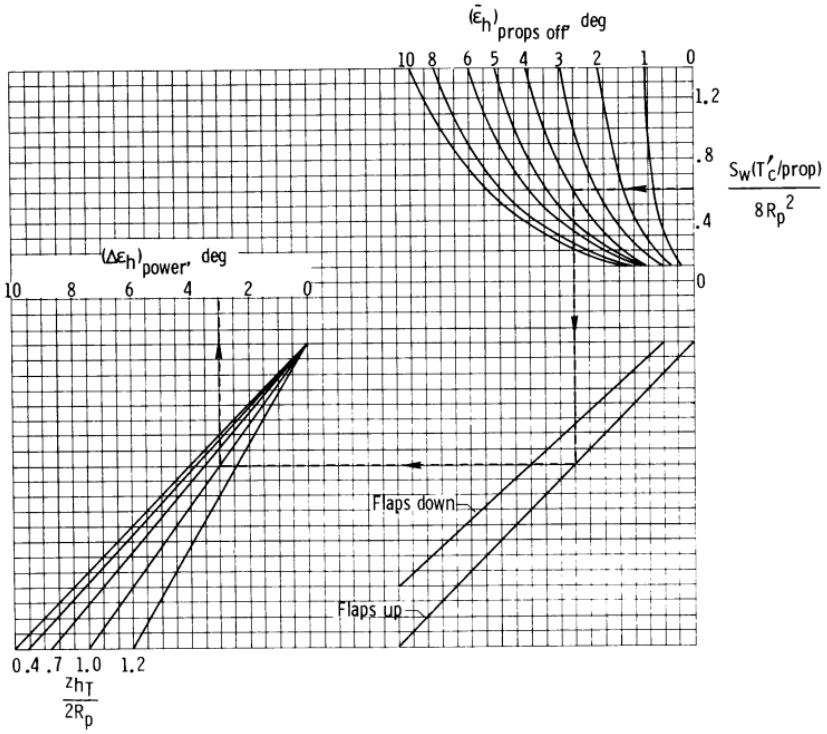

Figure 3.20: Increment in downwash due to propeller power for multiengine airplanes [7].

3.5.4. DYNAMIC PRESSURE AT THE HORIZONTAL TAIL DUE TO SLIPSTREAM

In Figure 3.17, the slipstream coverage of the horizontal tail is depicted. To estimate the dynamic pressure increase at the horizontal tail, the distance between the center of the slipstream and the horizontal tail needs to be found. This vertical distance is calculated with Equation 3.42, derived from Figure 3.21. The dynamic pressure increase is found using Figure 3.22.

$$z_{h_{\text{eff}}} = l'_h(\alpha_b - \epsilon_u - \epsilon_p - \bar{\epsilon}_{h_{\text{props off}}} - (\Delta\epsilon_h)_{\text{power}}) \tag{3.42}$$

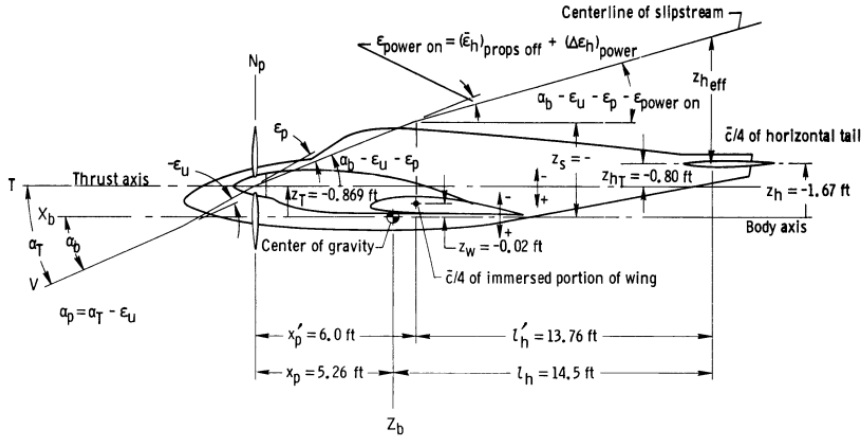

Figure 3.21: Definition sketch for calculation of propeller power effects [7].

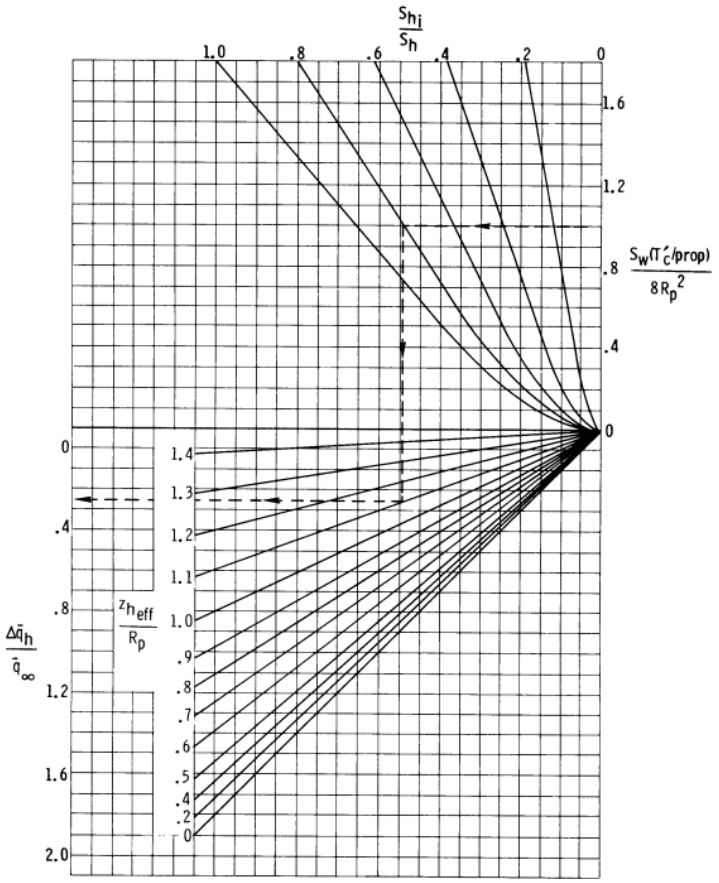

Figure 3.22: Definition sketches for calculation of immersed wing areas [7].

3.5.5. PROPELLER NORMAL FORCE COEFFICIENT

The normal force generated by the propeller can be approximated with Equation 3.43 [7]. Normal force factor is obtained from the propeller manufacturer or can be estimated with Equation 3.44, and normal force parameter can be estimated with Figure 3.23. The angle of attack of the propeller plane is described in Equation 3.45.

$$\left(C_{N_\alpha}\right)_p = \left[\left(C_{N_\alpha}\right)_p\right]_{K_N=80.7}\left[1+0.8\left(\frac{K_N}{80.7}-1\right)\right] \tag{3.43}$$

$$K_N = 262\left(\frac{b_p}{R_p}\right)_{0.3R_p} + 262\left(\frac{b_p}{R_p}\right)_{0.6R_p} + 135\left(\frac{b_p}{R_p}\right)_{0.9R_p} \tag{3.44}$$

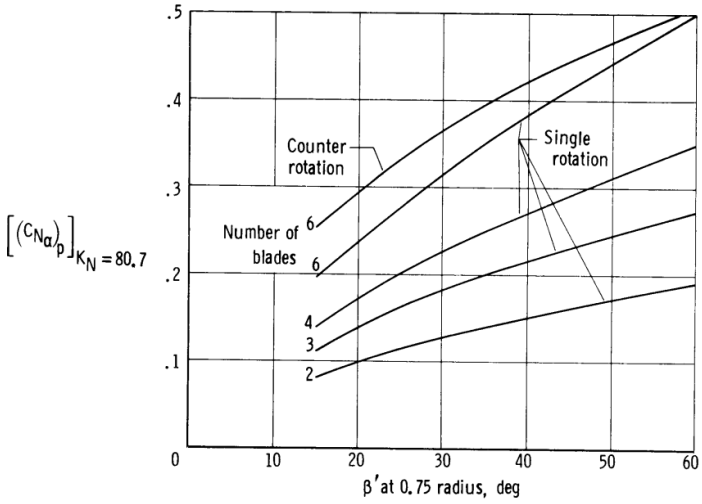

Figure 3.23: Propeller normal-force parameter [7].

$$\alpha_p = \alpha_T - \frac{\delta\epsilon_u}{\delta\alpha}(\alpha_w - \alpha_0) \tag{3.45}$$

3.6. LONGITUDINAL DYNAMIC STABILITY

One of the goals of this report is to predict the longitudinal dynamic stability of the aircraft. This consists of the short period and phugoid. These motions are described by natural frequency and damping. These quantities can be evaluated by formulas provided in Roskam's book [56]. The short period natural frequency and damping are estimated with Equation 3.46 and Equation 3.47, respectively. The phugoid natural frequency and damping are estimated with Equation 3.48 and Equation 3.49, respectively.

$$\omega_{n_{\text{sp}}} = \sqrt{\frac{Z_\alpha M_q}{U} - M_\alpha} \tag{3.46}$$

$$\zeta_{\text{sp}} = \frac{-(M_q + \frac{Z_\alpha}{U} + M_{\dot{\alpha}})}{2\omega_{n_{\text{sp}}}} \tag{3.47}$$

$$\omega_{n_{\text{ph}}} = \sqrt{\frac{-gZ_u}{U}} \tag{3.48}$$

$$\zeta_{\text{ph}} = \frac{-X_u}{2\omega_{n_{\text{ph}}}} \tag{3.49}$$

Static margin is an aircraft specification, which is part of static stability. On the other hand, it influences the short period performance. Thus, the short period results can be explained partly by knowing the static margin. It can be calculated with Equation 3.50

$$SM = -\frac{C_{m_\alpha}}{C_{L_\alpha}} \tag{3.50}$$

3.7. AIRCRAFT MANEUVERS

In this section, all of the relevant aircraft maneuvers are discussed. This also includes the approach to estimate the aircraft's behavior during these maneuvers.

3.7.1. TRIM

One of the responsibilities of the tail is to trim the aircraft. Thus, the tail has to produce a large enough force to keep the aircraft balanced. In general, only two forces (wing and horizontal tail lift) and two moments (wing and fuselage) are considered [10]. For this study the propeller normal force will also be included for relevant configurations, as seen in Figure 3.24. Weight is neglected, as the total moment is taken around the center of gravity. The moment of the horizontal tail and other forces are neglected due to their negligible contribution [10].

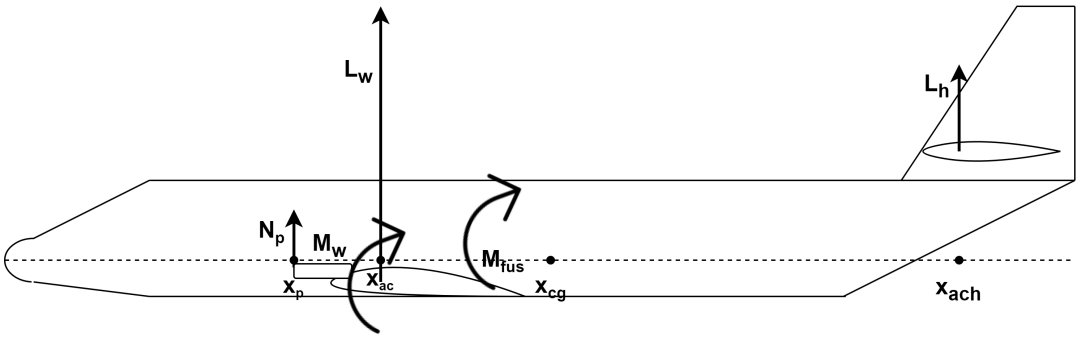

Figure 3.24: Aircraft forces and moments contributing to pitching moment.

This results in the moment equilibrium below (Equation 3.51). These two equations have two unknown variables angle of attack and tail incidence (or elevator deflection). Aircraft angle of attack will be obtained by matching wing lift to weight. The tail contribution to the lift can be neglected [10]. The configurations feature quite low payload and fuel mass; thus, the center of gravity ranges are low. Due to this, trim will be done only with the elevator. Having the angle of attack and using Equation 3.51 the minimum horizontal tail size will be estimated (using the maximum possible elevator deflection).

$$M_{fus} + L_w(x_{cg} - x_{ac}) + N_p(x_{cg} - x_p) - L_h(x_{ac_h} - x_{cg}) + M_w = 0 \tag{3.51}$$

3.7.2. ROLL

Ailerons are used to roll the aircraft. Sadraey [10] presents a good approach to doing the initial aileron sizing; however, this approach will be adjusted. The roll damping done by Sadraey can only be applied to conventional aircraft, thus, the method of Sadraey is adjusted by the roll damping estimation presented in Subsection 3.4.6. Moreover, it should be noted that an average lift slope should be taken for the aileron span part. Additionally, if a propeller blows over the aileron or part of it, it should be accounted for, as the effectiveness of the aileron increases. The lift coefficient due to aileron deflection was discussed in Subsection 3.4.7, and the roll damping was discussed in Subsection 3.4.6. An overview of the forces in a roll is shown in Figure 3.25. Aileron deflection creates a moment around the aircraft, which rolls it. However, during this motion, roll damping is created due to the change in the angle of attack at the control surfaces. These created moments resist the aileron moment, until both reach an equilibrium and a steady roll rate is achieved.

The roll analysis is done in a time-space. An aileron deflection is inputted, and the roll rate is estimated at every time step, including the created roll damping. Based on the result, the aileron size is then either increased or reduced until the desired roll time is achieved. A maximum aileron deflection of 20° is assumed [10] and the time to reach this deflection from neutral state is 0.5 s.

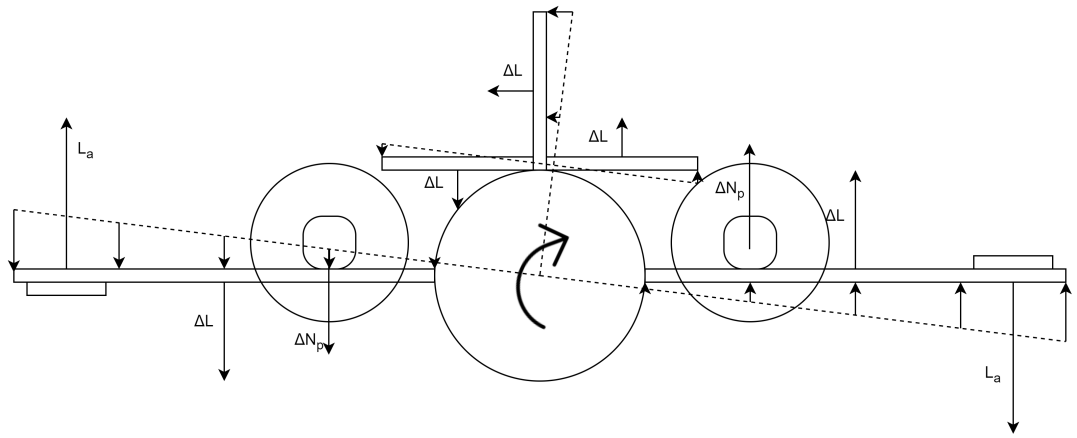

Figure 3.25: Overview of forces in a roll.

3.7.3. ROTATION

Usually, the most critical condition for elevator sizing is take-off. During this flight phase, flow speed is very low, and a large force is required to rotate the aircraft. An overview of forces and moments during take-off is shown in Figure 3.26. The elevator will need to provide a force big enough to meet the requirements set in Table 2.1. Again, only contributing forces are included in this preliminary analysis.

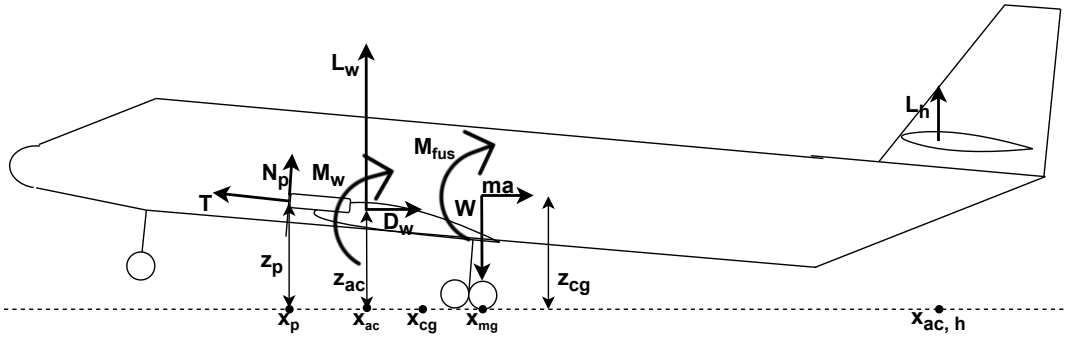

Figure 3.26: Forces and moments during take-off rotation.

Again, this analysis is done in a time-space. An elevator deflection is made, and the forces and moments generated at every time step are estimated. Then the rotation acceleration is achieved, which is used to estimate the new pitch angle. This analysis is repeated until the minimum horizontal tail size is found, which meets the requirements. The maximum elevator deflection is set to 30° [10]. Moreover, the elevator starts from 0° and reaches the maximum deflection in 0.3 s.

3.7.4. LONGITUDINAL STABILITY

In general, for an aircraft to be stable, the rate of change of the pitching moment coefficient concerning changes in the angle of attack and the rate of change of the pitching moment coefficient concerning the change in pitch rate has to be negative. The coefficients for longitudinal stability are found in Equation 3.52 and Equation 3.12 presented by Roskam [46].

$$C_{m_\alpha} = C_{L_{\alpha_w}}(\bar{x}_{cg} - \bar{x}_{ac_{wf}}) + C_{m_{\alpha_{\text{fus}}}} - C_{L_{\alpha_h}}\eta_h \frac{S_h}{S}(\bar{x}_{ac_h} - \bar{x}_{cg})(1 - \frac{d\epsilon}{d\alpha}) \tag{3.52}$$

4

VERIFICATION AND VALIDATION

In this chapter, the verification and validation of the tool created are presented. This step is crucial, as it allows ensuring the quality, reliability, and correctness of the process. First of all, the verification will be presented, and following it, the validation of the tool. Verification includes the downwash, wing wake, and propeller effects estimation. The verification of the moment of inertia estimation and aircraft maneuver modeling is neglected due to limited resources, however, validation for these modules is performed (the stability and control surface size, output of maneuver modeling, is compared to real-life aircraft in Chapter 5). The validation will cover aircraft moments and forces (including propeller effects) and the estimation of the moment of inertia. Additionally, a sensitivity analysis on ground effect and fixing constants (derived from validation of aircraft moments) is included in this chapter.

4.1. VERIFICATION

In this section, the verification of the propeller effects is discussed. The verification of these effects is done by comparing the results obtained by Reference [7] describing this methodology. To compare the results, the same geometry aircraft is put into the code to see if the same or similar outputs are received.

The majority of calculations were done by getting data from graphs. This graph data was digitized so it could be obtained by the code. Thus, some errors are expected due to the digitization process. Moreover, differences are also expected from the graph results obtained by the authors of Reference [7]. Due to this, the outputs will not match the exact figure but should be in a close range.

The key geometry parameters for the reference aircraft are shown in Table 4.1, other inputs can be obtained from Reference [7]. The units are imperial; however, the outputs are non-dimensional, thus, the units do not need to be converted. The reference aircraft is a smaller aircraft than the ones discussed in this study, however, it is a twin turboprop aircraft, which allows to verify the propeller effects.

Table 4.1: Reference aircraft specifications [7].

Parameter	Value
Wingspan (ft)	36
Wing area (ft^2)	178
Mean aerodynamic chord (ft)	4.96
Quarter chord sweep (deg)	-2.5
Aspect (-)	7.5
Taper (-)	0.513
Horizontal tail span (ft)	12.5
Horizontal tail area (ft^2)	32.5
Tail arm (ft)	14.5
Horizontal tail height (ft)	1.67
Propeller radius (ft)	3

4.1.1. DOWNWASH

First of all, the verification of the downwash is presented in Figure 4.1. There is some difference between the two results; however, this comes from the graph reading. The error is in the range of 0.9-2.3%.

4.1.2. WING WAKE

The wing wake verification is shown in Figure 4.2. However, all of the Reference [7] cases are outside of the wake. The same is true for the references in Datcom [45]. Thus, the results are the same, and there is no error between them. It should be noted that the position of the wing wake (which depends on the downwash - Figure 4.1), also, matches for Reference [7] and model.

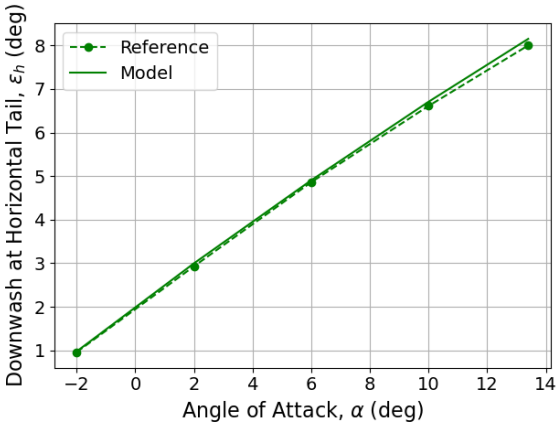

Figure 4.1: Wing downwash Reference [7] results compared to the model.

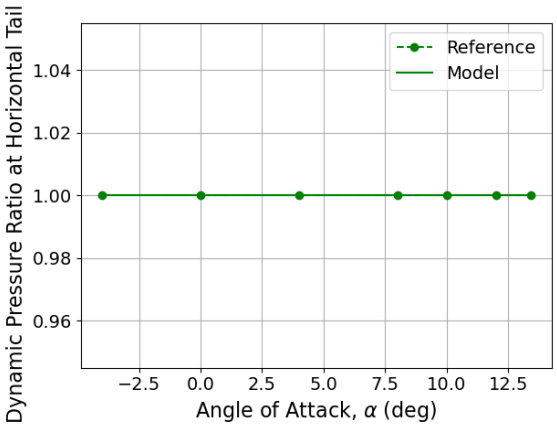

Figure 4.2: Wing wake Reference [7] results compared to the model.

4.1.3. PROPELLER EFFECTS

To verify the propeller effects, a propeller thrust coefficient of 0.1 (single propeller, normalized to wing area and free stream dynamic pressure) was used (same one used in Reference [7]). The verification was done for the increase in lift coefficient of the aircraft, as this was the result of Reference [7]. While the goal of this research is not to predict the lift of a DEP aircraft, a correct prediction of lift means that the effectiveness of the aerodynamic surface is estimated correctly. Thus, it can be applied to estimate balance and control forces (also lift).

The verification for the direct propeller contribution is shown in Figure 4.3. This includes the normal force and thrust force contribution to lift. Minimal differences are observed, thus, the prediction of the normal force is correct. The error ranges from -1.2% to -0.6%.

The increase in lift coefficients due to the increase of dynamic pressure over the wing is compared in Figure 4.4. Again, the results are very similar, and the error is at most 2.1%. It can be seen that the error increases with the airplane's angle of attack. This is mostly because the power-off lift coefficients are taken from a graph in Reference [7]. However, in the code, the lift curve slope is taken and multiplied by the angle of attack (neglecting the propeller effects). Thus, at larger angles of attack, a higher difference occurs because the slope starts slowly decreasing at high angles of attack.

Verification due to the local angle increase at the wing due to the propeller is presented in Figure 4.5. Again, the results are similar with an error ranging from -3.1% to 0.4%. Moreover, the results for the horizontal tail contribution are compared in Figure 4.6. The results closely match (error: -0.4%-0.7%).

The results of power effects do not perfectly match the ones in Reference [7]. However, the error is minimal and it mainly comes from the graph digitization and reading. Hence, the module responsible for estimating power effects is verified.

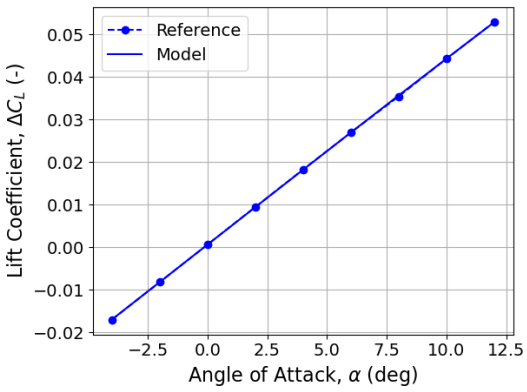

Figure 4.3: Propeller lift Reference [7] results compared to the model.

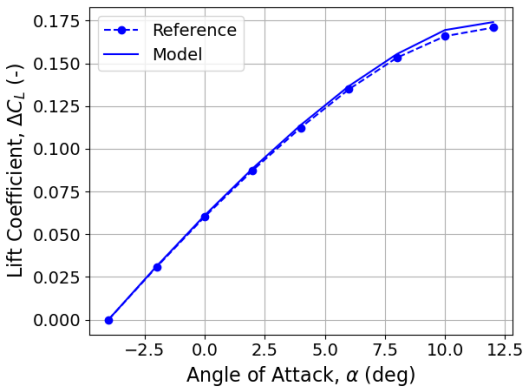

Figure 4.4: Lift increase due to dynamic pressure increase over the wing Reference [7] results compared to the model.

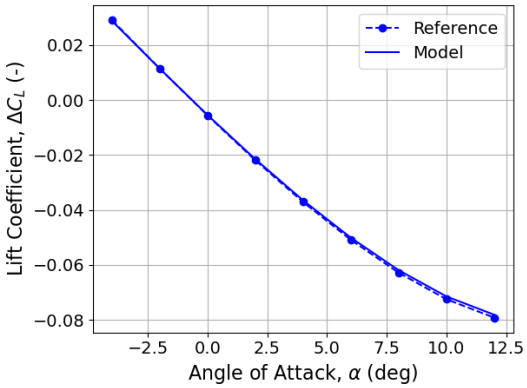

Figure 4.5: Lift increase due to change of local angle of attack at the wing Reference [7] results compared to the model.

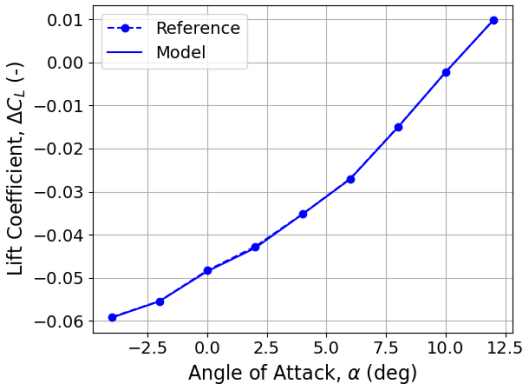

Figure 4.6: Lift increase at the horizontal tail Reference [7] results compared to the model.

4.2. VALIDATION

In this section, the validation of the tool is discussed. This ensures that the tool is able to model real-life aircraft performance. First of all, the propeller effect modeling is validated. This is done by comparing the model predicted aircraft lift and moment to Saab 340 with T-tail wind tunnel results [9]. After this, the moment of inertia calculation tool is also validated by comparing the model results to a X-57 (DEP aircraft) [57].

4.2.1. PROPELLER EFFECTS

For the validation of propeller effects, data from Bouquet's and Vos's paper [9] was taken, along with additional data from Obert's work [8]. This data was based on a Saab 340 with T-tail wind tunnel results. To compare the results, this aircraft geometry was used in the code to check if the outputs were similar.

It should be noted that not all aircraft specifications were provided. Some had to be derived from technical drawings or estimated manually (aerodynamic center location, airfoil lift curve slope). Due to this, some small deviations between the data should be expected. The key geometry parameters for the reference aircraft are shown in Table 4.2, and other inputs can be obtained from references [8, 9].

The tail-off lift versus angle of attack is presented for the model aircraft and wind tunnel test with no thrust in Figure 4.7. The results match closely; however, for higher angles of attack, the slope increases. This is due to the airfoil lift curve slope estimation. The model gets the airfoil lift curve slope by using graphical data of the airfoil lift curve. For the 8° angle of attack, the gradient is slightly overestimated due to the digitization of the data. The same is seen in Figure 4.8 for the 8° angle of attack and the whole aircraft lift.

The tail-off moment curve is shown for no thrust in Figure 4.9. In this case, the results are different, and there is a positive offset for the model. Considering that the tail-off lift matches closely and it consists of the wing lift only (fuselage lift is neglected in the model, minimal propeller lift due to no thrust), most likely, the

error is coming from the prediction of the fuselage moment or the wing moment (the moment due to lift is zero, as the moments are taken around the aerodynamic center). The fuselage moment prediction is a low-fidelity method based on one statistical graph and formula. Moreover, the method does not account for the zero angle of attack moment and only estimates the moment curve slope. Based on this, it is highly likely that the error is due to the missing fuselage zero angle of attack moment. In Figure 4.10, the total pitching moment curve is presented, where a similar trend is observed—a positive offset of the model.

Table 4.2: Saab 340 with T-tail specifications [8, 9].

Parameter	Value
Wingspan (m)	21.44
Wing area (m^2)	41.8
Mean aerodynamic chord (m)	2.04
Quarter chord sweep (deg)	2.62
Aspect (-)	11
Taper (-)	0.45
Horizontal tail span (m)	7.37
Horizontal tail area (m^2)	10.39
Tail arm (m)	9.35
Horizontal tail height[1] (m)	5.26
Propeller radius (m)	1.68

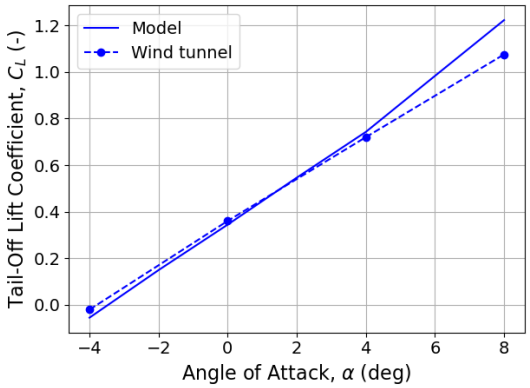

Figure 4.7: Tail-off lift curves for Saab 340 T-tail at T_C=0 [8, 9].

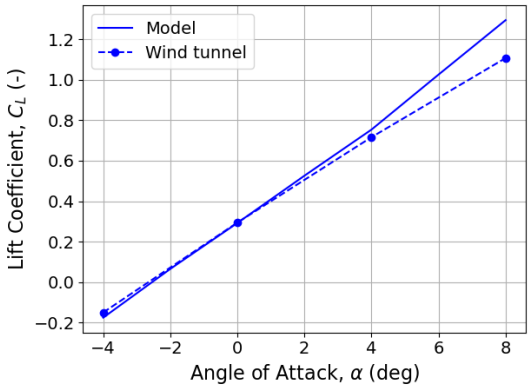

Figure 4.8: Lift curves Saab 340 T-tail at T_C=0 [8, 9].

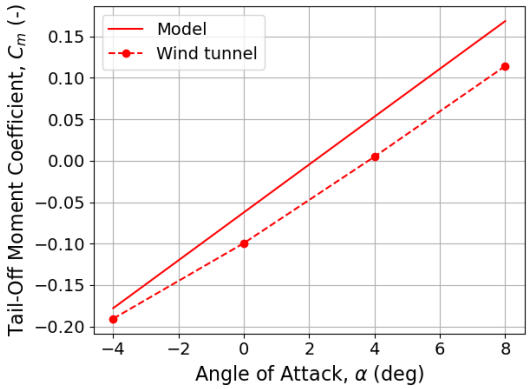

Figure 4.9: Tail-off moment curves Saab 340 T-tail at T_C=0 [8, 9].

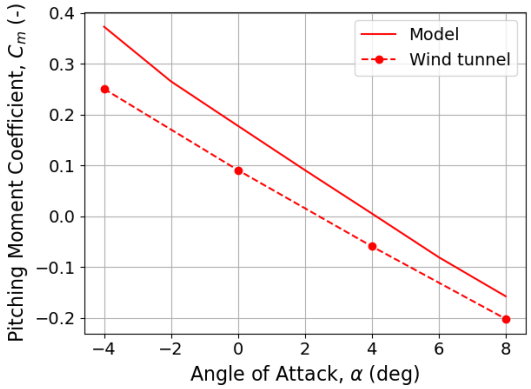

Figure 4.10: Moment curves Saab 340 T-tail at T_C=0 [8, 9].

[1] Vertical distance from wing aerodynamic center to horizontal tail aerodynamic center.

Moving to results with propeller thrust, a close relation between lift results is observed, as seen in Figures 4.11 and 4.12. The same higher gradient for 8° can be seen due to the lift curve slope estimation. In Figures 4.13 and 4.14, the moment curves are given, where again a positive model offset is observed.

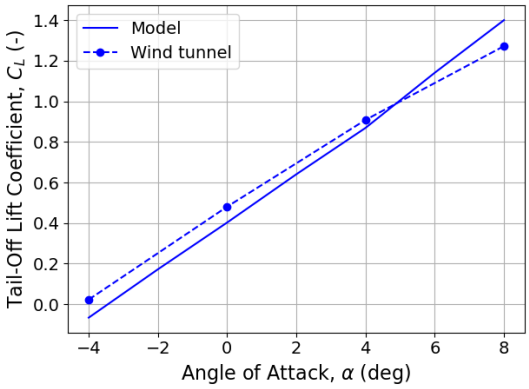

Figure 4.11: Tail-off lift curves Saab 340 T-tail at T_C=0.3 [8, 9].

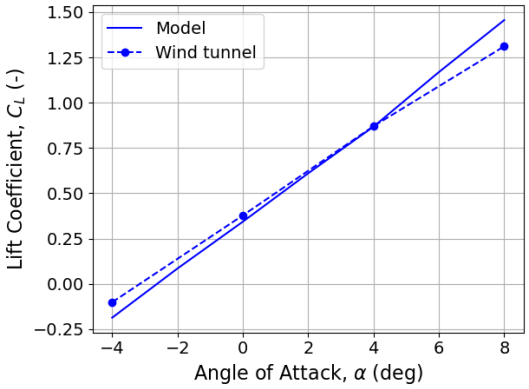

Figure 4.12: Lift curves Saab 340 T-tail at T_C=0.3 [8, 9].

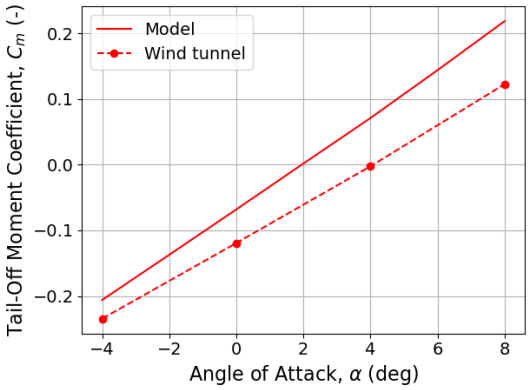

Figure 4.13: Tail-off moment curves Saab 340 T-tail at T_C=0.3 [8, 9].

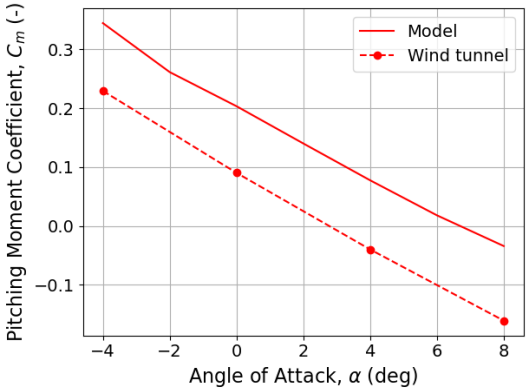

Figure 4.14: Moment curves Saab 340 T-tail at T_C=0.3 [8, 9].

Due to the moment offset, it was decided to introduce some constants to calibrate this. As the gradients are similar, these will not be adjusted. For adjusting the offset, two variables are chosen: the fuselage moment coefficient offset (ΔC_m) and the horizontal tail's incidence (Δi_h). The fuselage moment offset will be used to fix the tail-off moment curves, whereas the horizontal tail incidence will be used to fix the total moment curve if needed. Both of these variables do not affect the slope of the graphs. The values are presented in Table 4.3. These variables are used in order to calibrate the model for the wind tunnel data, as it is low/medium fidelity and can predict the moments with a certain range of error. However, this brings some uncertainty into the model. To see how this affects the model's results, a sensitivity analysis on these validation coefficients is done in Subsection 4.3.1.

Table 4.3: Coefficient values for fixing the model to validation data.

Coefficient	ΔC_m (-)	Δi_h (deg)
Value	-0.045	0.5

The calibrated model results versus the wind tunnel result with no thrust are presented in Figures 4.15 and 4.16. With the calibrated model, a slight difference in slope can be observed in Figure 4.16; however, due to it being minor and the complexity of accurately predicting the moment curves, it was decided to leave it as it is and not introduce another fixing variable. Additionally, the calibrated results are presented with thrust active on the propellers in Figure 4.17 and Figure 4.18. Again, some discrepancies are observed in the slope,

especially in Figure 4.17, however, the results still are similar. For further analysis, these non-dimensional fixing coefficients will be used.

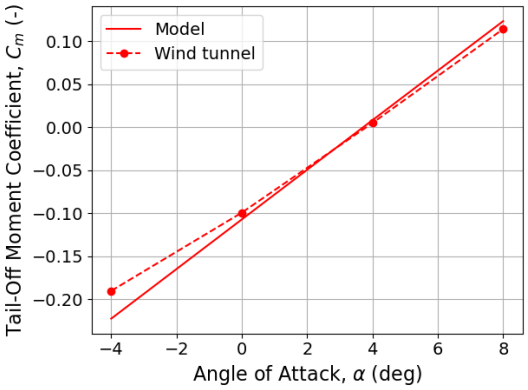

Figure 4.15: Tail-off moment curves Saab 340 T-tail at T_C=0 [8, 9] (model calibrated to experimental data).

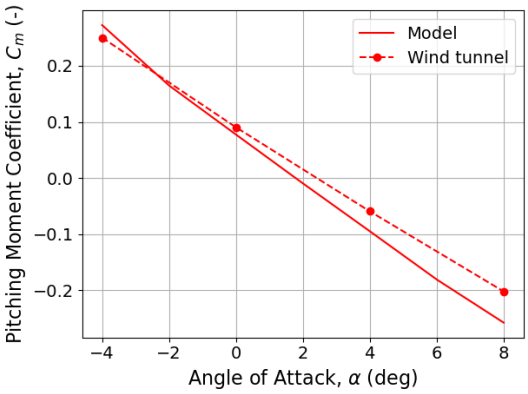

Figure 4.16: Moment curves Saab 340 T-tail at T_C=0 [8, 9] (model calibrated to experimental data).

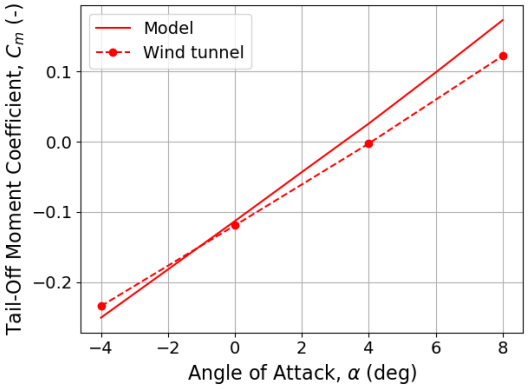

Figure 4.17: Tail-off moment curves Saab 340 T-tail at T_C=0.3 [8, 9] (model calibrated to experimental data).

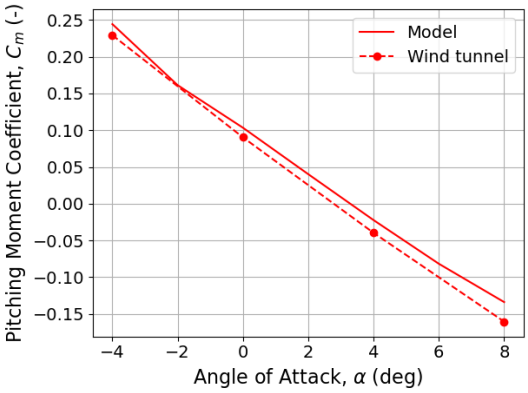

Figure 4.18: Moment curves Saab 340 T-tail at T_C=0.3 [8, 9] (model calibrated to experimental data).

4.2.2. MOMENT OF INERTIA

In this section, the module responsible for estimating the moment of inertia of the aircraft is validated. Firstly, the base case moment of inertia is estimated using Equation 3.1 and Equation 3.2. These equations are empirical and give the average moment of inertia for similar-size twin turboprop aircraft. Of course, some differences are expected, as this formula only gives an average and will vary per aircraft. This can be seen in Table 4.4, where the Cessna 172 [58] data is compared. The formulas can approximate the moment of inertia, however, some differences occur. In general, only in the final design stages an accurate moment of inertia estimation can be given when the complete mass distribution of the aircraft is known. For the design stage done in this report, this accuracy will be sufficient.

Table 4.4: Validation of empirical moment of inertia formula.

	Cessna 172 [58]	Model
I_{xx} (kgm^2)	1285	1434
I_{yy} (kgm^2)	1825	1874

Previously, Cessna 172 data was validated. This aircraft was also selected, as it is similar to X-57 [57] (a well-known electric distributed propulsion aircraft). The Cessna 172 moment of inertia will be adjusted

using the moment of inertia model to see how close the results match. In Table 4.5 the results are presented. This includes the adjustment for fuel, base engine, battery, and distributed propulsion.

Again there is some difference between the results. Due to the complexity of getting an accurate moment of inertia number, this is expected. However, the difference might also come from assumptions made. One of the assumptions used in the moment of inertia module is that engines are modeled as point masses. This is accurate for small engines located far away from the center of gravity (distributed propulsion), however, the same calculation was done for the Cessna 172 engine (a bigger engine, located at the spanwise center of gravity). The code was built for at least a twin-engine aircraft, as this is one of the configurations analyzed in this report. Due to this the moment of inertia for the Cessna 172 engine is underestimated. Moreover, there is not a lot of data on X-57, as it is a very new concept still being developed. Thus, some data had to be derived (like battery dimensions and location). This is also likely to cause the inaccuracy of the model. In general, the moment of inertia can be predicted in a larger range for the aircraft.

Table 4.5: Validation of moment of inertia model.

	Cessna 172 [58]	Cessna 172 engine	Fuel	Battery	Distributed propellers	Total	X-57 [35]
I_{xx} (kgm^2)	1285	0	-348	+32	+795	1764	1617
I_{yy} (kgm^2)	1825	-401	-122	+376	+44	1721	1927

4.3. SENSITIVITY TO MODEL ASSUMPTIONS

In this section, two sensitivity analyses are performed. First of all, one on the calibration of the model to see how they affect the results. Second sensitivity analysis is performed on the ground effect to see its influence and the influence of different effects of the ground effect on the results.

4.3.1. VALIDATION COEFFICIENTS

In this sensitivity analysis, Configuration 1 (twin turboprop with no propeller effects) and Configuration 2 (twin turboprop with propeller effects) are employed. Figure 4.19 illustrates the rotation performance of Configuration 1, displaying the minimal horizontal tail area for different wing locations. The impact of validation constants on the results is minimal, as evident in the graph. Figure 4.20 highlights the differences, which are more pronounced at lower wing positions due to the proximity to 0 (no horizontal tail area required). The moment constant diminishes rotation performance by inducing more pitching down, while horizontal tail incidence has both positive and negative effects. At low angles of attack, the pitching-up moment is lower, but at higher angles, the horizontal tail aids faster rotation. The negative effect dominates rotation performance. Similar trends are observed in Figure 4.21 and 4.22 for Configuration 2.

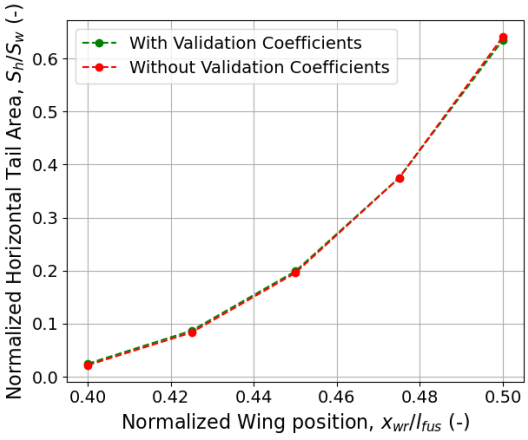

Figure 4.19: Configuration 1 minimum horizontal area (for different wing positions) for rotation and with and without validation coefficients.

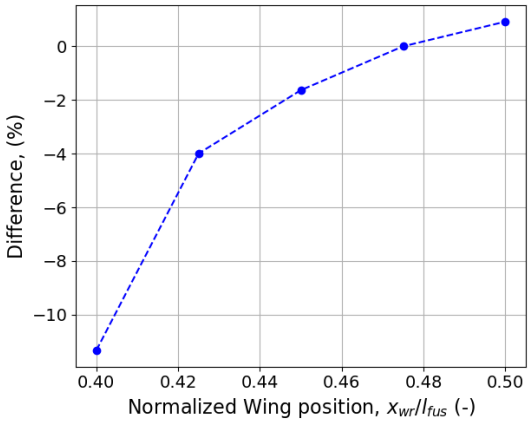

Figure 4.20: Sensitivity of validation coefficients for Configuration 1.

Shifting focus to stability, results for both Configurations remain consistent with and without validation coefficients. These coefficients have no bearing on the moment slope, thus leaving stability unaffected.

In conclusion, the impact of validation coefficients on the results is minimal, especially for more aft wing positions. Larger differences are noted for rotation in more forward wing positions. Consequently, the validation coefficients will be retained for further analysis, but it's crucial to note their minimal effect, particularly for aft wing positions.

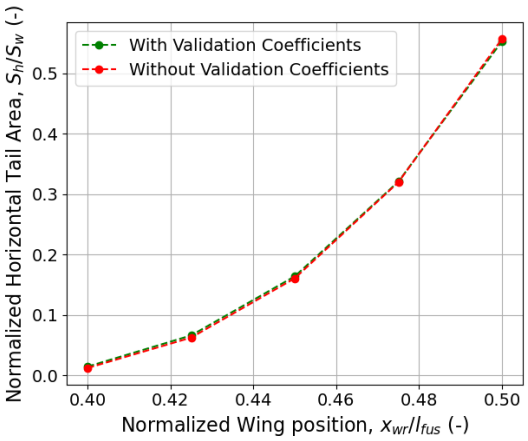

Figure 4.21: Configuration 2 minimum horizontal area (for different wing positions) for rotation and with and without validation coefficients.

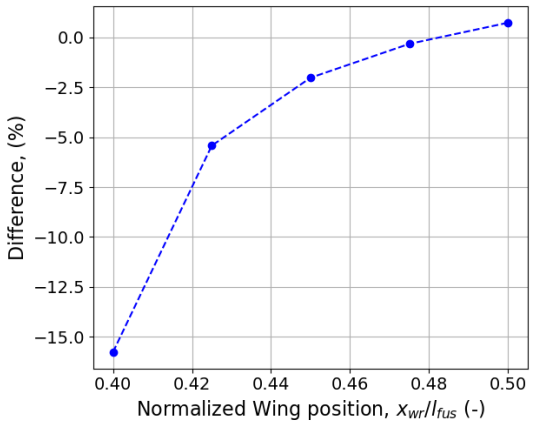

Figure 4.22: Sensitivity of validation coefficients for Configuration 2.

4.3.2. GROUND EFFECT

A sensitivity analysis is performed in order to see the effect of the ground effect on the model results, as shown in Figure 4.23. This is the rotation performance for Configuration 1. The difference is very small, as seen in Figure 4.24. Finally, the same results are observed for Configuration 2 (Figure 4.25 and Figure 4.26).

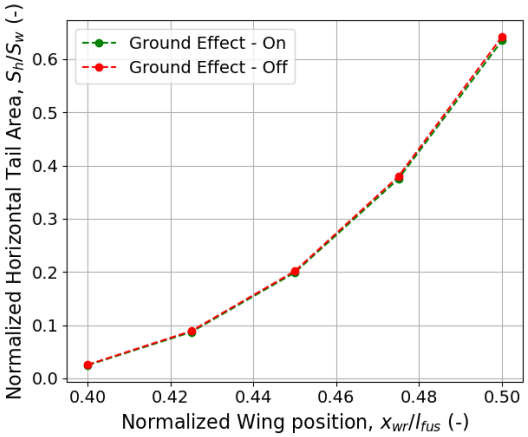

Figure 4.23: Configuration 1 minimum horizontal area (for different wing positions) for rotation and with and without ground effect.

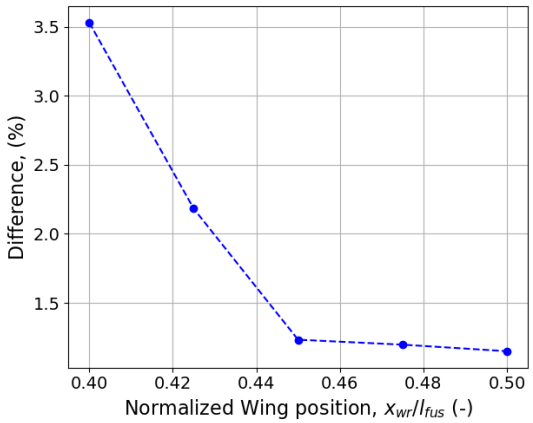

Figure 4.24: Sensitivity of ground effect for Configuration 1.

Moreover, a sensitivity analysis was performed on the lift curve slope. This was done to see the effect of a higher slope value on the results. The lift curve slope of the wing was increased by 10%. In Figure 4.27 the results for Configuration 1 and in Figure 4.29 results for Configuration 2 are shown. The increased lift curve slope has a noticeable effect on the results and reduces the needed horizontal tail size. However, with a lower (original) lift curve slope the tail size is only overestimated (safe design). Moreover, low tail values (below 0.1) should not be expected (for ATR-72 it is 0.19 [12]). This means that the error magnitude is in the range of 5%.

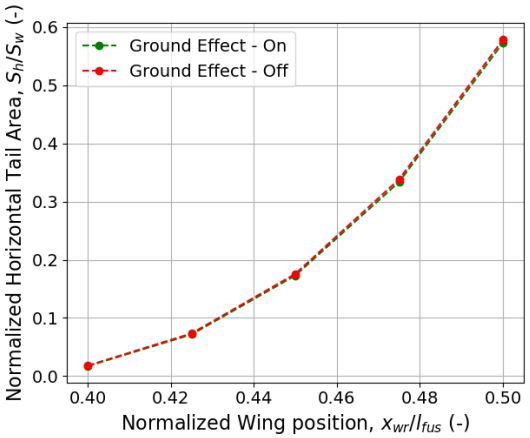

Figure 4.25: Configuration 2 minimum horizontal area (for different wing positions) for rotation and with and without ground effect.

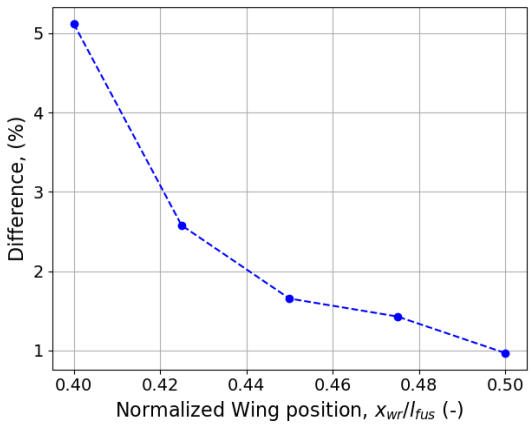

Figure 4.26: Sensitivity of ground effect of Configuration 2.

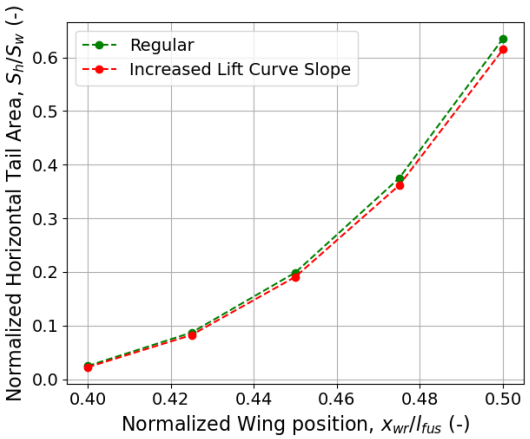

Figure 4.27: Configuration 1 minimum horizontal area (for different wing positions) for rotation and with and without increased lift curve slope.

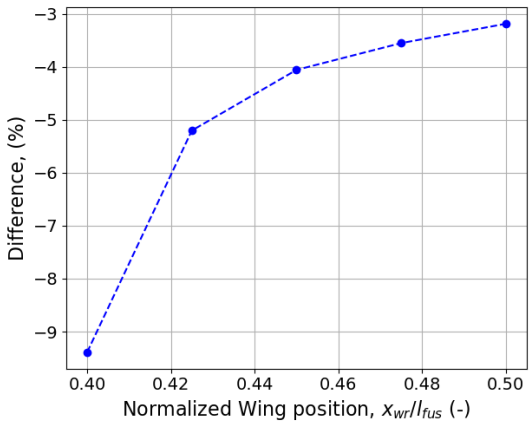

Figure 4.28: Sensitivity of lift curve slope for Configuration 1.

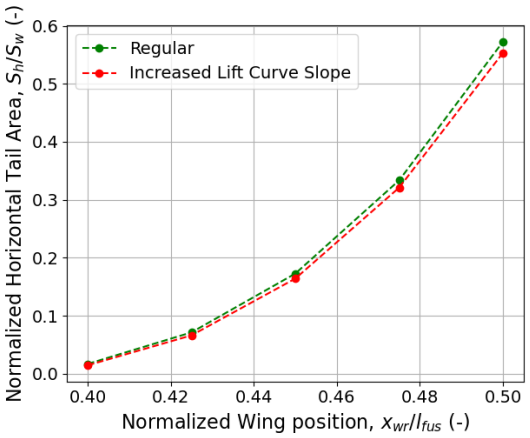

Figure 4.29: Configuration 2 minimum horizontal area (for different wing positions) for rotation and with and without increased lift curve slope.

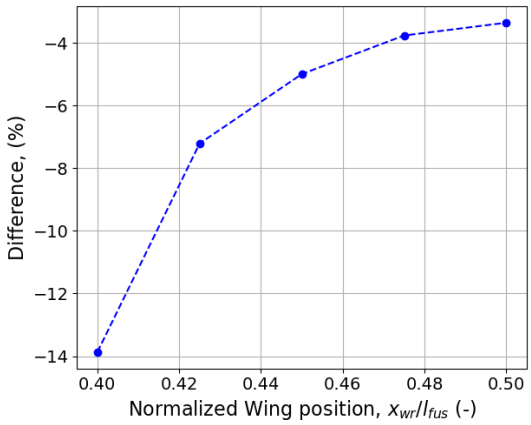

Figure 4.30: Sensitivity of lift curve slope for Configuration 2.

5

Results and Discussion

In this chapter, the results are presented. This includes the analysis of propeller effects, where Configurations 1 and 2 are compared for different flight conditions to see how propeller effects influence the aircraft. Later, the minimal tail and aileron size for each configuration is presented and discussed. Moreover, the longitudinal dynamic stability of each configuration is briefly discussed. Finally, a sensitivity analysis is performed on the DEP aircraft's vertical location of the horizontal tail, the placement of batteries in the wing, and the placement of reserve fuel in the fuselage.

5.1. Impact of Propeller Effects on Stability and Control of an Aircraft

To analyze the influence of propeller effects on the stability and control of a conventional aircraft configuration before adding the additional complexity of a distributed-propulsion system, Configuration 1 and 2 results were compared. Both of the configurations were kept with the same horizontal tail size (0.265, normalized to wing area) and wing position (0.459, normalized to fuselage length). In the subsections below, the influence of propeller effects for the same geometry is presented and discussed for stability, trim, rotation, and roll of the aircraft. Note that the aircraft meets the set-out requirements, but are not exactly sized for them, as the purpose of this chapter is to show the influence of propeller effects on the same aircraft configuration.

Both configurations feature the same weight distribution. Thus, the loading diagram is the same for both and is presented in Figure 5.1. The center of gravity of the aircraft is located in front of the aerodynamic center and ranges from about 0.03 to 0.17 of the mean aerodynamic chord. The range is small, as the fuel volume is low and the loading of payload is assumed to be evenly distributed.

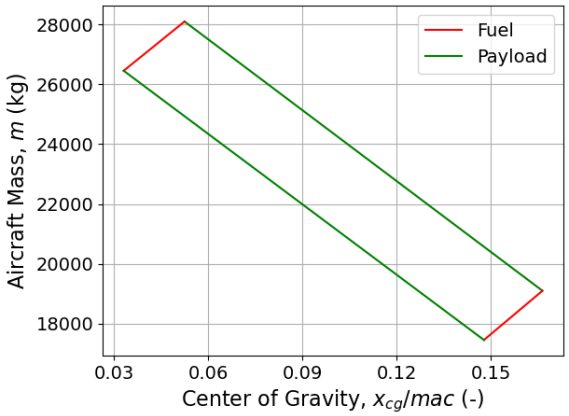

Figure 5.1: Loading diagram for Configuration 1 and 2.

5.1.1. STABILITY

As discussed before in Chapter 2, a propeller aircraft is less stable [9]. This is also the case for Configuration 2, as seen in Figure 5.2. In general, the requirement for horizontal tail size is higher for Configuration 2, as also discussed by Zhao [30]. Interestingly, the limiting condition for Configuration 1 and Configuration 2 is not the same. For Configuration 1, the limiting condition is the stall speed, whereas Configuration 2 suffers the most after take-off (lift-off).

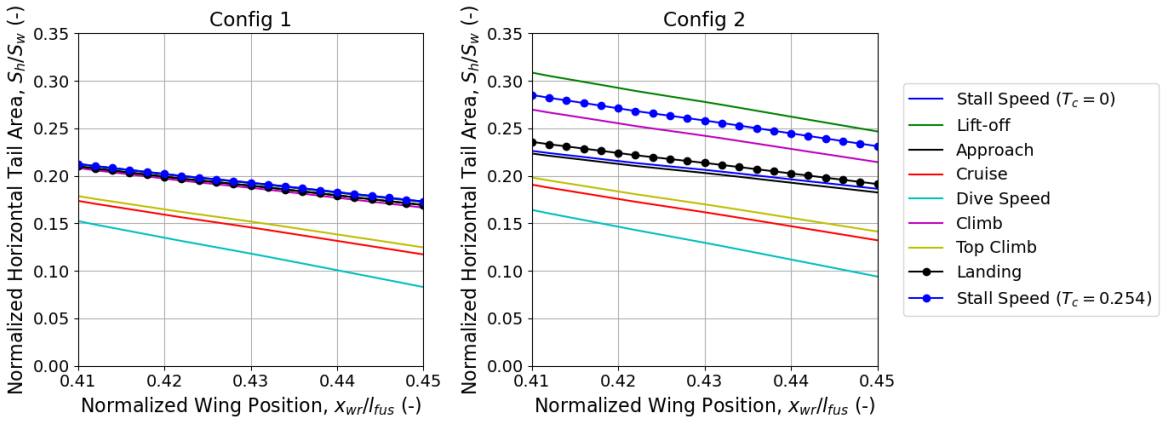

Figure 5.2: Minimum horizontal tail area size to ensure that the aircraft is stable for different conditions, wing position, and configurations for MTOW and most aft CG position.

Configuration 1 suffers the most for stability at stall speed due to the larger downwash created compared to other flight conditions. The lift coefficient at this condition is the highest; thus, the most downwash is generated during this condition. The high downwash reduces the effectiveness of the horizontal tail, as can be deduced from Equation 3.52.

On the other hand, Configuration 2 suffers even more at stall speed, as seen in Figure 5.3. As can be seen, Configuration 2 still has a lower magnitude slope, as expected. This lower stability is mainly caused by the propeller's normal force (Figure 5.4), as propellers are ahead of the center of gravity. The same conclusion has also been reached in Vaart's work [27].

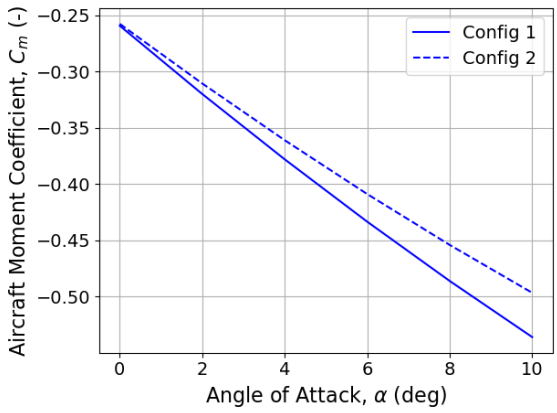

Figure 5.3: Aircraft moment coefficient versus angle of attack at stall speed for MTOW and most aft CG position (T_C=0).

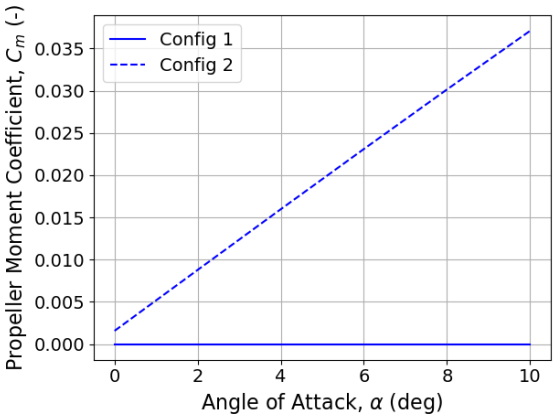

Figure 5.4: Propeller moment coefficient versus angle of attack at stall speed for MTOW and most aft CG position (T_C=0).

Configuration 2 suffers most after take-off because the thrust coefficient is highest. Due to the high thrust setting, a lot of downwash is generated, which lowers the effectiveness of the horizontal tail, as discussed previously. Also, this decrease in horizontal tail effectiveness due to downwash has been observed in Bouquet's work [9], and the importance of downwash in tail sizing was mentioned by Obert [4].

Again, after take-off, Configuration 2 is less stable, as can be seen from the slope of the pitching curve in Figure 5.5. The downwash increases with respect to angle of attack for Configuration 2 much more, as

presented in Figure 5.6. This is because the thrust setting is high (as this happens right after take-off), and this causes extra downwash due to the propeller slipstream. Thus, the effectiveness of the horizontal tail is reduced, as seen in Figure 5.7.

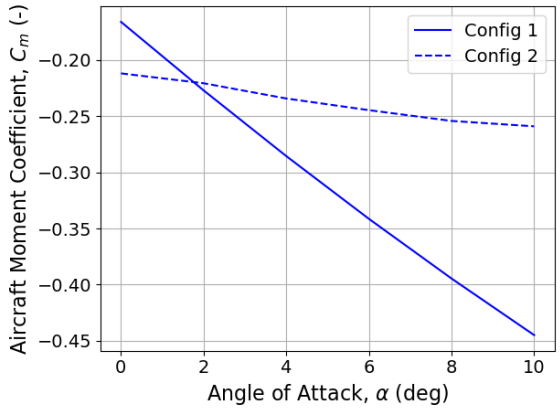

Figure 5.5: Aircraft moment coefficient versus angle of attack after take-off for MTOW and most aft CG position (T_C=0.368).

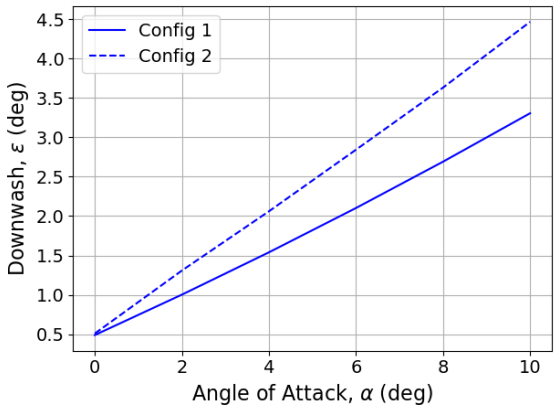

Figure 5.6: Downwash versus angle of attack after take-off for MTOW and most aft CG position (T_C=0.368).

Interestingly, no significant wing moment slope increase is observed in Figure 5.8. This contradicts the findings of Bouquet [32], where the author claimed that the slope increases due to the higher dynamic pressure over the wing caused by the propeller. However, in the paper, no lift reduction due to the change of angle of attack at the wing caused by the propeller downwash was included. The two effects counteract each other (discussed later in more detail in Subsection 5.1.3); thus, the lift increases due to propellers minimally scales with the angle of attack (Configuration 2 has a slightly higher magnitude slope). On the other hand, only an offset is added, as seen in Figure 5.8 due to the higher starting lift caused by the flaps (discussed in Subsection 5.1.3).

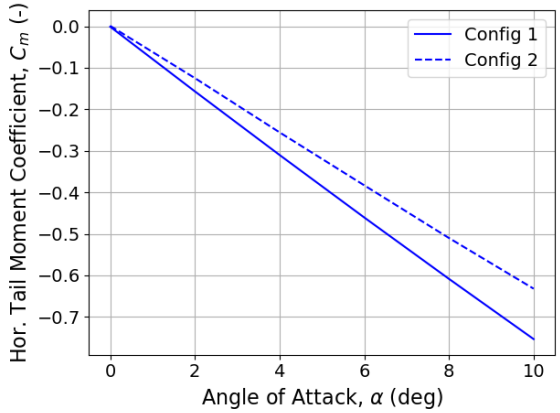

Figure 5.7: Horizontal tail moment coefficient versus angle of attack after take-off for MTOW and most aft CG position (T_C=0.368).

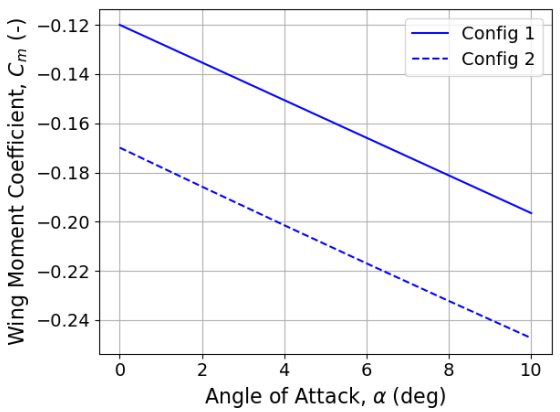

Figure 5.8: Wing moment coefficient versus angle of attack after take-off for MTOW and most aft CG position (T_C=0.368).

5.1.2. TRIM

To explain the effect of propellers on the trim of the aircraft, Figure 5.9 and Figure 5.10 can be used. In Figure 5.9, the trimming of an aircraft without propeller effects is depicted. On the y-axis is the horizontal tail lift coefficient and the x-axis shows the horizontal tail size (the scaling is not accurate, for illustration purposes). A positive elevator deflection leads to a more positive lift coefficient (more negative moment coefficient) and a negative elevator deflection does the opposite. For no elevator deflection, a horizontal tail has a positive lift coefficient (unless the horizontal tail features a negative incidence angle), which increases with tail size, as seen in Figure 5.9. To get the minimum needed horizontal tail size two extra curves can be added for

maximum positive and negative elevator deflection, as done in Figure 5.9. These are the limits for the horizontal tail lift coefficient. Then by putting in the needed lift coefficient and seeing where it interacts with the maximum or minimum horizontal tail lift line, the minimum tail size can be received (Figure 5.9).

The same curve is presented but for an aircraft with a propeller in Figure 5.10. The dashed line depicts the curve of the aircraft without a propeller and the solid line is for the propeller aircraft. Two factors play a role in the curve. The first one is the downwash created. Propeller aircraft generate more downwash at the horizontal tail, thus, the curves (also the maximum deflection curves) are scaled down, as less lift is generated (or more negative lift). This increases the performance if the tail-off moment is negative (pitch down), while reduces for positive tail-off moment (pitch up).

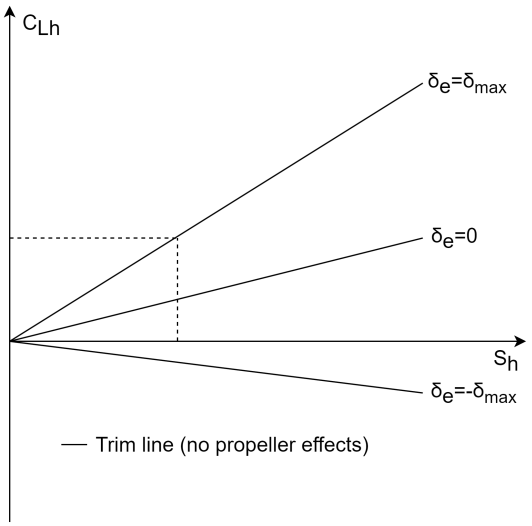

Figure 5.9: Conceptual sketch of aileron deflection effect on horizontal tail lift.

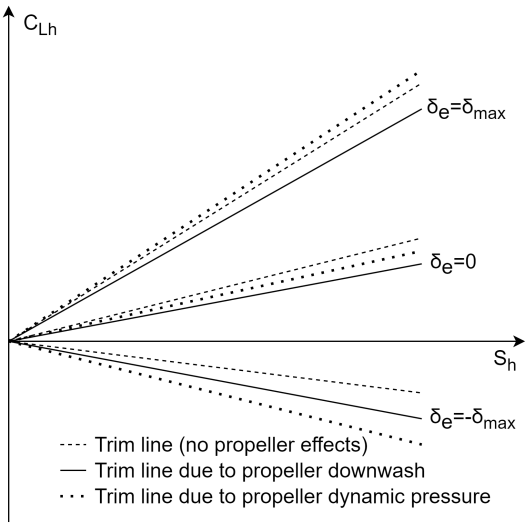

Figure 5.10: Conceptual sketch of aileron deflection effect on horizontal tail lift with propeller effects.

The second effect is the dynamic pressure increase at the horizontal tail, which increases the slope magnitude (depicted by a dotted line). This effect helps for both pitch-up and pitch-down tail-off moments. However, the configurations analyzed did not have any increase in dynamic pressure (the horizontal tail was not covered in the propeller slipstream for any flight conditions), thus, this is irrelevant for further discussion.

The minimum tail size (normalized) needed for different conditions and wing locations for Configuration 1 and 2 is presented in Figure 5.11. As can be seen, for conditions with high thrust setting the difference between Configuration 1 and 2 increases. Moreover, the trim requirement increases with lower speed. Thus, the most limiting condition is mostly stall speed (for the more forward wing, trim after take-off also becomes more limiting for Configuration 1).

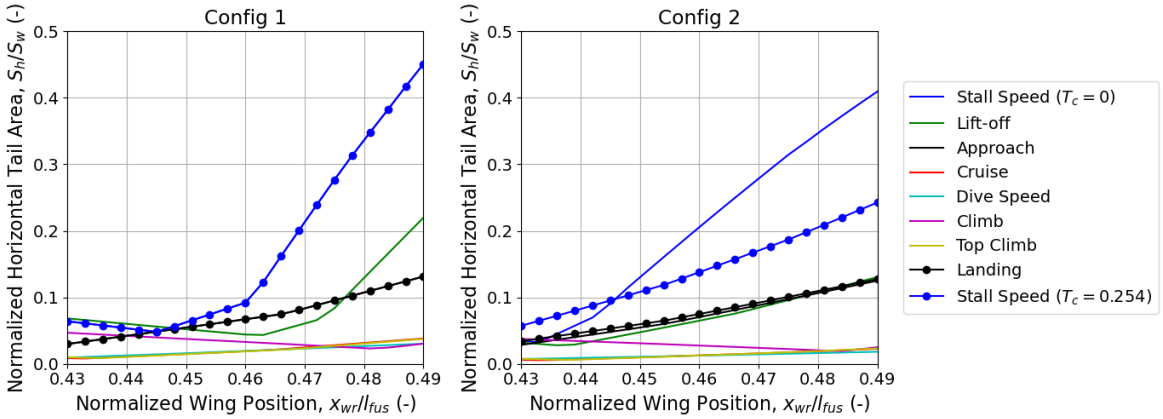

Figure 5.11: Minimum horizontal area size for trim and different conditions, wing position, and configurations.

The reader should note that for different wing positions different configurations are better. This is because propeller effects tend to increase the pitch-up moment of the aircraft (propeller normal force, extra downwash generated). Thus, for a forward placed wing propeller effects will usually increase the needed tail size, whereas for backward placed wing the tail size could be reduced. This effect can also be seen in Figure 5.11. Configuration 1 (solid lines) tail size increases much more with more aft wing position, whereas the same happens for Configuration 2 (dashed lines) for a wing position at the front. This correlates to Figure 5.10, where the effectiveness of an aircraft with propeller effects increases with a negative lift coefficient (more pitch up needed - aft wing position).

In general, one could expect a wing position where the needed horizontal tail size is zero (all moments balanced). This is true when considering a single center of gravity position and weight. However, the analysis was done with two different center of gravity locations (minimum and maximum) and aircraft mass (minimum and maximum). Due to this, the kinks can be observed for the horizontal tail size, which is limited by the highest minimum tail size needed for the four center of gravity possibilities. Finally, the reader should note that the horizontal tail area for trim is much less limiting than the one needed for rotation and stability. Thus, the designs discussed later are only limited by the rotation (controllability) and longitudinal stability.

5.1.3. ROTATION

While Configuration 1 is more stable, on the other hand, Configuration 2 showed a much better performance at rotation, as seen in Figure 5.12. Besides reaching the required lift sooner, Configuration 2 also features a lower pitch angle, as seen in Figure 5.13. This is beneficial considering the tail strike possibility.

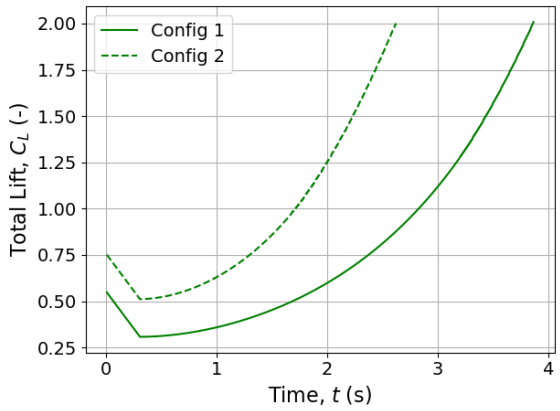

Figure 5.12: Aircraft lift coefficient during rotation for MTOW and most forward CG position (T_C=0.368, $\delta_{e_{max}}$=30°).

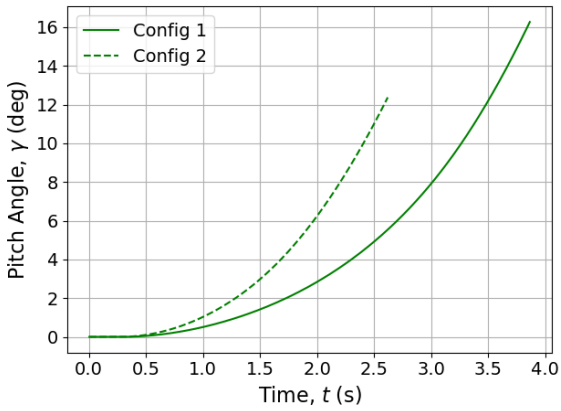

Figure 5.13: Aircraft pitch angle during rotation for MTOW and most forward CG position (T_C=0.368, $\delta_{e_{max}}$=30°).

The main reason, Configuration 2 has a better rotation performance, is the created lift at the start of rotation, as seen in Figure 5.12 (the offset between the two curves). This is because the wing generates more lift (and the wing is in front of main landing gear - generating more positive moment), as seen in Figure 5.14. Due to this the rotation starts slightly sooner (as a positive pitching moment is reached sooner) and reaches a higher initial angular acceleration (due to a higher net moment created), as depicted in Figure 5.15. The kink seen in Figure 5.12 is due to the horizontal tail generating increasing negative lift (reduction in total lift) until the aircraft starts to rotate (increasing total lift). Moreover, the zig-zag lines seen in Figure 5.15 are due to the controller limiting the acceleration of the aircraft at about 6 deg/s^2 [10].

The higher lift is caused by the increased dynamic pressure in the propeller slipstream. At take-off the propeller operates at high thrust settings, thus, a higher axial velocity is induced in the slipstream. This higher lift due to the propeller slipstream can be seen in Figure 5.16. On the other hand, the propeller slipstream also reduces the local angle of attack at the wing, reducing the lift generated, however, this effect is minimal at a low pitch angle, as seen in Figure 5.17.

Finally, the slipstream affects the flaps and they also generate more lift, as seen in Figure 5.18. The slight decrease observed for the Configuration 2 flap lift is due to the increasing pitch and the slipstream covering less of the wing. Adding the extra flap lift, extra lift due to dynamic pressure increase, and subtracting the lift decrease due to the change in angle of attack, a net positive lift increase is observed - increasing the performance of an aircraft with propeller effects.

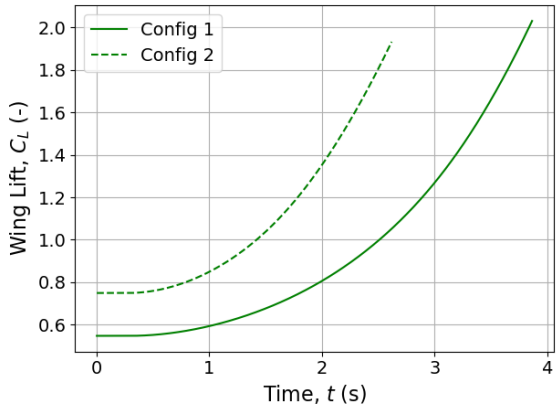

Figure 5.14: Wing lift coefficient during rotation for MTOW and most forward CG position (T_C=0.368, $\delta_{e_{max}}$=30°).

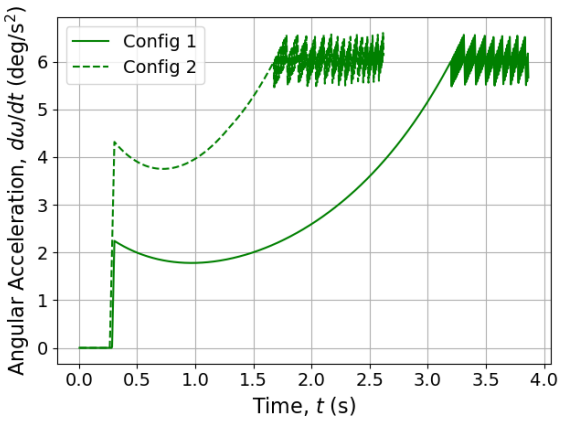

Figure 5.15: Aircraft angular acceleration during rotation for MTOW and most forward CG position (T_C=0.368, $\delta_{e_{max}}$=30°).

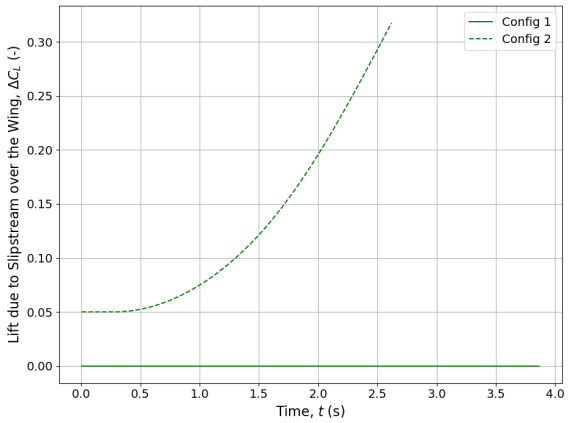

Figure 5.16: Extra lift generated due to increased dynamic pressure at the wing for MTOW and most forward CG position (T_C=0.368, $\delta_{e_{max}}$=30°).

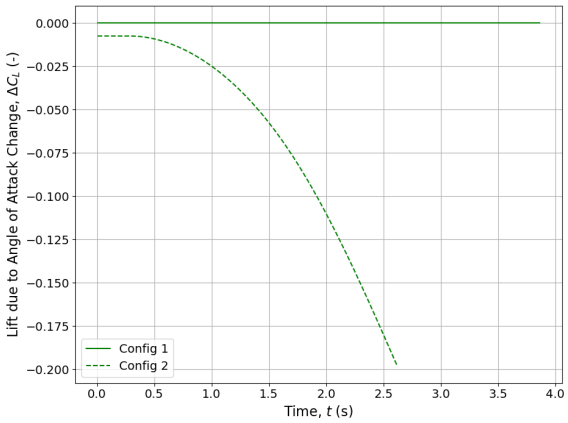

Figure 5.17: Extra lift generated due to change in angle of attack in propeller slipstream for MTOW and most forward CG position (T_C=0.368, $\delta_{e_{max}}$=30°).

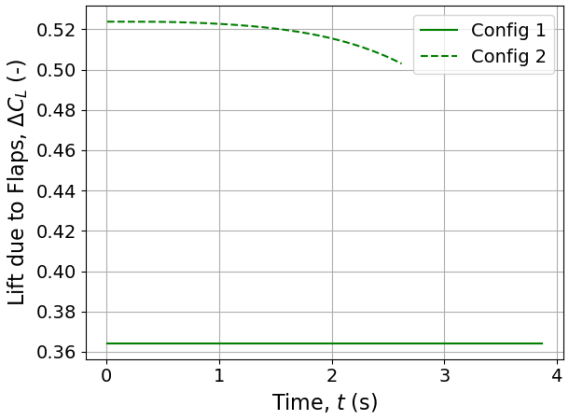

Figure 5.18: Extra lift generated due to flaps for MTOW and most forward CG position (T_C=0.368, $\delta_{e_{max}}$=30°).

5.1.4. ROLL

Regarding the roll performance, both configurations showed very similar results (Figure 5.19). However, Configuration 1 has a slightly better performance. It should be noted that the roll was done at approach speed,

as it is the most limiting condition due to low aerodynamic surface effectiveness (rolling at stall speed would stall the aircraft completely), while the moment of inertia is the same.

The reason Configuration 2 has a slightly lower roll performance is the propeller damping, as seen in Figure 5.20. Due to the roll motion, propellers generate normal force, which creates a moment acting against the motion. Due to this the angular speed and angular acceleration (Figure 5.21 and Figure 5.22, respectively) are slightly lower. Moreover, the parts of the wing covered in the propeller slipstream have a higher damping force due to the higher dynamic pressure. However, these results do not diverge, as the aerodynamic damping increases with higher roll speed. Thus, Configuration 1, stays close to Configuration 2. On the other hand, an aircraft with distributed propellers will feature a higher propeller damping, as the moment arm increases.

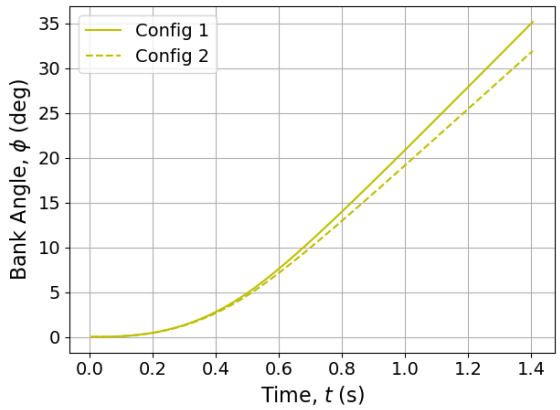

Figure 5.19: Aircraft bank angle during roll manoeuvre (T_C=0.254, δ_a=20°).

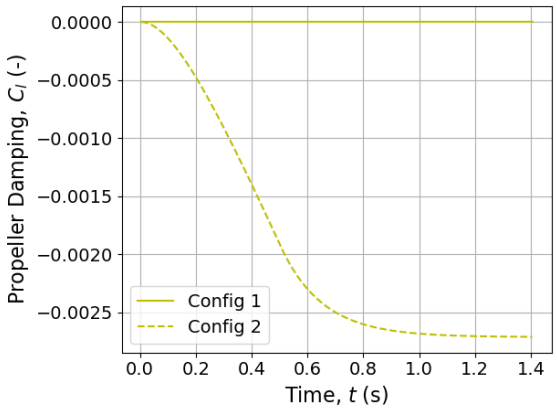

Figure 5.20: Propeller damping during roll maneuver (T_C=0.254, δ_a=20°).

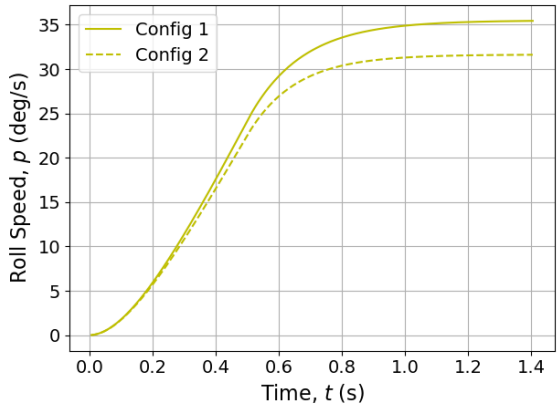

Figure 5.21: Aircraft angular speed during roll manoeuvre (T_C=0.254, δ_a=20°).

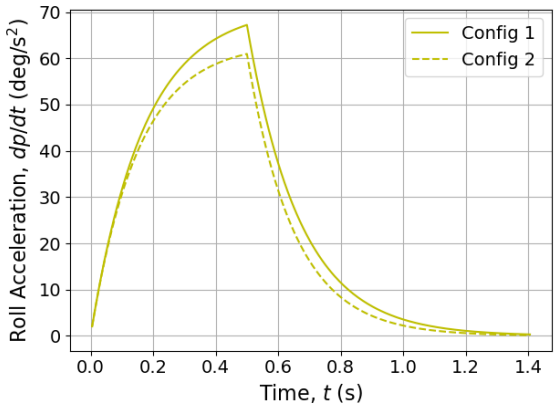

Figure 5.22: Aircraft angular acceleration during roll manoeuvre (T_C=0.254, δ_a=20°).

5.2. FINAL CONFIGURATION RESULT COMPARISON

In this section, the optimal designs for each configuration are presented. In Figure 5.23, the minimal tail size curves for different configurations and wing positions are shown. The optimal locations for all configurations are where the rotation and stability lines intersect (for Configuration 1 this is around [0.42, 0.20], for Configuration 2 - [0.44, 0.26], and for Configuration 3 - [0.42, 0.21]). In general, Configuration 1 is the most stable, whereas aircraft with propeller effects (Configuration 2 and 3) feature a better rotation performance, as also confirmed by Bouquet [9] for twin turboprop aircraft. Configuration 1 has the lowest tail ratio, closely followed by Configuration 3; Configuration 2 has the highest tail ratio. This is due to the lower stability, which is described in detail in later sections.

An overview of the final designs (sized for smallest horizontal tail size) is given in Table 5.1. The wing is more aft for Configuration 2 to compensate for the lower aircraft stability (more aft wing makes the aircraft more stable but reduces rotational performance). Moreover, the aileron area ratio is highest for Configuration 2 and 3. A more detailed explanation of each configuration's performance for different flight qualities is explained in the sections below.

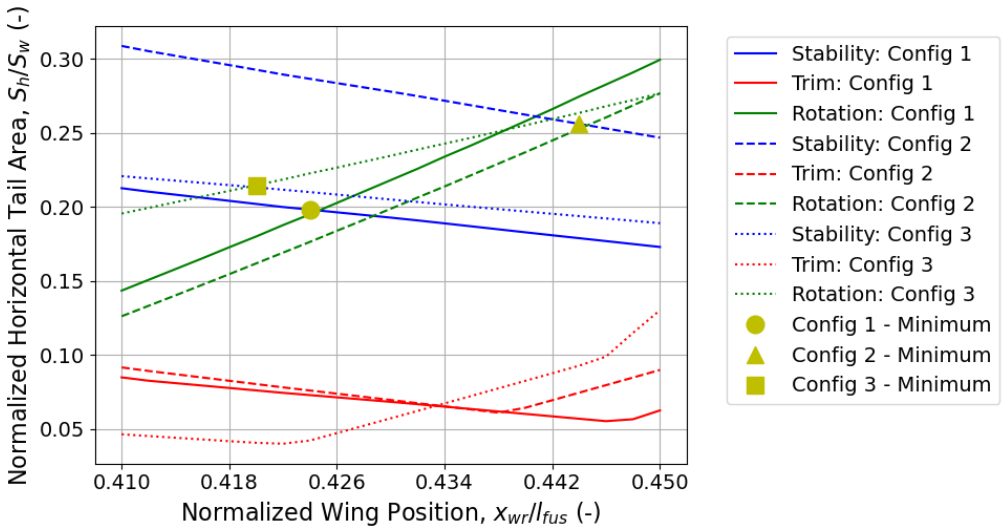

Figure 5.23: Minimal horizontal tail size for different wing positions and configurations.

Table 5.1: Aircraft parameters for each finalized configuration.

Parameter	Values			Normalization	Normalized values		
	Config 1	Config 2	Config 3		Config 1	Config 2	Config 3
Wing position (m)	12.88	13.48	14.17	x_{wr}/l_{fus}	0.424	0.444	0.42
Tail area (m^2)	12.72	16.44	31.68	S_h/S_w	0.20	0.26	0.21
Aileron area (m^2)	3.36	3.97	9.18	S_a/S_w	0.052	0.062	0.062
Aileron span (m)	3.53	4.08	5.39	b_a/b_w	0.26	0.29	0.26
I_{xx} (kgm^2)	135946	135946	1093578	$I_{xx}/m/b_w^2$	0.0063	0.0063	0.0082
I_{yy} (kgm^2)	733350	731474	2694020	$I_{yy}/m/l_{fus}^2$	0.028	0.028	0.031

The three configurations are compared to two other similar aircraft in Table 5.2. The aircraft are ATR 72 and Bombardier Q400. Both aircraft are twin turboprop with similar wingspan. However, the fuselage of Bombardier Q400 is longer than ATR 72. All aircraft have similar tail area ratios. Moreover, the tail volume coefficients are also within the range. Notice that a longer fuselage increases the tail volume, which is the case for real aircraft and configurations. This is because the fuselage is destabilizing, thus, due to a longer fuselage the tail needs to be larger. The aileron dimensions are also similar between the aircraft. Keep in mind that the aircraft have different aileron-to-chord ratios, thus, some difference between the aileron span and aileron area is expected. Moreover, Configuration 3 features folding wing tips, which reduce the aileron moment arm, but increase the force (larger wing surface affected by the aileron).

Table 5.2: Tail area, fuselage length, and tail volume coefficient for different aircraft [12].

Aircraft	S_h/S_w	l_{fus}/b_w	V_h	S_a/S_w	b_a/b_w
Config 1	0.20	1.10	1.31	0.052	0.26
Config 2	0.26	1.10	1.64	0.062	0.29
Config 3	0.21	0.80	1.03	0.062	0.26
ATR 72	0.19	1.00	1.13	0.074	0.26
Bombardier Q400	0.27	1.16	1.77	0.047	0.24

The loading diagrams for each configuration are presented in Figure 5.24, Figure 5.25, and Figure 5.26. It

can be seen that the wing of the DEP aircraft is placed in front of the center of gravity (all CG points are aft of 25% of the mean aerodynamic chord) while Configuration 1 features a wing placed close to the center of gravity (some CG points are forward and aft of 25% of the mean aerodynamic chord). Moreover, uncommonly for a DEP aircraft the center of gravity range is quite big. This is due to the reserve fuel tank being placed away from the center of gravity (fuselage end).

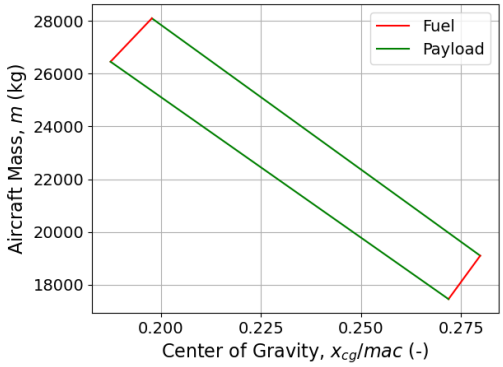

Figure 5.24: Configuration 1 loading diagram.

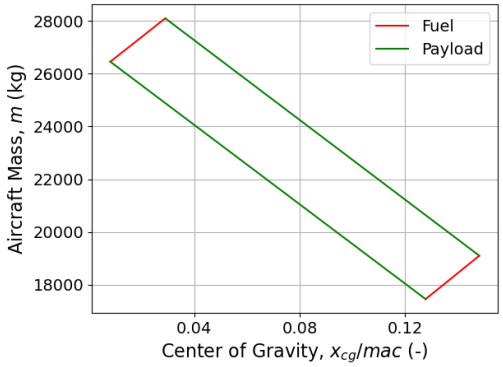

Figure 5.25: Configuration 2 loading diagram.

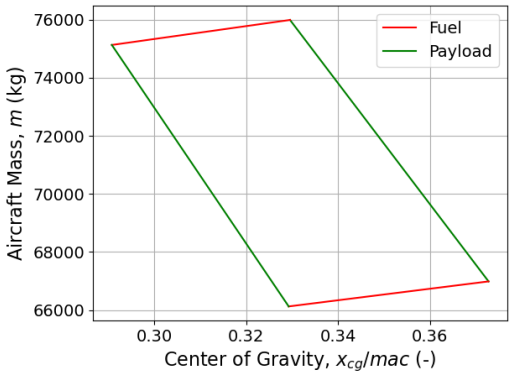

Figure 5.26: Configuration 3 loading diagram.

Finally, the reader should keep in mind that the graphs are discrete (Figure 5.23). Due to this, the best wing position and horizontal tail size are not the optimal ones due to discretization. In Figure 5.27 this is shown. Due to this, some results might seem that the horizontal tail can be even smaller (like the ones presented in Subsection 5.2.3 for Configuration 1 and 2 where the rotation time is much smaller than 5 seconds). This is because the selected point is on the left (Figure 5.27) and the most critical flight condition is stability while there is some buffer for the rotation (reducing the rotation time more than needed). However, it should be noted that the maximum difference between two neighboring wing positions is not more than 76 mm, ensuring that the discretization error is small.

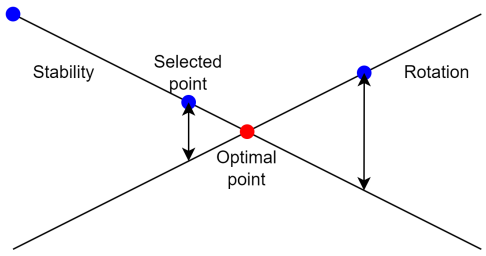

Figure 5.27: Discretization and optimal value of the results.

5.2.1. STABILITY

The moment curves of the final designs are presented in Figure 5.28. These are for lift-off (right after the aircraft takes off), as it is the most limiting condition (for propeller aircraft). As can be seen, the curves have a negative slope, thus, the aircraft are stable. Configuration 2 has a negative offset (compared to Configuration 1 and 3) due to the wing being placed more aft, as seen in Figure 5.29 (the wing generates higher magnitude and negative moment). In Figure 5.29, also the forward center of gravity wing placement of Configuration 1 and 3 can be seen (positive slope).

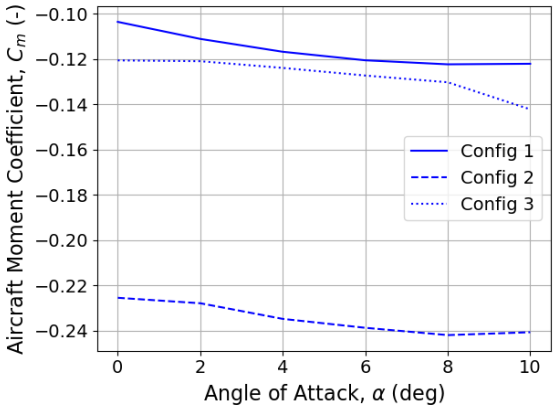

Figure 5.28: Moment curves of the final configurations for MTOW and most aft CG position ($T_{C_{1,2}}$=0.368, T_{C_3}=0.352).

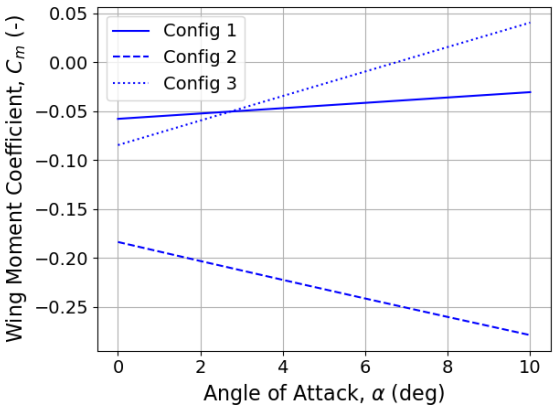

Figure 5.29: Wing moment curves of the final configurations for MTOW and most aft CG position ($T_{C_{1,2}}$=0.368, T_{C_3}=0.352).

The horizontal tail moment contribution is presented in Figure 5.30. Keep in mind that these curves are for the final designs. Thus, the low effectiveness of Configuration 3 tail is due to its size, as not much is needed due to the low fuselage moment, as presented in Figure 5.31. This is because the DEP aircraft features a relatively shorter fuselage (Table 5.2). Moreover, DEP aircraft propeller contribution to stability is better than Configuration 2, as seen in Figure 5.32. This is due to the propellers being close to the wing (more aft) and distributed (due to wing sweep outer propellers being more aft), as can be conceptually seen in Figure 3.4 and Figure 3.6. Thus, the moment is lower than compared to a twin turboprop aircraft. In Figure 5.33, the downash curves are given. It can be seen that Configuration 3 has the highest downwash, reducing the horizontal tail effectiveness, however, due to the low fuselage destabilizing moment and lower propeller destabilizing moment, Configuration 3 is more stable than Configuration 2. On the other hand, Configuration 1 is even still more stable with the higher fuselage contribution. This is also in line with Kim's work [36] where the authors state that the DEP aircraft stability is worse due to the propeller normal force. However, the downwash contribution is not mentioned in the article.

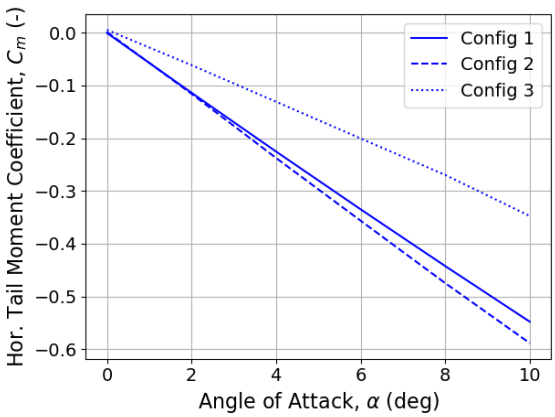

Figure 5.30: Horizontal tail moment curves of the final configurations for MTOW and most aft CG position ($T_{C_{1,2}}$=0.368, T_{C_3}=0.352).

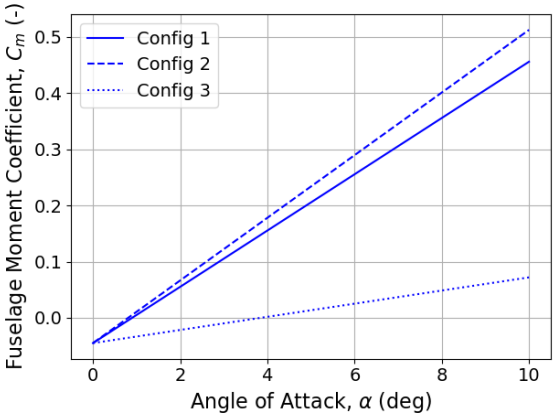

Figure 5.31: Fuselage moment curves of the final configurations for MTOW and most aft CG position ($T_{C_{1,2}}$=0.368, T_{C_3}=0.352).

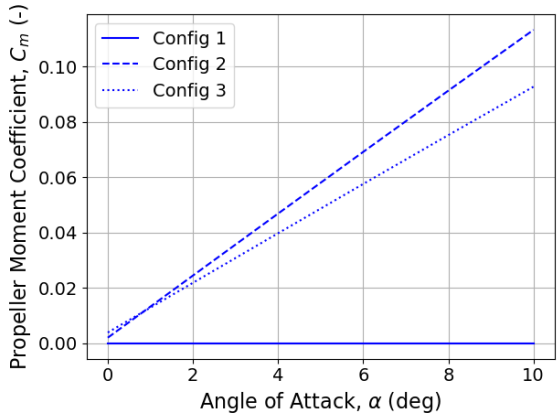

Figure 5.32: Propeller moment curves of the final configurations for MTOW and most aft CG position ($T_{C_{1,2}}$=0.368, T_{C_3}=0.352).

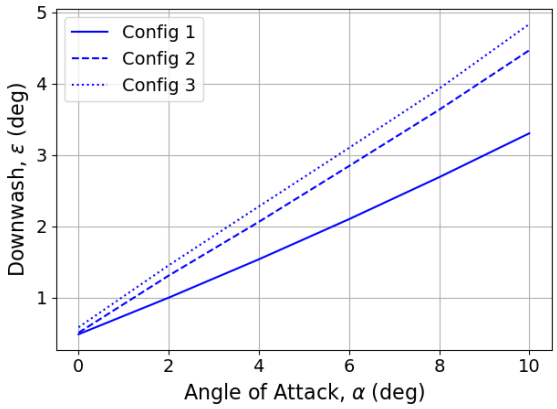

Figure 5.33: Downwash curves of the final configurations for MTOW and most aft CG position ($T_{C_{1,2}}$=0.368, T_{C_3}=0.352).

5.2.2. TRIM

Trim is not the limiting condition for the horizontal tail sizing (Figure 5.23), however, in this section, it will be analyzed to see the difference between trimming a DEP aircraft to a twin turboprop aircraft. To begin with, it's important to note that the DEP aircraft possess a shorter center of gravity range, which is positioned closer to the aerodynamic center (Figure 5.26). This lowers the trim requirement, as a lower debalancing moment is generated, however, the fuselage and the wing generate a moment (even if the wing aerodynamic center coincides with the center of gravity). Thus, even with an aerodynamic center close to the wing, there is still some moment to be balanced by the horizontal tail.

The minimum horizontal tail areas for different wing positions and conditions are presented for Configuration 2 and 3 in Figure 5.34. For both Configurations stall speed is the most limiting condition. This is limiting, as at low speed the aircraft tends to pitch up (high fuselage moment). Thus, the horizontal tail needs to generate positive lift to pitch down, however, due to the downwash created (and the extra downwash due to propellers) this is harder to reach (downwash generates negative lift). That is why the propeller aircraft have stall speed as limiting condition.

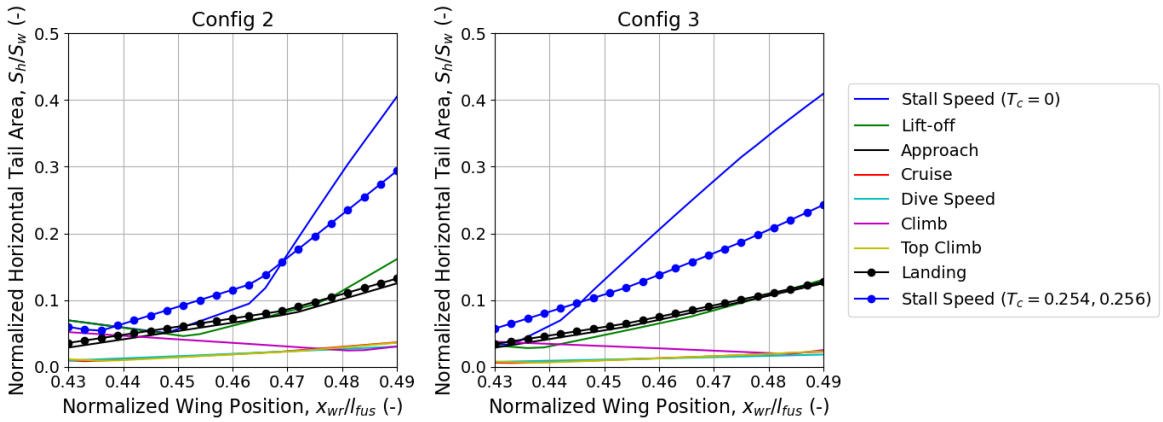

Figure 5.34: Minimum horizontal tail size for trim and different conditions, wing position, and configurations.

Interestingly, the stall speed without thrust becomes more limiting at more aft-placed wings. This is because the aft-placed wing generates a pitching down moment, meaning that it becomes larger than the fuselage moment and the aircraft has a tendency to pitch down. At this point the downwash contribution is good, however, with no thrust, there is less downwash generated. This is why the Configuration 3 trim performance can be seen to increase for more aft positions (lower slope) due to the higher downwash generated.

5.2.3. ROTATION

The results for rotation can be seen in Figure 5.35. Note that the final time is sensitive to the horizontal tail size, and a small increase in horizontal tail size can lead to a much lower take-off time. Looking at the results it can be seen that the DEP aircraft can take-off at an even lower pitch angle (reducing probability of tail strike). Looking at Figure 5.36 it can be seen that the configurations with propeller effects feature a higher starting lift, which was explained before. However, interestingly Configuration 2 and 3 feature a similar starting lift. This is because the increase in slipstream-induced lift over the wing (Figure 5.37) is compensated by the slipstream flap-induced lift (Figure 5.38). Configuration 2 features a bigger propeller positioned over the flap, thus, flap lift is higher than for Configuration 3. Moreover, the induced lift loss due to the change in the angle of attack in the propeller slipstream, also adds to this. The loss in lift due to changes in angle of attack is higher for Configuration 3 than for Configuration 2. Due to this, the net extra starting lift is the same for Configurations 2 and 3.

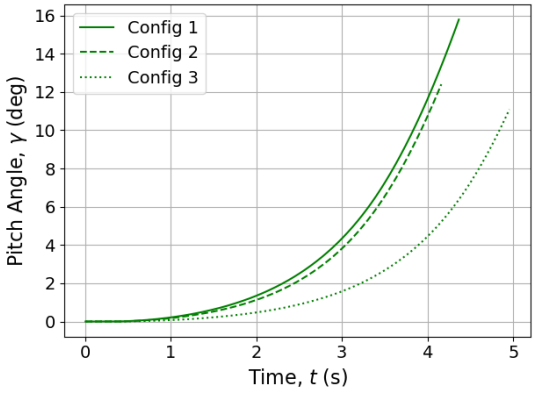

Figure 5.35: Aircraft pitch angle at rotation for final configurations for MTOW and most forward CG position ($T_{C_{1,2}}$=0.368, T_{C_3}=0.352, $\delta_{e_{max}}$=30°).

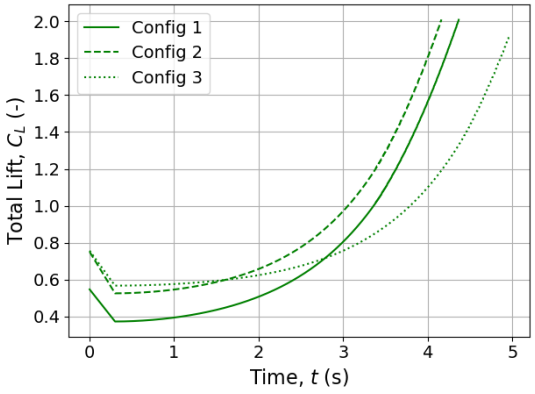

Figure 5.36: Total lift at rotation for final configurations for MTOW and most forward CG position ($T_{C_{1,2}}$=0.368, T_{C_3}=0.352, $\delta_{e_{max}}$=30°).

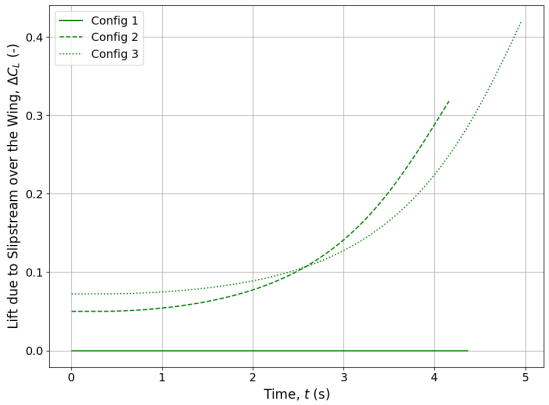

Figure 5.37: Lift increase due to slipstream over the wing at rotation for final configurations for MTOW and most forward CG position ($T_{C_{1,2}}$=0.368, T_{C_3}=0.352, $\delta_{e_{max}}$=30°).

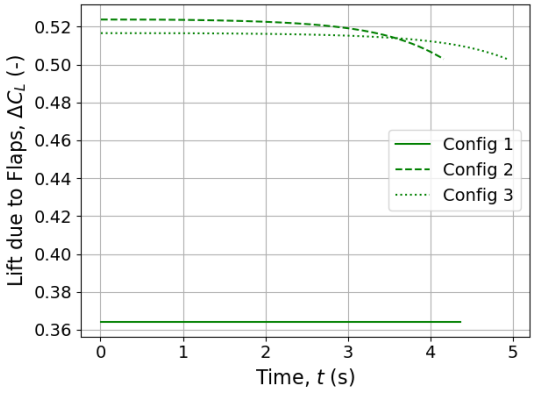

Figure 5.38: Lift increase due to flaps at rotation for final configurations for MTOW and most forward CG position ($T_{C_{1,2}}$=0.368, T_{C_3}=0.352, $\delta_{e_{max}}$=30°).

5.2.4. ROLL

For the roll, a high thrust condition with approach speed was selected. Stall speed is not possible, as one side would completely stall. As mentioned before, the lowest speed is the most limiting for roll, as the aerodynamic effectiveness decreases while the aircraft mass inertia stays the same. Moreover, the damping scales with speed, while the aileron moment with the square of speed. Thus, approach speed was selected. High thrust setting (the same as for the initial climb is selected), as propellers add damping (higher dynamic pressure over the wing increases damping).

The bank angle in time during roll for the three configurations is shown in Figure 5.39. Note that the requirement for Configuration 3 is lower (this is because the aircraft is heavier than 30 tons [10]). Moreover, the batteries are placed up to 34% of the half span to have the lowest possible moment of inertia (Figure 3.7). It can be seen in Figure 5.40 and Figure 5.41 that the DEP aircraft features a lower roll speed and acceleration, which is expected due to the 30% higher rolling inertia (Table 5.1). In addition, the propeller damping is much higher (Figure 5.43) even with the lower roll rate. Due to this, the total rolling damping is higher, as seen in Figure 5.44. However, this lower rolling performance is also with a more effective aileron (Figure 5.42) to compensate for the extra damping and moment of inertia.

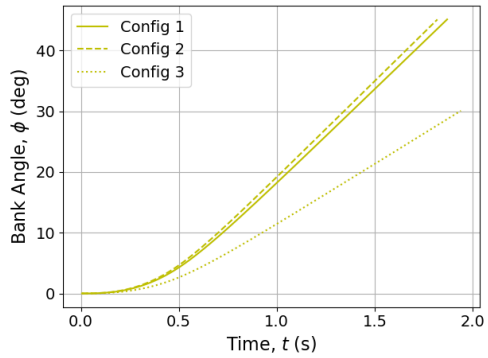

Figure 5.39: Bank angle of the configurations at roll ($T_{C_{1,2}}$=0.254, T_{C_3}=0.256, δ_a=20°).

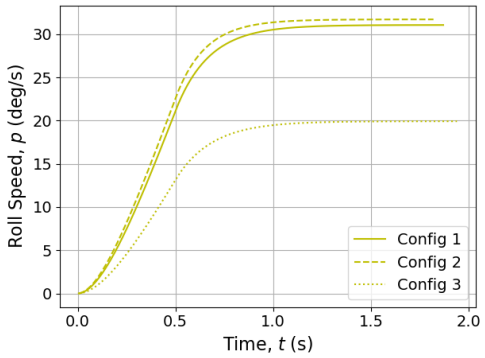

Figure 5.40: Rolling speed of the configurations at roll ($T_{C_{1,2}}$=0.254, T_{C_3}=0.256, δ_a=20°).

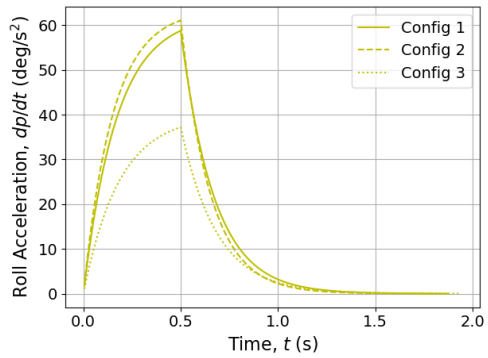

Figure 5.41: Rolling acceleration of the configurations at roll ($T_{C_{1,2}}$=0.254, T_{C_3}=0.256, δ_a=20°).

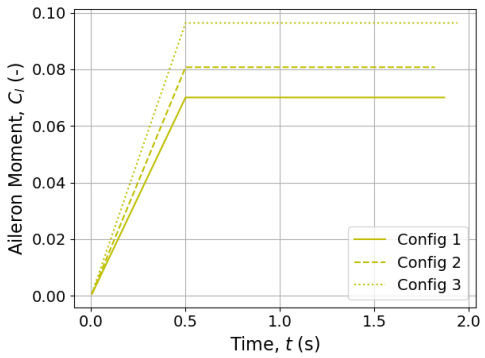

Figure 5.42: Aileron moment of the configurations at roll ($T_{C_{1,2}}$=0.254, T_{C_3}=0.256, δ_a=20°).

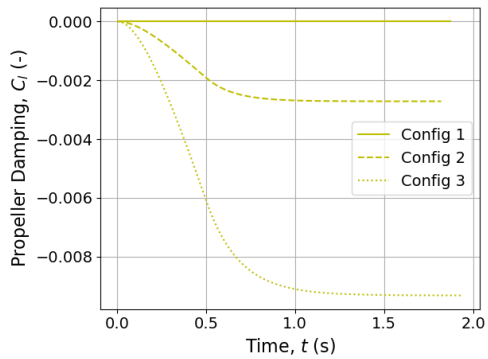

Figure 5.43: Propeller damping of the configurations at roll ($T_{C_{1,2}}$=0.254, T_{C_3}=0.256, δ_a=20°).

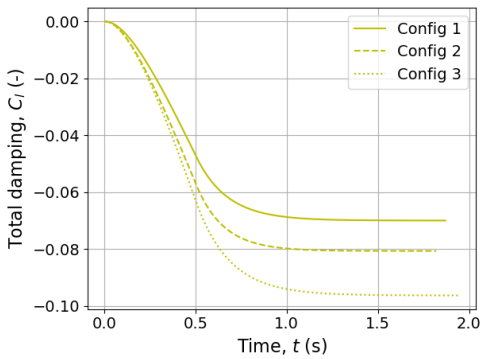

Figure 5.44: Total damping of the configurations at roll ($T_{C_{1,2}}$=0.254, T_{C_3}=0.256, δ_a=20°).

5.2.5. LONGITUDINAL DYNAMIC PERFORMANCE

In addition to ensuring static stability, it is crucial that the final designs also exhibit dynamic stability. The ranges of short-period and phugoid frequency and damping, along with the static margin range, are presented in Table 5.3 for all final configurations. Exact numbers for each flight condition, configuration, and mass distribution can be found in Appendix B. Upon examining the set requirements outlined in Chapter 2, it is evident that all configurations meet the suggested requirement for the short-period damping. However, the phugoid damping for some flight conditions is too low (mainly high-speed flight). It is important to note that these requirements are recommendations rather than strict mandates. Therefore, they can be surpassed for certification purposes. Nonetheless, a more comprehensive analysis is recommended for the short period and phugoid, or its consideration should be incorporated into the aircraft's tail-sizing process.

Table 5.3: Longitudinal dynamic motion frequency and damping for final configurations.

Parameter		Config 1	Config 2	Config 3
Short period	Natural frequency (rad/s)	0.525 - 3.172	0.674 - 4.180	0.579 - 3.085
	Damping	0.477 - 1.061	0.417 - 1.134	0.455 - 1.217
Phugoid	Natural frequency (rad/s)	0.078 - 0.258	0.078 - 0.258	0.077 - 0.243
	Damping	0.035 - 0.096	0.035 - 0.096	0.029 - 0.085
Static Margin		0.0176-0.280	0.0150-0.514	0.0167-0.246

The short period frequency is affected by static longitudinal stability, dynamic pressure, and the pitching moment of inertia [56]. Due to this, the lowest short period frequency is observed at low speeds for all configurations (lower dynamic pressure leads to lower frequency). All configurations have a similar normalized pitch moment of inertia (Configuration 3 has a slightly higher pitch moment of inertia due to the reserve fuel tank in the aft of the fuselage); thus, this does not bring any major differences. Finally, the frequency increases with a more negative moment slope—a higher static margin. As can be seen in Table 5.3, the maximum static margin values correspond to the short period maximum frequencies. The static margin is discussed later in this section.

The short period damping is also affected by the static margin. The main aircraft parameter affecting the short period damping is the aircraft dynamic damping [56]. This is mainly affected by the horizontal tail, as discussed in Chapter 3. Thus, an effective tail (high static margin) leads to much higher damping. This trend can also be observed in the results presented in Table 5.3.

For phugoid, the aircraft mass or center of gravity location does not have an effect. The phugoid shows how effectively the aircraft exchanges kinetic energy for potential energy and vice versa [56]. This means that the damping of the phugoid is highest when the lift-to-drag ratio is lowest. This is also the case for the final designs, where the highest damping is observed at approach or stall speed (flaps, gear extended). On the contrary, the lowest phugoid damping is observed at cruise speed, where the lift-to-drag ratio is highest. Note that the damping ratio for Configuration 3 is lower, meaning that the lift-to-drag ratio is higher. This is true; however, this is not due to propeller effects. The better lift and drag performance of a DEP aircraft is not accounted for in this study; thus, the higher lift-to-drag ratio comes from a different aircraft geometry. This is also verified by Configurations 1 and 2 having the same phugoid damping ratio.

The phugoid frequency is tied to the aircraft speed and is not related to any geometric or performance property [56]. A higher speed decreases the frequency. For all configurations, the lowest phugoid frequency is observed at dive speed. The highest frequency happens at stall speed for all configurations.

Additionally, static margins were checked, which affect short period values [56]. All of the static margins are positive, meaning that all configurations are stable. The lowest static margin is observed at the most critical condition for stability, for which the horizontal tail is sized. Thus, these are determined by the horizontal tail size. On the other hand, the maximum values show the difference in the final designs. One can see that Configuration 2 has the highest static margin. This is because the aircraft is sized for the most limiting conditions. The aircraft suffers from destabilizing propeller effects; thus, the horizontal tail size is increased and the wing is shifted back. On the other hand, in cruise, the propellers do not operate at high thrust settings; thus, they are less destabilizing. Due to this, the stability of the aircraft increases as the horizontal tail is oversized or the wing is too much shifted back. On the other hand, one can notice that the DEP aircraft features the lowest maximum static margin. This is because the wing is positioned very close to the center of gravity (Figure 5.26). Due to this, the wing does not affect the moment much, so the moment slope of the aircraft stays small while the lift slope remains the same.

5.3. DISTRIBUTED PROPULSION AIRCRAFT SENSITIVITY ANALYSIS

In this section, sensitivity analysis is performed for the DEP aircraft (Configuration 3). This is done based on three parameters. One of them is the horizontal-tail vertical position. This is done to see what could be an optimal tail configuration for a DEP aircraft. Three configurations are analyzed: T-tail, crucifix tail, and conventional tail. The second sensitivity analysis is done on battery distribution on the wing. A battery distributed along the whole wing span would be beneficial for the structure of the wing; however, the roll performance would suffer. The goal is to see if the aircraft is still capable of reaching the rolling requirement with the span reserved for the aileron or what would be the maximum length until the battery could be placed to meet the rolling requirement. Finally, the sensitivity of the reserve fuel position is analyzed to see the benefits of moving the fuel tank to the middle of the fuselage.

5.3.1. HORIZONTAL TAIL POSITION

To find the best horizontal tail configuration and the impact of the vertical position of the horizontal tail, a sensitivity analysis was performed. This was done by introducing three tail configurations: T-tail (original), crucifix and conventional. The longitudinal positional of all tail configurations was kept the same; T-tail was positioned at 92% of the vertical tail, crucifix - at 46%, and conventional tail was positioned at 0%.

The results for different tail configurations are presented in Figure 5.45; it can be seen that the T-tail performs the best. The cruciform tail and conventional tails perform similarly, featuring slightly bigger horizontal tail size. The aircraft becomes more stable with increasing horizontal tail height. Additionally, a better rotation performance for a conventional tail is observed.

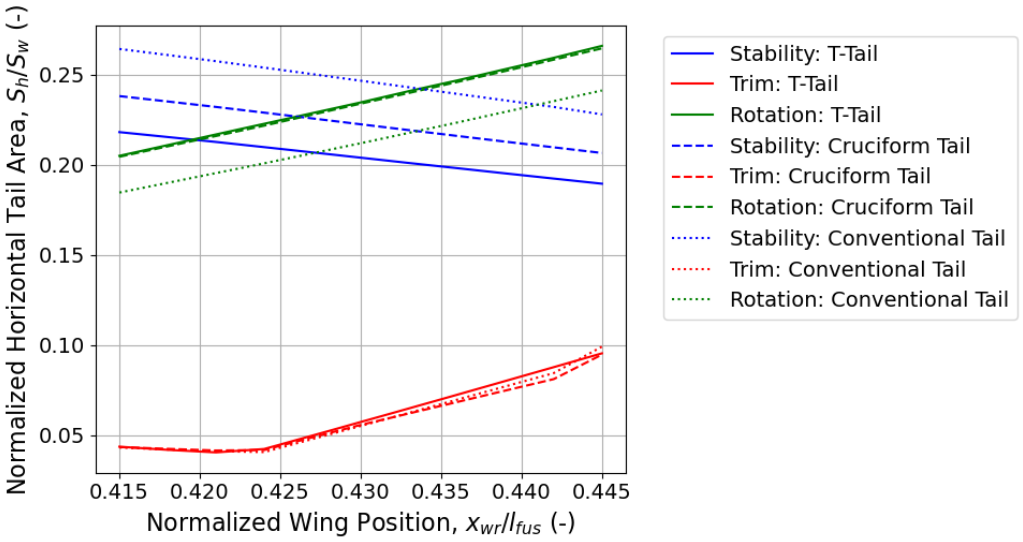

Figure 5.45: Minimal horizontal tail size for different horizontal tail configurations.

The conventional tail has the best performance for rotation, as seen in Figure 5.46. This is because the tail is covered in the propeller slipstream for the whole rotation maneuver, as seen in Figure 5.48 - at the start and as seen in Figure 5.49 - at the end. Due to this, an increase in down lift generated by the horizontal tail is observed (Figure 5.47 and Figure 5.50). This causes the aircraft to rotate faster (Figure 5.51). In contrast, the crucifix tail is barely in the slipstream at the end of the rotation, as seen in Figure 5.52. Thus, the T-tail and crucifix tail do not benefit from the propeller slipstream at take-off for the presented configurations.

For stability, the propeller slipstream helps, as it increases the effectiveness of the tail. However, the horizontal tail cannot be in the slipstream for all angles of attack (unless the slipstream is very big). Due to this, the horizontal tail effectiveness is increased for certain angles of attack. This can be seen in Figure 5.53 and Figure 5.54. The conventional tail features a much steeper slope until high angles of attack where it exits the slipstream. As seen in Figure 5.55, the conventional tail at a low angle of attack is covered in the propeller slipstream, and in Figure 5.56 the aircraft tail is still in the slipstream at a high angle of attack. However, the aircraft should be stable for all operational angles of attack, thus, the limiting condition is when the horizontal tail is outside the slipstream.

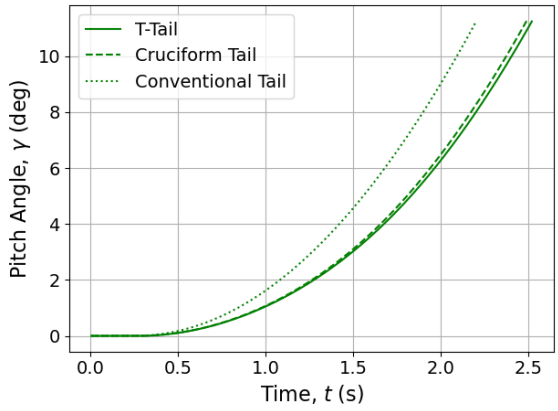

Figure 5.46: Config 3 pitch angle at rotation for different tail configurations for MTOW and most forward CG position (T_C=0.352, $\delta_{e_{max}}$=30°).

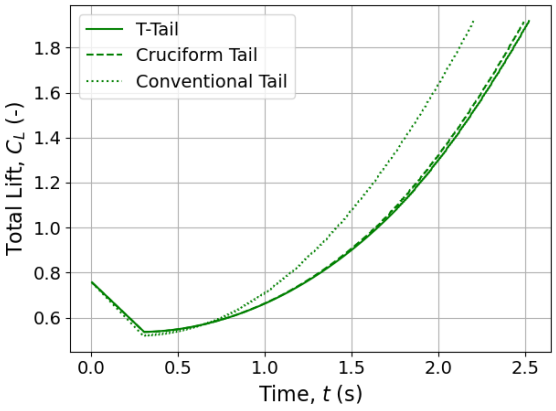

Figure 5.47: Config 3 total lift at rotation for different tail configurations for MTOW and most forward CG position (T_C=0.352, $\delta_{e_{max}}$=30°).

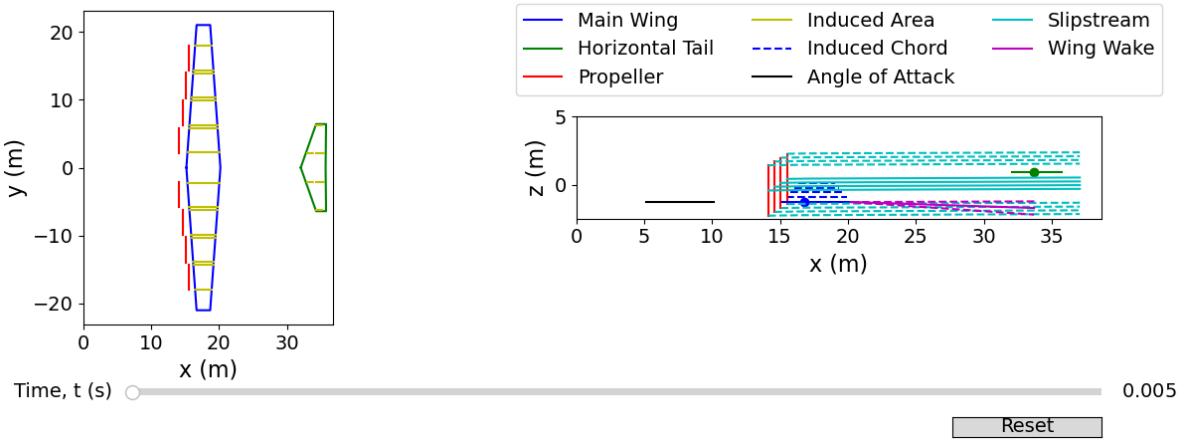

Figure 5.48: Slipstream of conventional tail configuration at the start of rotation (Config 3).

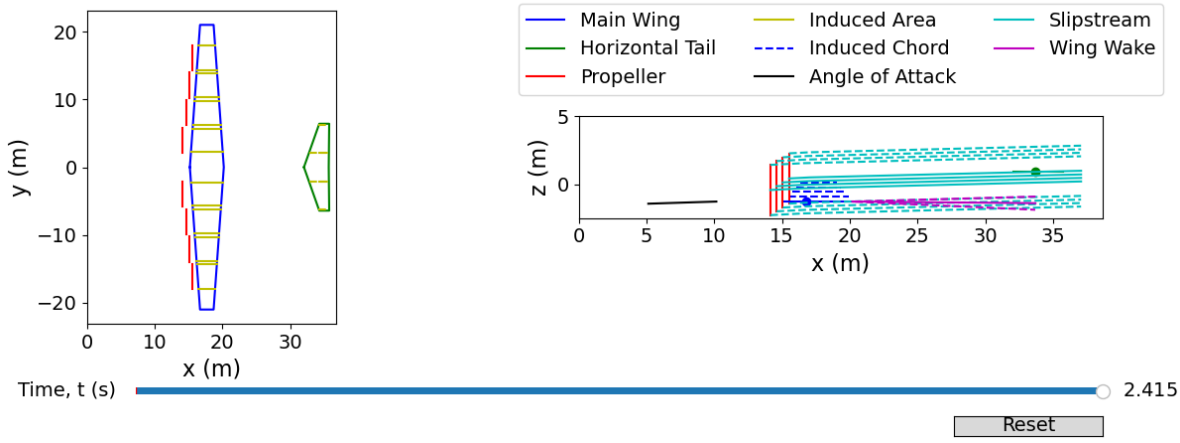

Figure 5.49: Slipstream of conventional tail configuration at the end of rotation (Config 3).

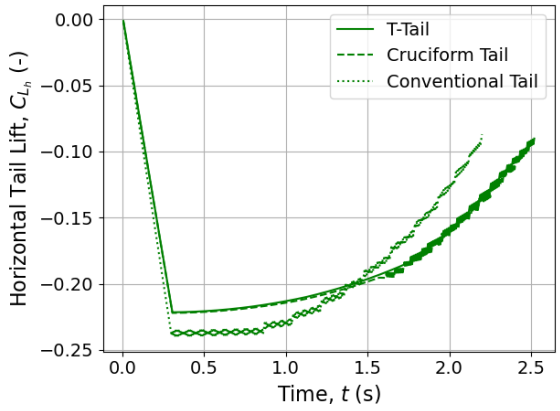

Figure 5.50: Config 3 horizontal tail lift at rotation for different tail configurations for MTOW and most forward CG position (T_C=0.352, $\delta_{e_{max}}$=30°).

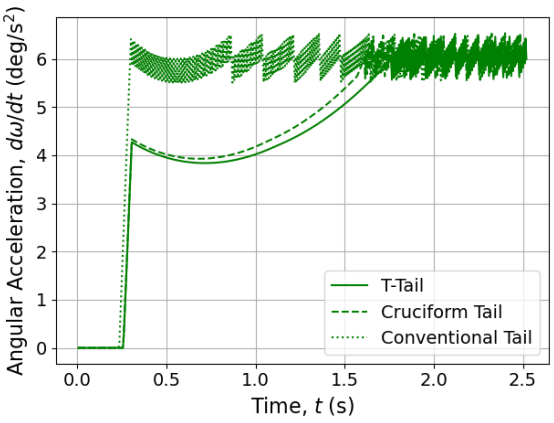

Figure 5.51: Config 3 angular acceleration at rotation for different tail configurations for MTOW and most forward CG position (T_C=0.352, $\delta_{e_{max}}$=30°).

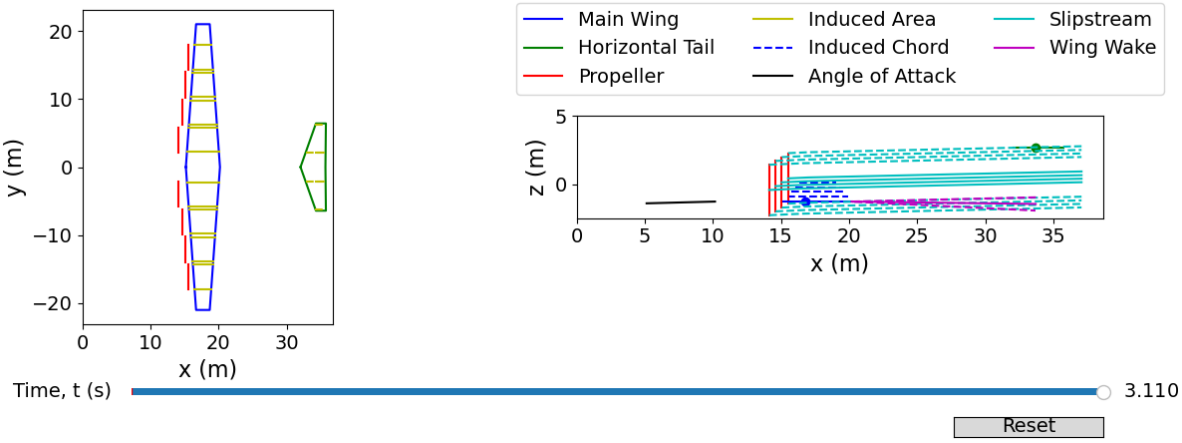

Figure 5.52: Slipstream of crucifix tail configuration at the end of rotation (Config 3).

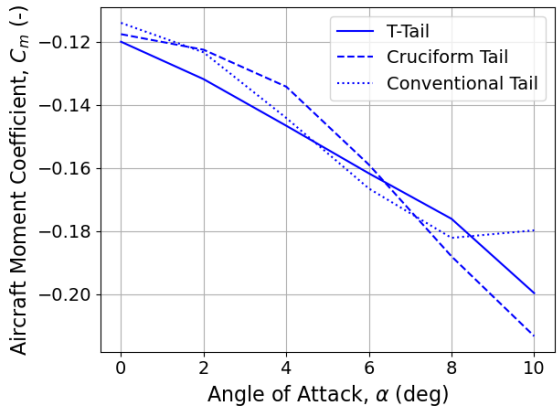

Figure 5.53: Config 3 moment curve after take-off for different tail configurations for MTOW and most aft CG position (T_C=0.352).

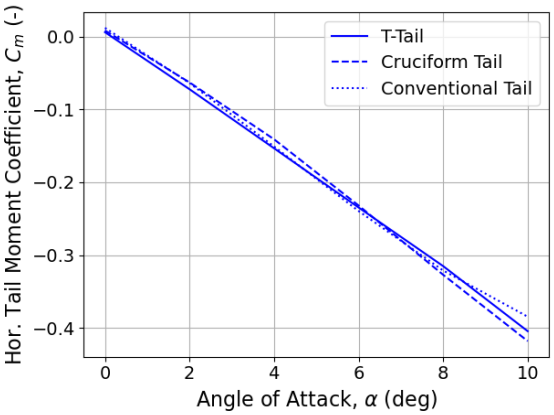

Figure 5.54: Config 3 horizontal tail moment curve after take-off for different tail configurations for MTOW and most aft CG position (T_C=0.352).

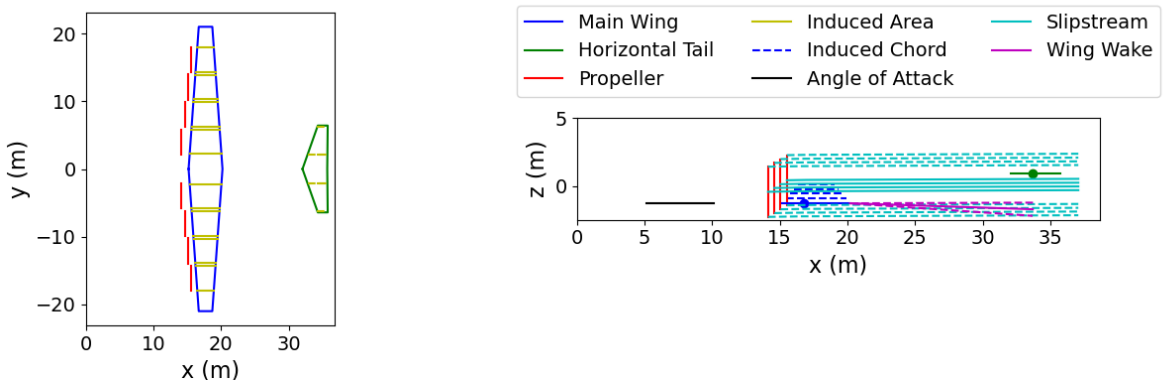

Figure 5.55: Slipstream of conventional tail configuration after take-off at low angle of attack (Config 3).

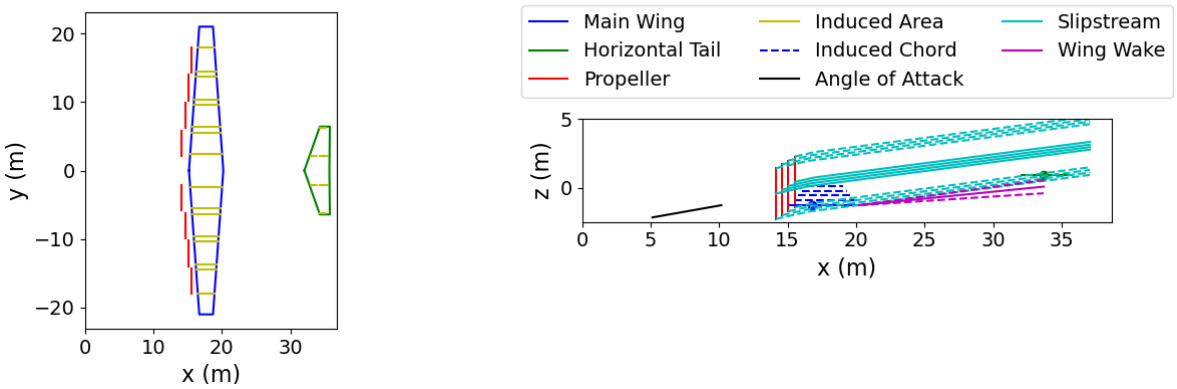

Figure 5.56: Slipstream of conventional tail configuration after take-off at high angle of attack (Config 3).

Similarly, the crucifix tail starts entering the slipstream at a medium angle of attack, as seen in Figure 5.57 and the T-tail only enters the slipstream at high angles of attack, as seen in Figure 5.58. However, once again the aircraft has to be stable for all flight angles, thus, the slipstream does not reduce the overall horizontal tail size.

The reason why the curves decrease (Figure 5.45) with horizontal tail height is the downwash generated. A higher downwash, as seen in Figure 5.59, reduces the horizontal tail effectiveness. Due to this, a larger tail is needed even if the slipstream covers the horizontal tail for a wider range of operational angles. To get the benefits of a slipstream for stability, the aircraft's horizontal tail has to be covered in it for all flight angles. However, this is not the case for the analyzed aircraft. Moreover, in case of engine failure, the aircraft should be stable even without the slipstream acting on the tail. Finally, due to the wing wake not accounting for the flow separation at higher angles of attack, a future study could be done on the horizontal tail position including the separation, as this would have an effect on different tail configurations.

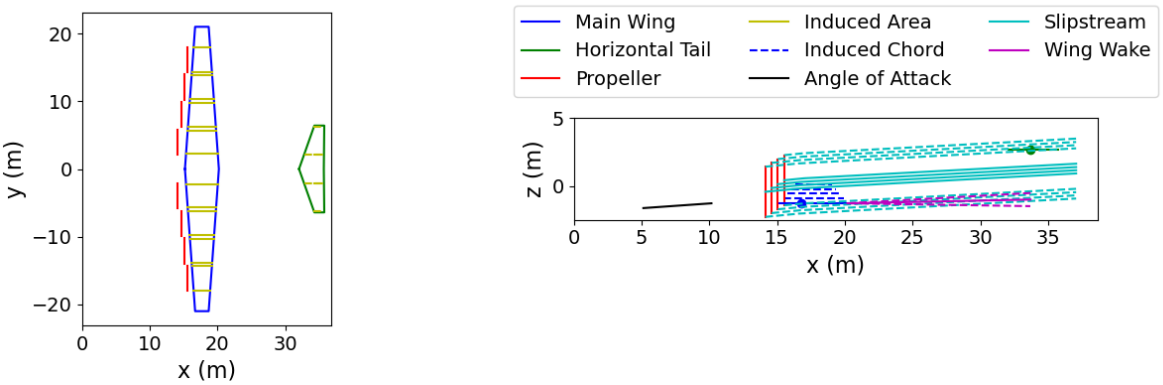

Figure 5.57: Slipstream of crucifix tail configuration after take-off at medium angle of attack (Config 3).

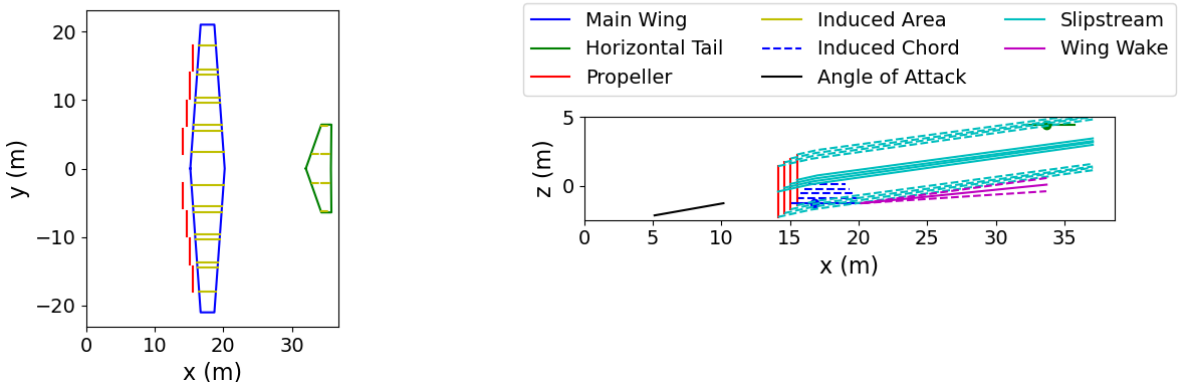

Figure 5.58: Slipstream of T-tail configuration after take-off at high angle of attack (Config 3).

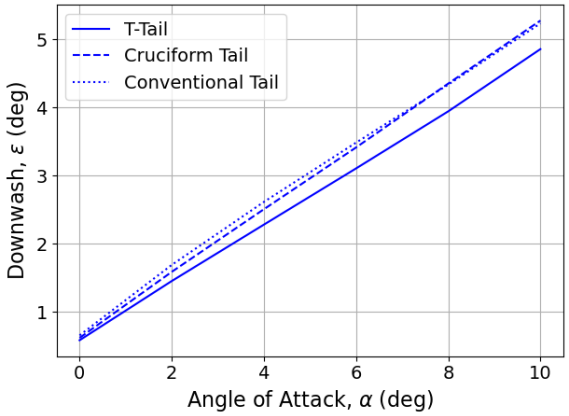

Figure 5.59: Config 3 downwash curve after take-off for different tail configurations for MTOW and most aft CG position (T_C=0.352).

5.3.2. BATTERY PLACEMENT

The effect of having batteries distributed along the whole span is discussed in this section. Note that the the aircraft has folding tips, thus, the batteries are only placed until the folding tip (also, the aileron is up to the folding tip). It can be seen in Table 5.4, that due to the batteries being placed more outside, the roll moment of inertia increases almost three times. Note that this significant increase is due to the significant battery mass and the quadratic scaling of the distance from the fuselage axis.

Table 5.4: Normalized roll moment of inertia for original, full span, and calibrated battery placement.

	Original battery	Full span battery	Calibrated battery
I_{xx}	0.0082	0.0223	0.0136

An aileron sizing was done for an aircraft with batteries placed along the whole span (until folding wing tips) and the results are presented in Figure 5.60. As can be seen in both configurations reach a 30° bank angle within 2 seconds. Moreover, the full span battery density is about 1038 kg/m^3, meaning that the battery can be put twice as sparsely. On the other hand, the aileron inboard edge does exceed the limit (58.6% spanwise position, as the inboard part is reserved for flaps - Figure 3.7). The aileron inboard edge is at 52.5%, making the design infeasible (or if this aileron positioning would be used, there would be less space for flaps).

Of course, the higher moment of inertia of the full-span battery leads to a lower acceleration at first (Figure 5.61). However, once the aileron reaches peak moment, as seen in Figure 5.62, the full span battery aircraft loses its acceleration slower, as the aircraft features a lower roll damping (Figure 5.63) due to the lower initial acceleration. Because of this the full-span battery aircraft catches up to the original configuration.

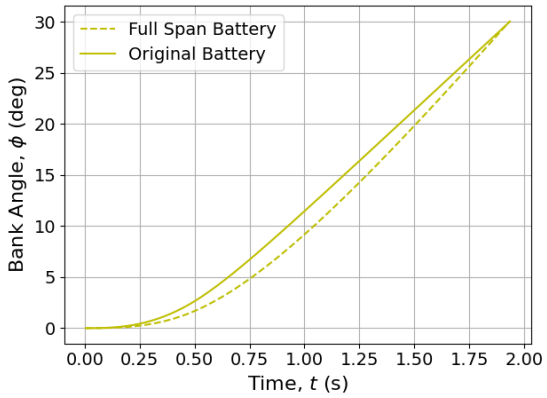

Figure 5.60: Aircraft bank angle during roll manoeuvre (T_C=0.256, δ_a=20°).

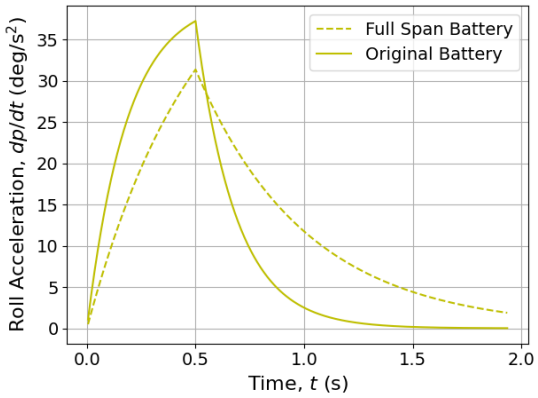

Figure 5.61: Aircraft angular acceleration angle during roll manoeuvre (T_C=0.256, δ_a=20°).

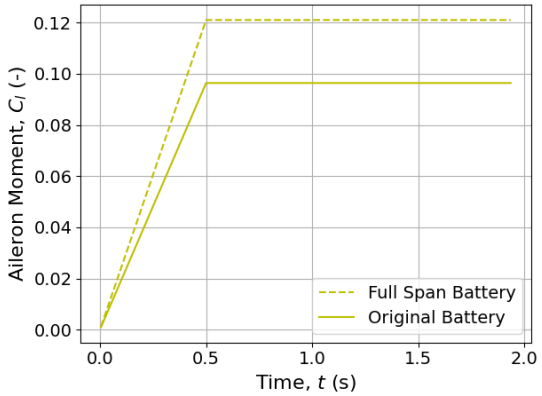

Figure 5.62: Aircraft aileron moment during roll manoeuvre (T_C=0.256, δ_a=20°).

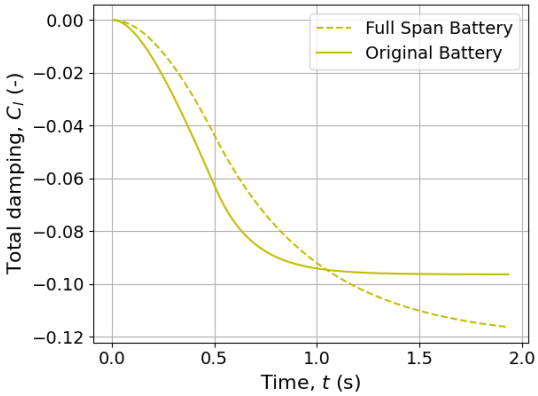

Figure 5.63: Aircraft damping moment during roll manoeuvre (T_C=0.256, δ_a=20°).

In order to find the best battery placement for the structure while meeting the roll requirement, its placement was adjusted to receive an aileron size at the limit. The limiting case is when the battery is placed up to 55% of the wing span (the original battery is placed up to 34% of the span). The normalized inertia for this case is presented in Table 5.4. As can be seen, the inertia increases by about 65% compared to the original battery placement. The density of the battery system is 1380 kg/m^3. This features, the same behaviour of the aircraft, as discussed above only with different magnitudes of moments and accelerations.

5.3.3. FUEL PLACEMENT

For the original Configuration 3 the reserve fuel is placed in the back of the fuselage. While the fuel mass is not high (about 1% of aircraft mass), the large distance from the center of gravity, shifts it back. This is not good for the stability of an aircraft. Thus, the goal of this section is to see what impact the positioning of the fuel closer to the center of gravity has on the size of the tail. To see this the fuel was placed in the middle of the fuselage and the results were compared to the original configuration, as seen in Figure 5.64.

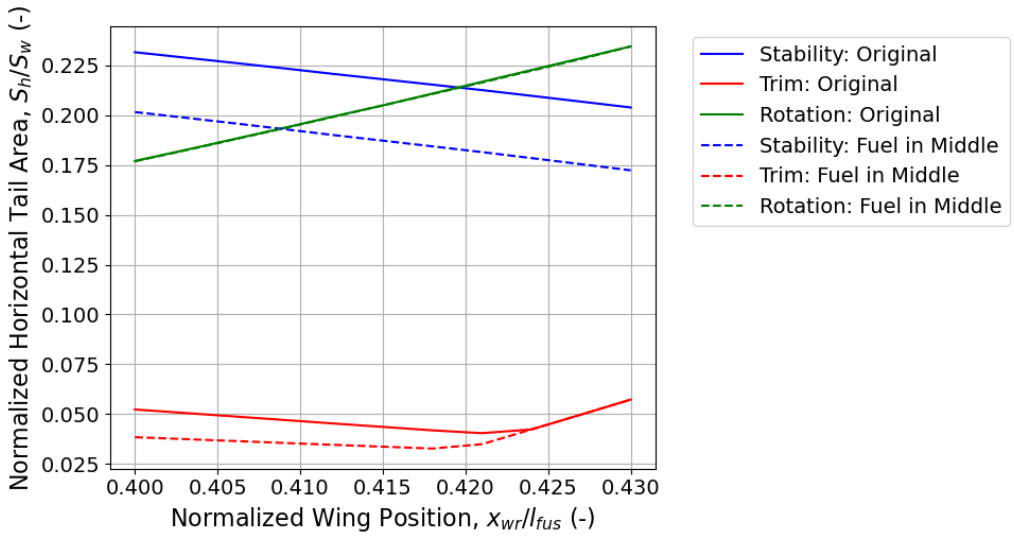

Figure 5.64: Minimal horizontal tail size for different fuel positions for Config 3.

The results indicate that in fact, the stability increases (lower tail size needed) for the aircraft with fuel placed in the middle. Due to this the tail size can be reduced by about 10%. There is no effect observed for rotation, as this is done by the most forward center of gravity location. As seen in Figure 5.65, this is not affected. For trim a slight difference is observed for forward wing positions, as moving the most aft center of gravity forward increases the tail arm and reduces the wing moment, thus, a reduction is observed. Note that the reserve fuel tank can be placed in the nose of the aircraft, further increasing stability, however, this would shift the most forward center of gravity location, reducing rotation performance.

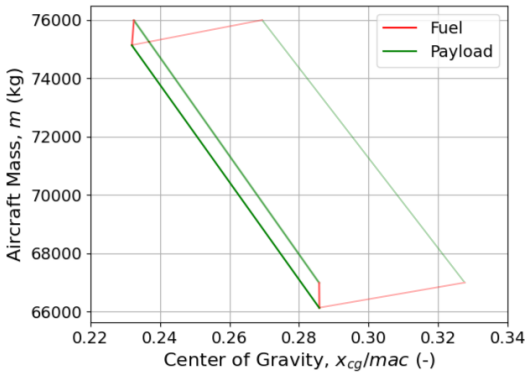

Figure 5.65: Loading diagram of Config 3 with fuel placed in the middle (shaded is the original).

6

CONCLUSION AND RECOMMENDATIONS

The conclusion and recommendations for future work are presented in this chapter. The primary objective of this study was to determine the minimum size required for the horizontal tail (including elevator) and aileron of a distributed propulsion aircraft, ensuring compliance with regulatory and recommended standards. This involved the creation of a low/medium fidelity model to estimate the aerodynamic forces acting on the aircraft, encompassing propeller forces and their effects, and to appropriately size the horizontal tail and aileron. The model operated by predicting the forces and moments produced by various aerodynamic surfaces, considering the alterations induced by the propeller on these surfaces. Noteworthy limitations of the model include its treatment of wing wake modeling and the absence of consideration for sideslip in roll motion. Despite these constraints, the model yielded results consistent with actual aircraft specifications, rendering it suitable for preliminary design purposes. The model could be even used for further design phases if the recommendations, mentioned below, are included in the model.

6.1. CONCLUSION

Firstly, propeller effects on an aircraft's stability and control were identified by comparing Configuration 1 (twin turboprop aircraft with no propeller interaction effects and out-of-plane forces) with Configuration 2 (twin turboprop with propeller effects). It was determined that propeller effects negatively impact aircraft stability, mainly due to the propeller-induced normal force acting ahead of the center of gravity, creating an additional destabilizing moment. Furthermore, propellers introduce extra downwash, reducing the effectiveness of the horizontal tail. Consequently, flight conditions for a propeller aircraft are limited by high thrust and low speed. However, propeller effects enhance the rotational performance of an aircraft by increasing the initial lift of the wing and aiding in generating a higher pitching-up moment during rotation.

Horizontal tail sizing for different wing locations was performed for all three configurations, now incorporating a Distributed Electric Propulsion (DEP) aircraft, to identify the optimal wing location and horizontal tail size. The sizing process revealed that Configuration 3 (DEP aircraft) exhibits greater stability than Configuration 2, attributed to the closer placement of distributed propellers on the wing, with outboard propellers positioned more aft due to the sweep. The DEP aircraft's relatively shorter fuselage, despite a larger wing, results in a lower normalized pitching-up moment and a reduced horizontal tail size. Although the DEP aircraft features slightly higher downwash than Configuration 2, the short fuselage prevents a significant increase in horizontal tail size. Nevertheless, the DEP aircraft still has a larger normalized tail size compared to Configuration 1, which lacks destabilizing propeller effects.

In terms of rotation performance, configurations 2 and 3 exhibited similar results, with both having higher initial wing lift for faster rotation. Configuration 3 had a slightly higher normalized inertia due to a fuel tank positioned at the rear of the fuselage, but this did not significantly impact rotation time.

A brief analysis of the longitudinal dynamic stability performance showed that all configurations met the minimum short period damping requirement, but phugoid damping was relatively low, particularly for the DEP aircraft. Although the requirement is only recommended, increasing the damping ratio would compromise lift-to-drag ratio and overall aircraft performance.

An analysis of the horizontal tail position for a DEP aircraft indicated that a T-tail is the optimal choice for improved stability, despite a conventional tail performing better during rotation. The T-tail's advantage lies

in experiencing smaller downwash at the horizontal tail. Additionally, increased horizontal tail effectiveness was observed when the slipstream covered it, but this effect was not consistent for all angles of attack, with the limiting case occurring when the horizontal tail is outside the slipstream.

The DEP aircraft demonstrated lower roll performance due to two main factors: a higher normalized moment of inertia (approximately 30% greater) due to heavy batteries and distributed propellers, and significant damping generated by the outboard propellers due to their large moment arm. Despite a lower roll requirement (attributed to a higher take-off mass), the aircraft necessitated the same normalized aileron size as Configuration 2. An analysis was conducted to assess aileron size when batteries were distributed along the entire span of the wing, revealing that the aircraft could still meet the rolling requirement, although the aileron exceeded the lower span limit reserved for flaps. In the event of placing the aileron along the entire reserved wing span, the battery placement could extend up to 55% of the wingspan instead of the original 34%. Lastly, an analysis of the Configuration 3 reserve fuel tank suggested that the tail size could be further reduced by 10% if the fuel tank were placed in the middle of the fuselage.

In summary, the DEP aircraft features a 19% smaller horizontal tail size compared to a twin turboprop aircraft with propeller effects. However, the normalized aileron size remains unaffected, given the lower roll requirement but higher roll damping and moment of inertia for the original, inboard battery placement.

6.2. RECOMMENDATIONS

In this section, the following recommendations for future studies are outlined:

- Implement a more advanced modeling technique for wing wake to account for separation, particularly at higher angles of attack where separated flow may impact the horizontal tail.
- Conduct a comprehensive study, incorporating more accurate wing wake modeling, to assess aircraft stability at high angles of attack and varying horizontal tail vertical positions.
- Enhance the modeling technique for propeller downwash by considering the mutual influence of separate propellers on each other's downwash, instead of assuming a simple average acting on the horizontal tail along with the wing downwash.
- Integrate the modeling of the reduction in downwash near the ground to accurately depict slipstream trajectory and horizontal tail effectiveness, for more accurate rotation results.
- Consider employing higher-fidelity methods for estimating fuselage and wing moments to enhance the accuracy of moment predictions.
- Increase the model's accuracy by utilizing an external aerodynamic tool (e.g., AVL) or a database of aerodynamic data, especially at higher angles of attack where the linear lift slope assumption may lead to inaccuracies.
- Include rolling moment due to sideslip to achieve more precise roll results, potentially introducing extra damping to the roll maneuver.
- Incorporate horizontal tail sizing for short period and phugoid into the minimal horizontal tail estimation for a more comprehensive analysis.
- Explore the possibility of analyzing lower phugoid damping to maintain higher aerodynamic efficiency.
- Conduct further analysis on reducing flap area or incorporating flaperons to facilitate optimal battery placement across the entire wing and reduce structural weight.

A

CS-25 Requirements

CS 25.143 General

(a) The aeroplane must be safely controllable and manoeuvrable during:

(1) take-off;

(2) climb;

(3) level flight;

(4) descent;

(5) approach and go-around; and

(6) approach and landing.

(b) It must be possible to make a smooth transition from one flight condition to any other flight condition without exceptional piloting skill, alertness, or strength, and without danger of exceeding the aeroplane limit-load factor under any probable operating conditions, including:

(1) The sudden failure of the critical engine;

(2) For aeroplanes with three or more engines, the sudden failure of the second critical engine when the aeroplane is in the en-route, approach, or landing configuration and is trimmed with the critical engine inoperative; and

(3) Configuration changes, including deployment or retraction of deceleration devices; and

(4) Go-around manoeuvres with all engines operating. The assessment must include, in addition to controllability and manoeuvrability aspects, the flight crew workload and the risk of a somatogravic illusion.

(h) The manoeuvring capabilities in a constant speed coordinated turn at forward centre of gravity, as specified in the following table, must be free of stall warning or other characteristics that might interfere with normal manoeuvring.

Configuration	Speed	Manoeuvring bank angle in a coordinated turn	Thrust/power setting
Take-off	V_2	30°	Asymmetric wat-limited
Take-off	V_2+xx	40°	All engines operating climb
En-route	V_{FTO}	40°	Asymmetric wat-limited
Landing	V_{REF}	40°	Symmetric for - 3° flight path angle

CS 25.147 Directional and lateral control

(a) It must be possible, with the wings level, to yaw into the operative engine and to safely make a reasonably sudden change in heading of up to 15° in the direction of the critical inoperative engine. This must be shown at 1.3 VSR1, for heading changes up to 15° (except that the heading change at which the rudder pedal force is 667 N (150 lbf) need not be exceeded), and with –

(1) The critical engine inoperative and its propeller (if applicable) in the minimum drag position;

(2) The power required for level flight at 1.3 V_{SR1}, but not more than maximum continuous power;

(3) The most unfavourable centre of gravity;

(4) Landing gear retracted;

(5) Wing-flaps in the approach position; and

(6) Maximum landing weight.

(b) Aeroplanes with four or more engines must meet the requirements of sub-paragraph (a) of this paragraph except that –

(1) The two critical engines must be inoperative with their propellers (if applicable) in the minimum drag position;

(3) The wing-flaps must be in the most favourable climb position.

(c) It must be possible to make 20° banked turns, with and against the inoperative engine, from steady flight at a speed equal to 1.3 V_{SR1}, with –

(1) The critical engine inoperative and its propeller (if applicable) in the minimum drag position;

(2) The remaining engines at maximum continuous power;

(3) The most unfavourable centre of gravity;

(4) Landing gear both retracted and extended;

(5) Wing-flaps in the most favourable climb position; and

(6) Maximum take-off weight;

(d) With the critical engine inoperative, roll response must allow normal manoeuvres. Lateral control must be sufficient, at the speeds likely to be used with one engine inoperative, to provide a roll rate necessary for safety without excessive control forces or travel.

(e) Aeroplanes with four or more engines must be able to make 20° banked turns, with and against the inoperative engines, from steady flight at a speed equal to 1.3 V_{SR1}, with maximum continuous power, and with the aeroplane in the configuration prescribed by sub-paragraph (b) of this paragraph.

(f) With the engines operating, roll response must allow normal manoeuvres (such as recovery from upsets produced by gusts and the initiation of evasive manoeuvres). There must be enough excess lateral control in sideslips (up to sideslip angles that might be required in normal operation), to allow a limited amount of manoeuvring and to correct for gusts. Lateral control must be enough at any speed up to V_{FC}/M_{FC} to provide a peak roll rate necessary for safety, without excessive control forces or travel.

CS 25.149 Minimum control speed

(b) V_{MC} is the calibrated airspeed, at which, when the critical engine is suddenly made inoperative, it is possible to maintain control of the aeroplane with that engine still inoperative, and maintain straight flight with an angle of bank of not more than 5°.

(c) V_{MC} may not exceed 1.13 V_{SR} with –

(1) Maximum available take-off power or thrust on the engines;

(2) The most unfavourable centre of gravity;

(3) The aeroplane trimmed for take-off;

(4) The maximum sea-level take-off weight (or any lesser weight necessary to show V_{MC});

(5) The aeroplane in the most critical take-off configuration existing along the flight path after the aeroplane becomes airborne, except with the landing gear retracted;

(6) The aeroplane airborne and the ground effect negligible; and

(7) If applicable, the propeller of the inoperative engine –

(i) Windmilling;

(ii) In the most probable position for the specific design of the propeller control; or

(iii) Feathered, if the aeroplane has an automatic feathering device acceptable for showing compliance with the climb requirements of CS 25.121.

(d) The rudder forces required to maintain control at V_{MC} may not exceed 667 N (150 lbf) nor may it be necessary to reduce power or thrust of the operative engines. During recovery, the aeroplane may not assume any dangerous attitude or require exceptional piloting skill, alertness, or strength to prevent a heading change of more than 20°.

(e) V_{MCG}, the minimum control speed on the ground, is the calibrated airspeed during the take-off run at which, when the critical engine is suddenly made inoperative, it is possible to maintain control of the aeroplane using the rudder control alone (without the use of nose-wheel steering), as limited by 667 N of force (150 lbf), and the lateral control to the extent of keeping the wings level to enable the take-off to be safely continued using normal piloting skill. In the determination of V_{MCG}, assuming that the path of the aeroplane accelerating with all engines operating is along the centreline of the runway, its path from the point at which the critical engine is made inoperative to the point at which recovery to a direction parallel to the centreline is completed, may not deviate more than 9.1 m (30 ft) laterally from the centreline at any point. V_{MCG} must be established, with –

(1) The aeroplane in each take-off configuration or, at the option of the applicant, in the most critical take-off configuration;

(2) Maximum available take-off power or thrust on the operating engines;

(3) The most unfavourable centre of gravity;

(4) The aeroplane trimmed for take-off; and

(5) The most unfavourable weight in the range of take-off weights.

(f) V_{MCL}, the minimum control speed during approach and landing with all engines operating, is the calibrated airspeed at which, when the critical engine is suddenly made inoperative, it is possible to maintain control of the aeroplane with that engine still inoperative, and maintain straight flight with an angle of bank of not more than 5°. V_{MCL} must be established with –

(1) The aeroplane in the most critical configuration (or, at the option of the applicant, each configuration) for approach and landing with all engines operating;

(2) The most unfavourable centre of gravity;

(3) The aeroplane trimmed for approach with all engines operating;

(4) The most unfavourable weight, or, at the option of the applicant, as a function of weight;

(5) For propeller aeroplanes, the propeller of the inoperative engine in the position it achieves without pilot action, assuming the engine fails while at the power or thrust necessary to maintain a 3 degree approach path angle; and

(6) Go-around power or thrust setting on the operating engine(s).

(g) For aeroplanes with three or more engines, V_{MCL-2}, the minimum control speed during approach and landing with one critical engine inoperative, is the calibrated airspeed at which, when a second critical engine is suddenly made inoperative, it is possible to maintain control of the aeroplane with both engines still inoperative, and maintain straight flight with an angle of bank of not more than 5°. V_{MCL-2} must be established with –

(1) The aeroplane in the most critical configuration (or, at the option of the applicant, each configuration) for approach and landing with one critical engine inoperative;

(2) The most unfavourable centre of gravity;

(3) The aeroplane trimmed for approach with one critical engine inoperative;

(4) The most unfavourable weight, or, at the option of the applicant, as a function of weight;

(5) For propeller aeroplanes, the propeller of the more critical engine in the position it achieves without pilot action, assuming the engine fails while at the power or thrust necessary to maintain a 3 degree approach path angle, and the propeller of the other inoperative engine feathered;

(6) The power or thrust on the operating engine(s) necessary to maintain an approach path angle of 3o when one critical engine is inoperative; and

(7) The power or thrust on the operating engine(s) rapidly changed, immediately after the second critical engine is made inoperative, from the power or thrust prescribed in subparagraph (g)(6) of this paragraph to –

(i) Minimum power or thrust; and

(ii) Go-around power or thrust setting.

CS 25.161 Trim

(a) Each aeroplane must meet the trim requirements of this paragraph after being trimmed, and without further pressure upon, or movement of, either the primary controls or their corresponding trim controls by the pilot or the automatic pilot.

(b) The aeroplane must maintain lateral and directional trim with the most adverse lateral displacement of the centre of gravity within the relevant operating limitations, during normally expected conditions of operation (including operation at any speed from 1.3 V_{SR1}, to V_{MO}/M_{MO}).

(c) The aeroplane must maintain longitudinal trim during –

(1) A climb with maximum continuous power at a speed not more than 1.3 V_{SR1}, with the landing gear retracted, and the wing-flaps (i) retracted and (ii) in the take-off position;

(2) Either a glide with power off at a speed not more than 1.3 V_{SR1}, or an approach within the normal range of approach speeds appropriate to the weight and configuration with power settings corresponding to a 3° glidepath, whichever is the most severe, with the landing gear extended, the wing-flaps retracted and extended, and with the most unfavourable combination of centre of gravity position and weight approved for landing; and

(3) Level flight at any speed from 1.3 V_{SR1}, to V_M/M_{MO}, with the landing gear and wing-flaps retracted, and from 1.3 V_{SR1} to V_{LE} with the landing gear extended.

(d) The aeroplane must maintain longitudinal, directional, and lateral trim (and for lateral trim, the angle of bank may not exceed 5°) at 1.3 V_S, during the climbing flight with –

(1) The critical engine inoperative;

(2) The remaining engines at maximum continuous power; and

(3) The landing gear and wing-flaps retracted.

(e) Each aeroplane with four or more engines must also maintain trim in rectilinear flight with the most unfavourable centre of gravity and at the climb speed, configuration, and power required by CS 25.123(a) for the purpose of establishing the en-route flight path with two engines inoperative.

CS 25.171 General

The aeroplane must be longitudinally, directionally and laterally stable in accordance with the provisions of CS 25.173 to 25.177. In addition, suitable stability and control feel (static stability) is required in any condition normally encountered in service, if flight tests show it is necessary for safe operation.

CS 25.173 Static longitudinal stability

Under the conditions specified in CS 25.175, the characteristics of the elevator control forces (including friction) must be as follows:

(a) A pull must be required to obtain and maintain speeds below the specified trim speed, and a push must be required to obtain and maintain speeds above the specified trim speed. This must be shown at any speed that can be obtained except speeds higher than the landing gear or wing flap operating limit speeds or V_{FC}/M_{FC}, whichever is appropriate, or lower than the minimum speed for steady unstalled flight.

(b) The airspeed must return to within 10% of the original trim speed for the climb, approach and landing conditions specified in CS 25.175(a), (c) and (d), and must return to within 7.5% of the original trim speed for the cruising condition specified in CS 25.175(b), when the control force is slowly released from any speed within the range specified in sub-paragraph (a) of this paragraph.

CS 25.177 Static directional and lateral stability

(a) The static directional stability (as shown by the tendency to recover from a skid with the rudder free) must be positive for any landing gear and flap position and symmetrical power condition, at speeds from 1.13 V_{SR1}, up to V_{FE}, V_{LE}, or V_{FC}/M_{FC} (as appropriate).

(b) The static lateral stability (as shown by the tendency to raise the low wing in a sideslip with the aileron controls free) for any landing gear and wingflap position and symmetric power condition, may not be negative at any airspeed (except that speeds higher than V_{FE} need not be considered for wingflaps extended configurations nor speeds higher than V_{LE} for landing gear extended configurations) in the following airspeed ranges:

(1) From 1.13 V_{SR1} to V_{MO}/M_{MO}.

(2) From V_{MO}/M_{MO} to V_{FC}/M_{FC}, unless the divergence is –

(i) Gradual;

(ii) Easily recognisable by the pilot; and

(iii) Easily controllable by the pilot

CS 25.181 Dynamic stability

(a) Any short period oscillation, not including combined lateral-directional oscillations, occurring between 1.13 V_{SR} and maximum allowable speed appropriate to the configuration of the aeroplane must be heavily damped with the primary controls –

(1) Free; and

(2) In a fixed position.

(b) Any combined lateral-directional oscillations ('Dutch roll') occurring between 1.13 V_{SR} and maximum allowable speed appropriate to the configuration of the aeroplane must be positively damped with controls free, and must be controllable with normal use of the primary controls without requiring exceptional pilot skill.

CS 25.237 Wind velocities

(a) The following applies:

(1) A 90° cross component of wind velocity, demonstrated to be safe for take-off and landing, must be established for dry runways and must be at least 37 km/h (20 kt) or 0·2 V_{SR0}, whichever is greater, except that it need not exceed 46 km/h (25 kt).

CS 25.253 High-speed characteristics

(b) V_{FC}/M_{FC}. V_{FC}/M_{FC} is the maximum speed at which the requirements of CS 25.143(g), 25.147(f), 25.175(b)(1), 25.177(a) through (c), and 25.181 must be met with wing-flaps and landing gear retracted. Except as noted in CS 25.253(c), V_{FC}/M_{FC} may not be less than a speed midway between V_{MO}/M_{MO} and V_{DF}/M_{DF}, except that, for altitudes where Mach Number is the limiting factor, M_{FC} need not exceed the Mach Number at which effective speed warning occurs.

CS 25.671

(d) The aeroplane must be designed so that, if all engines fail at any time of the flight:

(1) it is controllable in flight;

(2) an approach can be made;

(3) a flare to a landing, and a flare to a ditching can be achieved; and

(4) during the ground phase, the aeroplane can be stopped.

B

Short Period, Phugoid, and Static Margin Values

Note that phugoid damping only depends on the aircraft mass and natural frequency does not depend on the mass or CG position.

Table B.1: Short period natural frequency (rad/s) for Config 1.

Condition	Max. mass forward CG	Max. mass aft CG	Min. mass, forward CG	Min. mass, aft CG
Stall speed (T_c=0)	0.696	0.525	0.785	0.636
Lift-off	0.761	0.572	0.86	0.695
Approach	0.981	0.746	1.111	0.906
Cruise	1.893	1.538	1.996	1.66
Dive speed	3.01	2.563	3.172	2.746
Climb	1.089	0.822	1.223	0.989
Top climb	1.811	1.455	1.92	1.585
Landing	0.981	0.746	1.111	0.906
Stall speed (T_c=0.254)	0.696	0.525	0.785	0.636

Table B.2: Short period damping (-) for Config 1.

Condition	Max. mass forward CG	Max. mass aft CG	Min. mass, forward CG	Min. mass, aft CG
Stall speed (T_c=0)	0.797	1.04	0.87	1.061
Lift-off	0.791	1.035	0.864	1.056
Approach	0.779	1.008	0.857	1.038
Cruise	0.483	0.585	0.574	0.682
Dive speed	0.477	0.552	0.572	0.653
Climb	0.75	0.977	0.83	1.014
Top climb	0.509	0.623	0.601	0.719
Landing	0.779	1.008	0.857	1.038
Stall speed (T_c=0.254)	0.797	1.04	0.87	1.061

Table B.3: Phugoid Natural Frequency and Damping for Config 1.

Condition	Natural Frequency (rad/s)	Damping (-)	
		Max. mass	Min. mass
Stall speed (T_c=0)	0.258	0.085	0.075
Lift-off	0.236	0.065	0.052
Approach	0.188	0.08	0.096
Cruise	0.086	0.035	0.043
Dive speed	0.078	0.038	0.053
Climb	0.163	0.04	0.038
Top climb	0.089	0.036	0.044
Landing	0.188	0.08	0.096
Stall speed (T_c=0.254)	0.258	0.085	0.075

Table B.4: Stability margin (-) for Config 1.

Condition	Forward CG	Aft CG
Stall speed (T_c=0)	0.11	0.018
Lift-off	0.111	0.019
Approach	0.118	0.026
Cruise	0.225	0.132
Dive speed	0.28	0.187
Climb	0.124	0.031
Top climb	0.211	0.118
Landing	0.118	0.026
Stall speed (T_c=0.254)	0.11	0.018

Table B.5: Short period natural frequency (rad/s) for Config 2.

Condition	Max. mass forward CG	Max. mass aft CG	Min. mass, forward CG	Min. mass, aft CG
Stall speed (T_c=0)	1.037	0.863	1.119	0.956
Lift-off	0.95	0.674	1.07	0.828
Approach	1.453	1.213	1.573	1.348
Cruise	2.614	2.216	2.715	2.329
Dive speed	4.019	3.502	4.18	3.678
Climb	1.452	1.117	1.597	1.294
Top climb	2.51	2.112	2.617	2.233
Landing	1.42	1.165	1.546	1.309
Stall speed (T_c=0.254)	0.906	0.682	1.006	0.805

Table B.6: Short period damping (-) for Config 2.

Condition	Max. mass forward CG	Max. mass aft CG	Min. mass, forward CG	Min. mass, aft CG
Stall speed (T_c=0)	0.631	0.739	0.704	0.806
Lift-off	0.826	1.134	0.888	1.122
Approach	0.622	0.726	0.698	0.797
Cruise	0.417	0.479	0.49	0.559
Dive speed	0.422	0.472	0.498	0.554
Climb	0.709	0.896	0.782	0.944
Top climb	0.44	0.509	0.514	0.59
Landing	0.654	0.776	0.73	0.843
Stall speed (T_c=0.254)	0.776	1.005	0.842	1.03

Table B.7: Phugoid Natural Frequency and Damping for Config 2.

Condition	Natural Frequency (rad/s)	Damping (-)	
		Max. mass	Min. mass
Stall speed (T_c=0)	0.258	0.085	0.075
Lift-off	0.236	0.065	0.052
Approach	0.188	0.08	0.096
Cruise	0.086	0.035	0.043
Dive speed	0.078	0.038	0.053
Climb	0.163	0.04	0.038
Top climb	0.089	0.036	0.044
Landing	0.188	0.08	0.096
Stall speed (T_c=0.254)	0.258	0.085	0.075

Table B.8: Stability margin (-) for Config 2.

Condition	Forward CG	Aft CG
Stall speed (T_c=0)	0.331	0.191
Lift-off	0.155	0.015
Approach	0.34	0.2
Cruise	0.441	0.302
Dive speed	0.514	0.374
Climb	0.23	0.09
Top climb	0.419	0.28
Landing	0.307	0.167
Stall speed (T_c=0.254)	0.193	0.053

Table B.9: Short period natural frequency (rad/s) for Config 3.

Condition	Max. mass forward CG	Max. mass aft CG	Min. mass, forward CG	Min. mass, aft CG
Stall speed (T_c=0)	0.846	0.717	0.861	0.733
Lift-off	0.811	0.587	0.828	0.61
Approach	1.108	0.938	1.128	0.961
Cruise	2.076	1.737	2.1	1.764
Dive speed	3.045	2.583	3.085	2.628
Climb	1.151	0.906	1.176	0.938
Top climb	1.965	1.631	1.99	1.66
Landing	1.089	0.909	1.11	0.934
Stall speed (T_c=0.256)	0.749	0.579	0.756	0.588

Table B.10: Short period damping (-) for Config 3.

Condition	Max. mass forward CG	Max. mass aft CG	Min. mass, forward CG	Min. mass, aft CG
Stall speed (T_c=0)	0.583	0.675	0.606	0.698
Lift-off	0.899	1.217	0.908	1.209
Approach	0.576	0.667	0.6	0.692
Cruise	0.455	0.533	0.478	0.558
Dive speed	0.481	0.556	0.506	0.583
Climb	0.707	0.879	0.731	0.899
Top climb	0.482	0.569	0.505	0.594
Landing	0.624	0.733	0.649	0.757
Stall speed (T_c=0.256)	0.848	1.075	0.842	1.063

Table B.11: Phugoid Natural Frequency and Damping for Config 3.

Condition	Natural Frequency (rad/s)	Damping (-)	
		Max. mass	Min. mass
Stall speed (T_c=0)	0.243	0.085	0.08
Lift-off	0.213	0.061	0.056
Approach	0.188	0.076	0.076
Cruise	0.084	0.029	0.029
Dive speed	0.077	0.029	0.032
Climb	0.158	0.038	0.035
Top climb	0.088	0.029	0.03
Landing	0.188	0.076	0.076
Stall speed (T_c=0.256)	0.243	0.085	0.08

Table B.12: Stability margin (-) for Config 3.

Condition	Forward CG	Aft CG
Stall speed (T_c=0)	0.221	0.139
Lift-off	0.099	0.017
Approach	0.222	0.14
Cruise	0.235	0.153
Dive speed	0.246	0.164
Climb	0.153	0.071
Top climb	0.223	0.141
Landing	0.202	0.12
Stall speed (T_c=0.256)	0.124	0.042

BIBLIOGRAPHY

[1] B. J. Brelje and J. R. Martins, *Electric, hybrid, and turboelectric fixed-wing aircraft: A review of concepts, models, and design approaches,* Progress in Aerospace Sciences **104**, 1 (2019).

[2] L. Veldhuis, *Propeller Wing Aerodynamic Interference,* Ph.D. thesis, Delft University of Technology (2005).

[3] T. Theodorsen, *The theory of propellers - Part III, The slipstream contraction with numerical values for two-blade and four-blade propellers,* Tech. Rep. Report 777 (NACA, 1944).

[4] E. Obert, *Aerodynamic Design of Transport Aircraft* (IOS Press under the imprint Delft University Press, Delft, 2009).

[5] M. F. M. Hoogreef and J. S. E. Soikkeli, *Flight dynamics and control assessment for differential thrust aircraft in engine inoperative conditions including aero-propulsive effects,* CEAS Aeronautical Journal **13**, 739 (2022).

[6] S. Biser, M. Filipenko, M. Boll, N. Kastner, G. Atanasov, M. Hepperle, D. Keller, D. Vechtel, and M. Noe, *Design space exploration study and optimization of a distributed turbo-electric propulsion system for a regional passenger aircraft,* in 2020 AIAA/IEEE Electric Aircraft Technologies Symposium (EATS) (2020) pp. 1–27.

[7] C. Wolowics and R. Yancey, *Longitudinal Aerodynamic Characteristics of Light, Twin-engine Propeller Driven Airplanes,* Tech. Rep. TN D-6800 (NASA, 1972).

[8] E. Obert, *The Effect of Propeller Slipstream on the Longitudinal Characteristics of a Model of the Saab 340 with a T-tail,* Tech. Rep. LR-761 (Delft University of Technology, 2016).

[9] T. Bouquet and R. Vos, *Modeling the propeller slipstream effect on lift and pitching moment,* in 55th AIAA Aerospace Sciences Meeting (Grapevine, Texas, 2017) https://arc.aiaa.org/doi/pdf/10.2514/6.2017-0236 .

[10] M. H. Sadraey, *Aircraft Design: A Systems Engineering Approach* (A John Wiley Sons, Ltd, Chichester, 2013).

[11] D. Raymer, *Aircraft Design: A Conceptual Approach* (AIAA Education Series, Reston, 2012).

[12] D. Ciliberti, *An improved preliminary design methodology for aircraft directional stability prediction and vertical tailplane sizing,* Ph.D. thesis (2016).

[13] European Commission and Directorate-General for Mobility and Transport and Directorate-General for Research and Innovation, *Flightpath 2050 : Europe's vision for aviation : maintaining global leadership and serving society's needs* (Publications Office, 2011).

[14] S. Pinheiro Melo, A. Barke, F. Cerdas, C. Thies, M. Mennenga, T. S. Spengler, and C. Herrmann, *Sustainability assessment and engineering of emerging aircraft technologies—challenges, methods and tools,* Sustainability **12** (2020), 10.3390/su12145663.

[15] M. D. Moore, *Misconceptions of electric aircraft and their emerging aviation markets,* in 52nd Aerospace Sciences Meeting (National Harbor, Maryland, 2014) https://arc.aiaa.org/doi/pdf/10.2514/6.2014-0535 .

[16] G. Ameyugo, M. Taylor, and R. Singh, *Distributed propulsion feasibility studies,* in 25th International Congress of the Aeronautical Sciences (Hamburg, Germany, 2006).

[17] A. M. Stoll, J. Bevirt, M. D. Moore, W. J. Fredericks, and N. K. Borer, *Drag reduction through distributed electric propulsion,* in 14th AIAA Aviation Technology, Integration, and Operations Conference (Atlanta, Georgia, 2014) https://arc.aiaa.org/doi/pdf/10.2514/6.2014-2851 .

[18] T. Johnson and A. Joshi, *Review of vehicle engine efficiency and emissions,* SAE International Journal of Engines **11**, 1307 (2018).

[19] A. S. Gohardani, G. Doulgeris, and R. Singh, *Challenges of future aircraft propulsion: A review of distributed propulsion technology and its potential application for the all electric commercial aircraft,* Progress in Aerospace Sciences **47**, 369 (2011).

[20] B. T. Schiltgen, M. W. Green, and A. R. Gibson, *Analysis of terminal area operations and short field performance of hybrid electric distributed propulsion,* in 2013 International Powered Lift Conference (Los Angeles, California, 2013) https://arc.aiaa.org/doi/pdf/10.2514/6.2013-4265 .

[21] G. T. Klunk and J. L. Freeman, *Vertical tail area reduction for aircraft with spanwise distributed electric propulsion,* in 2018 AIAA/IEEE Electric Aircraft Technologies Symposium (Cincinnati, Ohio, 2018) https://arc.aiaa.org/doi/pdf/10.2514/6.2018-5022 .

[22] H. D. Kim, A. T. Perry, and P. J. Ansell, *A review of distributed electric propulsion concepts for air vehicle technology,* AIAA Propulsion and Energy Forum , 1 (2018).

[23] E. Nguyen Van, D. Alazard, P. Pastor, and C. Döll, *Towards an aircraft with reduced lateral static stability using differential thrust,* in 2018 Aviation Technology, Integration, and Operations Conference (Atlanta, Georgia, 2018) https://arc.aiaa.org/doi/pdf/10.2514/6.2018-3209 .

[24] J. L. Freeman and G. T. Klunk, *Dynamic flight simulation of spanwise distributed electric propulsion for directional control authority,* in 2018 AIAA/IEEE Electric Aircraft Technologies Symposium (EATS) (2018) pp. 1–15.

[25] P. Kou, J. Wang, and D. Liang, *Powered yaw control for distributed electric propulsion aircraft: A model predictive control approach,* IEEE Transactions on Transportation Electrification **7**, 3006 (2021).

[26] M. Fouda, R. Haq, H. N. Naeem, M. A. Saeed, S. N. Wanyonyi, N. Cigal, C. Beker, M. Yayla, and D. F. Kurtulus, *Design methodologies of a distributed propulsion aircraft,* in 10th Ankara International Aerospace Conference (Ankara, Turkey, 2019) pp. 1–37.

[27] J. van der Vaart and H. Muhammad, *Static longitudinal stability and control characteristics of the Fokker F27 'Friendship' calculated by simple handbook methods*, Tech. Rep. LR-394 (Technical University of Delft, 1983).

[28] E. Nguyen, P. Troillard, J. Jézégou, D. Alazard, P. Pastor, and C. Döll, *Reduction of vertical tail using differential thrust : Influence on flight control and certification,* in AEGATS 2018 (Toulouse, France, 2018) pp. 1–8.

[29] N. J. van Wonderen, *Analysis of propeller slipstream effects on the directional stability using a potential flow model*, Master's thesis, Delft University of Technology, Netherlands (2017).

[30] S. Zhao, J. Li, Z. Yang, R. Qian, and R. Xu, *Propeller rotation effects on pitching moment for transport aircraft with conventional tail,* Journal of Aircraft **0**, 1 (0), https://doi.org/10.2514/1.C036578 .

[31] P. Van Den Borne and J. Van Hengst, *Investigation of propeller slipstream effects on the Fokker 50 through in-flight pressure measurements,* in Flight Simulation Technologies Conference and Exhibit (Dayton, Ohio, 1990) https://arc.aiaa.org/doi/pdf/10.2514/6.1990-3084 .

[32] T. Bouquet, *Modelling the Propeller Slipstream Effect on the Longitudinal Stability and Control*, Master's thesis, Delft University of Technology, Netherlands (2016).

[33] M. Schroijen, L. Veldhuis, and R. Slingerland, *Propeller slipstream investigation using the Fokker F27 wind tunnel model with flaps deflected,* 26th International Congress of the Aeronautical Sciences , 1 (2008).

[34] D. Keller and R. Rudnik, *Investigation and improvement of directional stability and control under slipstream effects,* in 2018 AIAA Aerospace Sciences Meeting (Kissimmee, Florida, 2018) https://arc.aiaa.org/doi/pdf/10.2514/6.2018-1793 .

[35] J. Soikkeli, *Vertical Tail Reduction Through Differential Thrust*, Master's thesis, Delft University of Technology, Netherlands (2020).

[36] D. Kim, Y. Lee, S. Oh, Y. Park, J. Choi, and D. Park, *Aerodynamic analysis and static stability analysis of manned/unmanned distributed propulsion aircrafts using actuator methods,* Journal of Wind Engineering and Industrial Aerodynamics **214**, 104648 (2021).

[37] O. Pfeifle, M. Frangenberg, S. Notter, J. Denzel, D. Bergmann, J. Schneider, W. Scholz, W. Fichter, and A. Strohmayer, *Distributed electric propulsion for yaw control: Testbeds, control approach, and flight testing,* in AIAA Aviation 2021 Forum (Virtual Event, 2021) https://arc.aiaa.org/doi/pdf/10.2514/6.2021-3192 .

[38] E. Nguyen Van, D. Alazard, C. Döll, and P. Pastor, *Co-design of aircraft vertical tail and control laws using distributed electric propulsion,* IFAC-PapersOnLine **52**, 514 (2019), 21st IFAC Symposium on Automatic Control in Aerospace ACA 2019.

[39] C. Courtin and R. J. Hansman, *Safety considerations in emerging electric aircraft architectures,* in 2018 Aviation Technology, Integration, and Operations Conference (Atlanta, Georgia, 2018) https://arc.aiaa.org/doi/pdf/10.2514/6.2018-4149 .

[40] European Union Aviation Safety Agency, *CS-25 large aeroplanes,* https://www.easa.europa.eu/sites/default/files/dfu/CS-25_Amdt%203_19.09.07_Consolidated%20version.pdf (2007), accessed on March 7, 2023.

[41] R. de Vries, R. E. Wolleswinkel, M. Hoogreef, and R. Vos, *A new perspective on battery-electric aviation, part II: Conceptual design of a 90-seater,* in AIAA SciTech Forum (Orlando, Florida, 2024).

[42] all Time ReSet, *Fuel system,* https://alltimereset.weebly.com/fuel.html#:~:text=The%20fuel%20in%20the%20ATR,part%20of%20the%20wing%20structure., accessed on May 24, 2023.

[43] epec, *Battery cell comparison,* https://www.epectec.com/batteries/cell-comparison.html, accessed on December 12, 2023.

[44] J. Roskam, *Airplane Design* (Roskam Aviation and Engineering Corporation, Kansas, USA, 1990) parts I through VIII.

[45] *USAF Stability and Control Datcom*, United States Air Force (1978), available at: https://apps.dtic.mil/sti/citations/ADB072483.

[46] J. Roskam, *Airplane Design* (Design, Analysis and Research Corporation, Lawrence, 2018).

[47] A. J. Santosh, *Influence of Ground Effect on the Flying V aircraft*, Master's thesis, Delft University of Technology, Netherlands (2020).

[48] S. Gudmundsson, *General Aviation Aircraft Design : Applied Methods and Procedures* (Elsevier, Oxford, United Kingdom, 2022).

[49] K. A. Salem, G. Palaia, M. Bianchi, D. Zanetti, V. Cipolla, and V. Binante, *Preliminary take-off analysis and simulation of prandtlplane commercial aircraft,* Aerotecnica Missili Spazio **99**, 203 (2020).

[50] M. S. Seif and M. a. Tavakoli, *A practical method for investigation of aerodynamic and longitudinal static stability of wing-in-ground effect,* International Journal of Maritime Technology **4** (2015), http://ijmt.ir/article-1-436-en.pdf .

[51] M. L. Sueur, *Ground Effect on the Take-off and Landing of Airplanes*, Tech. Rep. NACA-TM-771 (NACA, 1935).

[52] S. T. Kim, Y. Kim, and T. K. Reu, *CFD computation of the ground effect on airplane with high aspect ratio wing,* 28th International Congress of the Aeronautical Sciences , 1 (2012).

[53] O. Schrenk, *A simple approximation method for obtaining the spanwise lift distribution,* The Aeronautical Journal **45**, 331–336 (1941).

[54] *Flow Fields of Free Air Jets - A Report Bibliography*, Tech. Rep. DDC-ARB-41 (Defense Doc Center, 1965).

[55] M. J. Abzug, *Effect of Jet and Rocket Operation on Static Longitudinal and Directional Stability*, Tech. Rep. (Bureau of Aeronautics, 1945).

[56] J. Roskam, *Airplane Flight Dynamics and Automatice Flight Controls Part I* (DARcorporation, Lawrence, Kansas, 1995).

[57] NASA, *X-57 maxwell,* https://www.nasa.gov/aeronautics/x-57-maxwell/ (2018), accessed on March 7, 2023.

[58] *Metrics for various aircraft,* https://jsbsim.sourceforge.net/MassProps.html, accessed on January 16, 2024.